Predicting the Risk of Crystallization for Suspensions of Amorphous Spray Dried Dispersions from Structural, Thermal and Hydrophilicity Properties

By
James D. Ormes

Submitted to the graduate degree program in Pharmaceutical Chemistry and the Graduate Faculty of the University of Kansas in partial fulfillment of the requirements for the degree of Master of Arts.

_____
Chairperson Dr. Jeffrey Krise

_____
Dr. Laird Forrest

_____
Dr. Patrick Marsac

Date Defended: May 23, 2014

The Thesis Committee for James D. Ormes
certifies that this is the approved version of the following thesis:

Predicting the Risk of Crystallization for Suspensions of Amorphous Spray Dried Dispersions from Structural, Thermal and Hydrophilicity Properties

_____

Chairperson Dr. Jeffrey Krise

Date approved: May 23, 2014

Abstract:

Suspensions of spray dried amorphous dispersions are a valuable tool for enhancing the exposure of poorly soluble compounds in preclinical animal models. However, limitations in drug supply and time/cost of manufacture in the drug discovery space make it desirable to predict the likelihood of obtaining a physically stable (free from detectable crystallization) suspension prior to synthetic scale-up and processing of a candidate compound. Background information on this topic is covered in Chapter 1.

*For 33.3% drug load amorphous dispersions in Hydroxypropylmethyl cellulose acetate succinate (HPMCAS) suspended in 0.5% methocellulose (MC) + 0.25% sodium lauryl sulfate (SLS) + 5 mM HCl, a platform formulation frequently used in discovery, a 2-tiered model can be used to correctly predict the physical stability of 22 of 24 model compounds. First, the model considers the humidity adjusted glass transition temperature of the amorphous dispersion ($T_{g,dispersion,100\%\ RH}$). For compounds where $T_{g,dispersion,100\%\ RH}$ is >30 °C, the amorphous dispersion is typically free from crystallization within 3 hours of preparation, which is attributed to a decrease in molecular mobility. 3 hours was selected as the timeframe between suspension preparation and dosing for the purpose of the present research. For compounds where $T_{g,dispersion,100\%\ RH}$ is <30 °C, the amorphous dispersion has elevated molecular mobility, and can undergo rapid crystallization within a 3 hour dosing window. For these compounds analysis of melting temperature/entropy of fusion (must be <5500 K^2*mol/KJ to be predicted stable) and molecular weight x LogP (must be >1000 to be predicted stable) can be used to successfully predict a 3 hour shelf-life. A decision tree, resulting from this dissertation research, is outlined in Figure 1.*

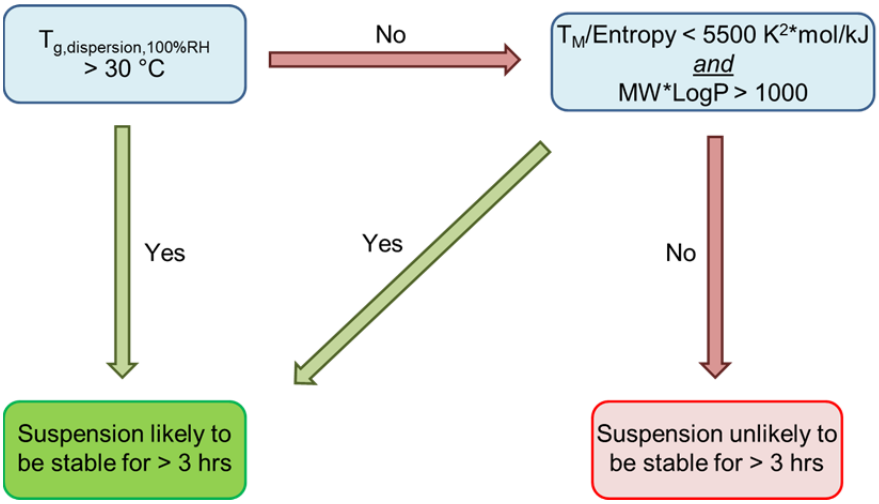

Figure 1. Decision tree for assessing the physical stability of a model compound spray dried to form an amorphous dispersion at 33.3% drug load in HPMCAS and suspended in 0.5% methocellulose + 0.25% SLS + 5 mM HCl.

Acknowledgements: I would like to acknowledge my thesis panel including Dr. Jeff Krise, Dr. Patrick Marsac and Dr. Laird Forrest. I would like to acknowledge Dr. Annette Bak for input throughout the thesis process. I would like to acknowledge Dr. Caroline McGregor, Dr. Brian Farrer, Dr. Nara Variankaval, and Dr. Elizabeth Kwong, all of which helped with thesis guidance along the way. In addition I would like to thank the Merck Research Labs for funding my Masters education.

Table of Contents:

Chapter 1: Introduction and Background

Chapter 1 focuses on providing background rational and design of subsequent chapters. The need for solubilization and dissolution rate enhancement in the preclinical space, in order to support pharmacology and toxicology animal studies, is first demonstrated. Next, the chapter discusses the available solubilization strategies, potential differences between crystalline and amorphous materials, and the benefit and risk associated with utilizing suspensions of amorphous solid dispersions for animal studies. The background further delves into why spray drying is the preferred method to prepare 'suspendable' amorphous material, and lastly this thesis chapter describes the critical need to predict the crystallization mode of failure, for a potential compound, based upon the physicochemical descriptors of that compound.

1. Utility of amorphous dispersions in the drug discovery space:

Current industry trends seem to favor molecules which, without the use of technologies to enhance exposure, demonstrate poor oral bioavailability[1,2]. Reasons for this include increased molecular weight, increased lipophilicity and a decrease in the solubility of many candidate molecules relative to drug prepared from 1980 to 2000[1,2]. As a result, amorphous solid dispersions have increased in utility in recent years as a tool to enhance oral bioavailability in both a clinical and preclinical setting[3-10].

The ways in which amorphous dispersions enhance exposure are four-fold. First, in the amorphous state, the energy barrier to dissolve is decreased relative to the crystalline state, as no crystal lattice energy is present[11]. Typically this results in an enhanced apparent kinetic solubility and can lead to faster dissolution[12-15] and super saturation[16-19]. Second, the amorphous dispersion may dissolve in such a way so as to form colloidal species in solution, which reduces the drug particle size and increases the surface area, thus improving the dissolution rate[16,18]. Third, typical amorphous dispersion polymers tend to have some hydrophilic character, depending upon the polymer selected, and can facilitate dissolution through increased wetting[12-15]. Lastly, the amorphous dispersion polymer can act as a precipitation and crystallization inhibitor thus sustaining supersaturation[12,14,17,18].

Several key differences exist between the formulation presentation for a commercial/clinical (human) preparation and a preclinical (animal) study. Typically, the primary difference between these two presentations is the need to prepare suspensions for preclinical studies, whereas solid oral dosage forms, such as a tablet, are frequently used for clinical studies and as the preferred commercial dosage form. Nonetheless preclinical animal studies are an integral and important foundation for developing effacious and safe drugs. From this perspective, this thesis explores how physicochemical and structural properties of a model compound can be used to predict the potential for crystallization from a model system. These empirical structure property relationships, which can be rationalized through thermondynamic first principals, are of utmost importance in a drug discovery setting, where limitations in drug supply and time/cost of manufacture in the drug discovery space make it desirable to predict the likelihood of obtaining a physically stable suspension prior to synthesis, scale-up and processing of a candidate compound[2].

A better understanding of the empirical structure property relationships observed in suspension crystallization studies can be obtained by considering the potential modes of failure for a suspension of amorphous spray dried dispersions. It can be hypothesized that two primary modes of failure could include (1) dissolution of the model compound out into the suspending vehicle followed by crystallization in the suspending vehicle, or (2) permeation of the water into the amorphous solid dispersions followed by plastization/anti-solvation, which can lead to elevated drug mobility and an enhanced nucleation rate[20-26].

When considering failure mode 1, one must first consider whether the suspended material exhibits properties of a glass or a super cooled liquid, where it is hypothesized that the drug can more readily partition out of a material in a supercooled liquid state rather than a glass state. In addition the lipophilicity of the drug is important as it represents a potential to partition into a water phase, and may affect the rate of crystallization from this failure mode. Once in the bulk suspending media, the supersaturation and solubility of the drug in the suspending media needs to be considered as it represents a thermodynamic driving force for crystallization[27-34]. Lastly the rate of nucleation in solution will be dependent upon structural (such as molecular weight and number of rotatable bonds) and thermodynamic (melting temperature, enthalpy and entropy of fusion) features of the model molecule[29,30,31,33]. Each of these parameters are key components to classical nucleation theory, which will be discussed in more detail later in this chapter.

When considering failure mode 2, properties such as the glass transition temperature, or the glass transition temperature in the presence of moisture, may be critical in understanding the crystallization tendency of the model amorphous dispersion[20-22,24-26]. These factors will be impacted by the glass transition temperature of the drug, the glass transition temperature of the amorphous dispersion, and the hygroscopicity of the amorphous dispersion, as water will serve as a plasticizer. In addition, it is hypothesized, for amorphous dispersions in the super cooled liquid state, where molecular mobility is elevated, the rate of nucleation in the solid state will have increased sensitivity to structural (such as molecular weight and number of rotatable bonds) and thermodynamic (melting temperature, enthalpy and entropy of fusion) features of the model molecule.

Certain properties, which are predictive of the driving force, or ease of undergoing nucleation, are equally important to each model. Regardless of the failure mode, amorphous dispersions in the glassy state should be more stable than amorphous dispersions in the super cooled liquid state due to decreased molecular mobility. In addition other properties that affect nucleation rates, such as molecular weight, number of rotatable bonds, melting termperature and other thermodynamic parameters play a critical role in each failure mode.

2. Key differences between amorphous versus crystalline materials:

The primary difference between a crystalline and amorphous material is the existence of long range lattice order[11]. Crystalline materials are arranged in a lattice consisting of a repeating orientation/pattern in three dimensions. These materials possess crystalline lattice energy and undergo a melting event (solid-liquid phase transformation) at a defined melting temperature. In contrast, amorphous materials do not possess long range order. These materials exist in a meta-stable state in which the material possesses a higher Gibbs free energy relative to the crystalline state[11].

Differentiation of crystalline and amorphous materials can be made using several solid state characterization techniques including: differential scanning calorimetry (measuring the presence or absence of a melting temperature and glass transition temperature), powder x-ray diffraction (using x-rays to look for diffraction peaks) and polarized light microscopy (observing birefringence under cross polarized light)[35-39].

Amorphous materials, having a higher Gibbs free energy than crystalline materials, contain a thermodynamic driving force to spontaneously crystallize[11,40,41] and reduce the Gibbs free energy of the system. This presents an inherent physical stability risk. For this reason amorphous drugs are generally prepared as amorphous dispersions within a polymer matrix. In these amorphous dispersions the polymer plays a key role in the stabilization of the amorphous state[42,43]. The polymer helps stabilize a drug, and prevent crystallization by raising the glass transition temperature. This decreases the molecular mobility of the drug in the polymer dispersion. The polymer also acts as nucleation inhibitor and slows growth of already formed crystalline material[42,43]. The polymer may also impart a reduction in the chemical potential of the drug to crystallize (reduce the thermodynamic driving force for crystallization)[42,43]. Additional details on the polymer selection criteria for this thesis appear in Chapter 2.

Achieving an adequate dissolution profile and a high solubility in the gastrointestinal milieu are key steps in enhancing oral exposure as many drugs have dissolution rate limited oral exposure[44]. The mechanism by which amorphous solid dispersions improve oral bioavailability has been discussed in the literature, with most discussion centering around the Noyes-Whitney equation (equation 1), where *D is* the diffusivity through the boundary layer, *l* is the boundary layer. Reduction in the surface area (*A*) or a increase in the kinetic/apparent solubility over the thermodynamic solubility (C_S) result in a faster dissolution rate and therefore elevated absorption *in vivo*[6,45-47].

$$\text{Dissolution Rate} = \frac{DA}{l}(C_S - C) \qquad (1)$$

For amorphous materials C_S is the apparent amorphous solubility, which is elevated relative to the thermodynamic solubility, and provides a faster dissolution driving force and an elevated solubility for compounds with dissolution rate limited absorption. In addition to dissolution rate, an elevation C_S can help improve exposure for solubility limited compounds[7-10], which will be described in more detail. The elevation of the apparent amorphous solubility limit, relative to the crystalline equilibrium solubility, is described at length in the literature[11,48-51]. A first calculation was proposed by Hancock and Parks[11] as shown in (2) where $\sigma_{amorphous}$ and $\sigma_{crystalline}$ are the solubility values for the amorphous and crystalline material, and $\Delta G_{a\text{-}c}$ is Gibbs free energy difference between the amorphous and crystalline materials. An approximation for $\Delta G_{a\text{-}c}$ can be provided by the Hoffman equation[41] (3), where ΔH_f is the enthalpy of fusion, ΔT is

the difference between the melting temperature and room temperature, and *Tm* is the melting temperature.

$$\frac{\sigma_{amorphous}}{\sigma_{crystalline}} = \exp\left(\frac{\Delta G_{a-c}}{RT}\right) \quad (2)$$

$$\Delta G_{a-c} = \frac{\Delta H_f}{RT}\left(\frac{\Delta T \cdot T}{T_m{}^2}\right) \quad (3)$$

A more sophisticated calculation of the amorphous solubility limit has been proposed by Murande and Pikal[48-51]. This equation employs an additional correction factor (4) based upon the Gibbs-Duhem equation[48]. The Gibb-Duhem correction accounts for the free energy difference between the crystalline and hydrated amorphous state. Equation 4 is given for an unionized molecule.

$$\frac{\sigma_{amorphous}}{\sigma_{crystalline}} = \exp\left(\frac{\Delta G_{a-c}}{RT}\right) \times \left(e^{[-I(a_2)]}\right) \quad (4)$$

From these thermodynamic and rate equations, and the literature referenced, it is clear that an amorphous dispersion can improve both the dissolution rate and apparent solubility of a model molecule. If one could accurately measure the solubility difference between the amorphous and crystalline forms experimentally, the thermodynamic driving force of crystallization could be obtained. Correlating this value with the physical stability of suspensions of amorphous materials could be useful for developing a predictive physical stability model, however measuring this amorphous/crystalline solubility ratio has proven difficult to do experimentally due to the driving force to crystallize[11,49,50]. Nonetheless, these equations demonstrate a correlation between the driving force crystallization and properties such as melting temperature, and other thermodynamic properties, and thus these properties could play a key role in building a predictive model for physical stability of suspensions of amorphous dispersions.

3. Preparation of amorphous materials via spray drying:

While amorphous solid dispersions have seen increased usage as a clinical formulation strategy, it is only recently that advances in technology have afforded utility of this approach in the preclinical space[52]. This has been primarily due to challenges in making amorphous solid dispersions robustly at the milligram scale given the short development time and low material availability, which is necessary to support drug discovery programs. Numerous ways exist to prepare amorphous solid dispersions including spray drying, hot melt extrusion, spray congealing, milling and co-precipitation[7,9,10]. Spray drying has some unique advantages in the drug discovery space[53,54] and platform conditions can be utilized to produce spray dried dispersions with a relatively short development time[53,54]. Spray drying is a scalable process which can be used to produce material at the milligram to kilogram scale, although numerous considerations and challenges need to be taken into account when scaling the spray drying process[53,54].

In the drug discovery space, where formulations are typically dosed as suspensions to rodent and non-rodent species for pharmacology and toxicology studies, spray drying allows for some level of particle design and control (i.e., control of particle size and morphology). In addition the rapid drying times associated with spray drying are advantageous for preparing a uniform amorphous dispersion[53,54]. Thus, a preclinical formulation scientist can design particle attributes to provide good suspension characteristics. These attributes make spray drying an ideal unit operation for producing amorphous solid dispersions in the drug discovery space. The process of spray drying appears in Figure 2.

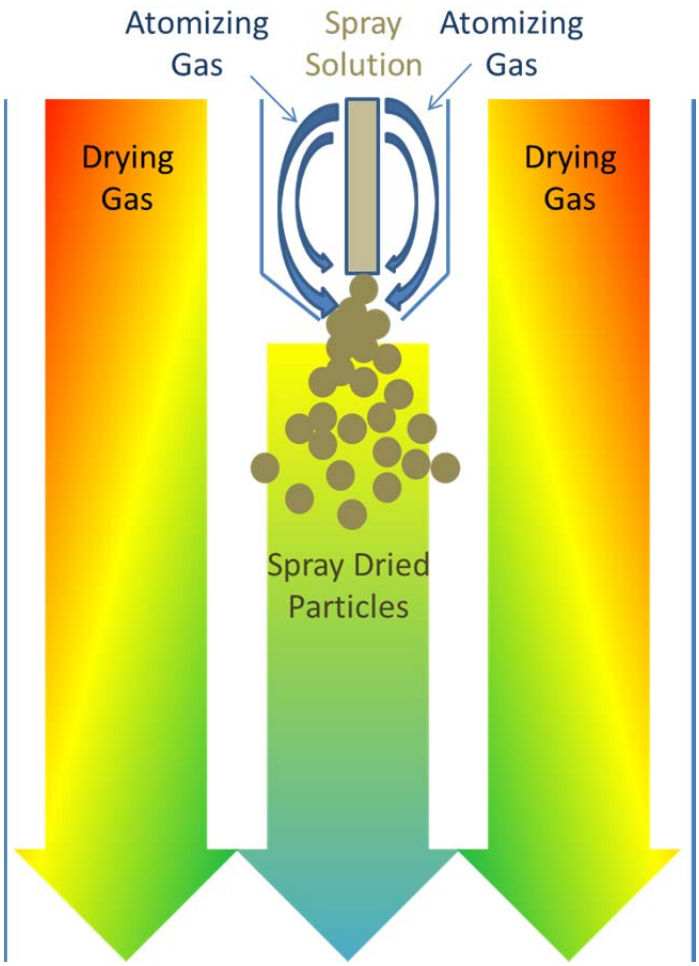

Figure 2. Diagram of spray drying unit operation.

In the spray drying process, an amorphous dispersion is prepared by first dissolving a drug and polymer in a volatile organic solvent. This mixture is then sprayed through an atomizing nozzle into a stream of hot drying gas. The solvent is rapidly evaporated leaving a powder containing the drug and polymer in an amorphous dispersion. The goal of this process is to dry the material at a sufficient rate that crystallization is unable to occur and that the material is a homogenous (single phase) amorphous dispersion[53,54]. Concerns do exist that the material may be heterogeneous based upon the drying kinetics, or that residual solvent may be contained within the spray dried particle and require secondary drying. While platform operating conditions are generally employed in the drug discovery space, downstream activities will require significant process definition to optimize operating conditions. Failure to adequately prepare a homogenous amorphous dispersion, prior to testing in a suspension physical stability

model, could result in an erroneous rapid crystallization rate (either by failure mode 1 or failure mode 2). For this reason each material is characterized thoroughly before physical stability studies are conducted.

In a preclinical setting, the spray dried powder can be dispersed in a carrier vehicle and dosed as a suspension. Numerous parameters are critical to the spray drying process including, selection of the processing equipment, inlet and outlet temperatures, selection of the solvent and carrier polymer, spray rate and atomization pressure to name a few. Details behind the selection of these parameters appear in Chapter 2 of this thesis.

4. Possible modes of failure for suspensions of spray dried dispersions:

A suspension of a spray dried amorphous dispersion can undergo several modes of formulation failure. Three hypothesized modes of failure include crystallization, poor flow/suspension properties and chemical degradation. Amongst these three modes of failure, crystallization is a large concern due to the meta-stable nature of the amorphous dispersion, and is the sole focus of this thesis. Within the crystallization mode of failure, there are two primary modes of failure as mentioned previously, (1) dissolution of drug into the suspending vehicle followed by crystallization or (2) crystallization of the drug within the suspended amorphous dispersion particle.

Numerous papers exist focusing on attempts to predict the shelf-life and performance of amorphous solid dispersions[35,36,39,40,43]. These papers are focused on the preparation of clinical solid oral dosage formulations rather than suspensions. From this literature, it has been well established that the physical stability of an amorphous solid dispersion can be enhanced by (1) increasing the polymer to drug ratio, (2) decreasing the storage temperature and (3) protecting the amorphous dispersion from moisture[20-26]. Unfortunately, in the preclinical space, where suspensions of spray dried dispersions are utilized, there is limited ability to control any of these three factors. First, target doses, especially for high dose safety studies, may necessitate a high drug loading in the amorphous solid dispersion. This can limit the maximum achievable dose which can lead to a gumming, gelling or caking of the material at high dose (a commonly encountered mode of failure). Second, suspensions of amorphous solid dispersions encounter 100% relative humidity via direct contact with the aqueous environment of the suspending

vehicle. As previously mentioned this can promote crystallization, by increasing the thermodynamic driving force for crystallization, through two modes of failure, as it allow for both a plasticizing effect anti-solvation effect on the amorphous dispersion particles. This can lower the glass transition temperature from a glassy state to a super cooled liquid state as water penetrates the solid particles. This can also promote crystallization with the solid state material (failure mode 2) or can solubilize drug into the bulk suspending media, where the drug is free to crystallize in the absence of the undissolved polymer to inhibit crystallization (failure mode 1).

Upon examining crystallization of suspensions of spray dried dispersions, it is critical to understand the difference between nucleation and growth of crystals[29,30]. Nucleation is the spontaneous formation of a crystalline material. Growth involves monitoring the increasing size of the crystalline material. This thesis focuses on detecting the onset of crystallization (nucleation) rather than on monitoring the growth of already formed crystalline material, as the formulation would need to be dosed prior to observable crystalline content (prior to failure/nucleation). The inability of a preclinical formulation scientist to accurately assess the impact of low levels of crystallization on bioperformance/oral absorption, and the inability to accurately quantify the crystallized content in suspension, precludes the use of partially crystallized suspensions reliably in the drug discovery setting.

The nucleation process can be described by classical nucleation theory (CNT). CNT describes the precipitation of particles from supersaturated solutions. In CNT, nucleation centers evolve until a critical size of repeating molecules is reached[29,30]. Equation 5 describes the most basic view of classical nucleation theory where K_0 is a pre-exponential factor, ΔG_{crit} is driving force for nucleation, and k_B is the Boltzman constant. Of importance to this thesis are parameters which can affect ΔG_{crit} and K_0. Factors affecting ΔG_{crit} include thermodynamic factors, such as melting temperature, and entropy and enthalpy of fusion. ΔG_{crit} can also be related to the supersaturation of the drug, either in the suspending media (failure mode 1) or in the amorphous solid dispersion matrix (failure mode 2)[29-34]. K_0 can be related to structural features associated with the ease of molecular stacking into a crystal lattice. These parameters could be affected by molecular descriptors such as molecular weight, number of rotatable bonds or surface tension[29,30].

$$NucleationRate = K_0 \exp\left(-\frac{\Delta G_{crit}}{k_B T}\right) \quad (5)$$

5. Predicting crystallization of suspensions of amorphous dispersions:

In the drug discovery/preclinical setting it is clear that suspensions of amorphous dispersions can provide a useful tool for exposure enhancement of compounds with low solubility[3-10]. This potential exposure enhancement may come with a risk of formulation failure, of which crystallization is the critical concern. However, the current literature lacks tools to predict which compounds are likely to encounter failure due to crystallization when formulated as suspensions of amorphous dispersions. Literature does exist to predict crystallization of amorphous materials in the solid state in a dry environment[35,39,42,43], in a humid environment[20-26] and predict crystallization from solution[38-34]. However, none of the current literature adequately predicts what will happen to suspensions of spray dried dispersions. Limitations in drug supply and time/cost of manufacture in the drug discovery space make it desirable to predict the likelihood of obtaining a stable (free from detectable crystallization) suspension prior to synthesis, scale-up and processing of a candidate compound.

In order to experimentally determine which properties impact the potential of the model system to show signs of crystallization, 24 poorly water soluble model compounds were selected with a wide range of physicochemical properties (details appear in Chapter 2). These poor solubility model compounds were selected in order to represent random model compounds which could appear in a drug discovery pipeline. Additional details regarding selection criteria appear in Chapter 2.

The following structural descriptors were assessed for each model compound: molecular weight, number of rotatable bonds, number of hydrogen bond donors and number of hydrogen-bond acceptors. Each of these parameters helps to characterize the model compounds in terms of size, shape and propensity to participate in hydrogen bonding. In addition, several of these properties can be explored as a ratio, for instance normalizing by molecular weight.

The following thermal properties were assessed for each model compound: melting temperature, enthalpy of fusion, entropy of fusion, Gibbs free energy, as well as the glass transition temperature of the drug substance and dry amorphous dispersion.

The following hydrophilicity properties were assessed for each model compound: water solubility, water solubility calculated from the general water solubility equation, platform vehicle

solubility, hygroscopicity (as defined by moisture weight gain at 90% RH) and the glass transition temperature of the amorphous dispersion at 100% RH. Interactions with water are of utmost importance to amorphous suspension formulations since the amorphous spray dried dispersions encounters 100% humidity. Both failure mode 1 and failure mode 2 describe interactions with water either as a solvent/anti-solvent, a plasticizer or a bulk solution in which the drug can dissolve into.

In addition to assessing properties in a uni-variate fashion, a multi-variate model was developed in this thesis which incorporates numerous parameters. Preclinical scientists will be able to utilize the output from this thesis to predict which compounds will have adequate crystallization stability in a platform suspension. As mentioned previously, this will save resource expenditure in the drug discovery space with time and drug substance supply are limited.

Chapter 2: Amorphous Dispersion Suspension Crystallization Studies

Chapter 2 outlines the selection of the model systems used in this thesis. The chapter illustrates how compounds were selected based upon a need for a diverse set of physicochemical properties. The drivers for selecting a 33.3% drug load HPMCAS-L amorphous solid dispersion and the model suspending vehicle (0.5% methocellulose + 0.25% Sodium Lauryl Sulfate + 5 mM HCl) are also described in detail. In addition to the selection of the model systems, important details around the spray drying process and characterization of material are discussed. Lastly, the chapter outlines how crystallization studies were conducted and presents the composite data from those studies.

1. Selection of the model polymer/dispersion system:

Hydroxypropylmethyl cellulose acetate succinate L grade (HPMCAS-L) was selected as a model dispersion polymer. This polymer was selected for several reasons including (1) precedent in the literature[55,56], (2) an elevated glass transition temperature which helps stabilize the amorphous dispersion from crystallization[55,56], (3) acidic/enteric nature of the succinate moiety of the polymer (useful from a solubilization control versus pH standpoint) and (4) hydrophilic/surface active properties at neutral pH (useful from an *in vivo* anti-nucleation standpoint)[55-57]. The pH-dependent nature of this polymer is of particular importance to the design of the suspensions. The pH-dependent solubility of the polymer allows for the preparation of a stable suspension below pH 5.5, while still allowing for release of the drug at neutral/intestinal pH[55-57]. In addition upon release of the drug at pH 5.5, the polymer acts as an anti-nucleation agent[55-57].

A platform drug loading of 33.3% w/w drug/polymer was selected for the model amorphous dispersions. This drug loading was selected based upon literature precedence as a model drug loading[14,55]. In addition, this drug loading can be rationalized in the following way. For drug loadings below 20%, the maximum dose-able concentration decreases since the majority of each solid particle is comprised of polymer, this is important since several drug discovery studies (e.g., pharmacology and toxicology) require high doses. For drug loadings

above 50%, there is an inherent crystallization stability risk in both the solid state and the suspended state[55].

2. Selection of the model compounds:

The following 24 model compounds were selected for this thesis: nevirapine, piroxicam, griseofulvin, chlorpropamide, tolazamide, indoprofen, fenofibrate, carbamazepine, telmisartan, aprepitant, felodipine, omperizole, bifonazole, telaprevir, ketonconazole, miconazole, itraconazole, indomethacin, clofoctol, ritonavir, efavirenz, clotrimazole, torcetrapib, and celecoxib. These molecules were selected, after careful consideration, based upon the following criteria. First, a large number of these molecules have been prepared as amorphous dispersions in the pharmaceutical literature, and therefore historical data can be leveraged and these compounds have precedence as representing poorly water soluble pharmaceutical molecules. Second, the physical chemical properties of these molecules cover a large range of physicochemical space. Key properties include molecular weight (200 to 800 dalton), number of rotatable bonds (0 to 10), ionization state (acidic, basic, neutral and zwitterionic) glass transition temperatures (-20 to 100 °C), Log P (0 to 9) and melting temperature (100 to 300 °C). By covering a large range of the possible physicochemical properties in a pharmaceutical development pipeline, this data set helps us identify which parameter, or parameters, are most predictive of the amorphous suspension physical stability of amorphous dispersions of future molecules. In addition these properties bracket the range of molecules which are typically considered drug like[1,2] with all molecules reaching phase IIB in clinical trials or the market.

3. Selection of a model/platform suspending vehicle:

A model suspending vehicle for a suspension of amorphous spray dried material, containing a pH-dependent polymer, generally contains three key components. The first component is a pH modifier, in this case 5 mM HCl was selected. Other pharmaceutically acceptable potential options could include buffering agents such as citrate, tartrate, acetate or other weak acids. HCl was selected, due to a simple ionic structure, which is less likely to act as an anti-nucleation agent, and confound the measurements. This component acidifies the pH and

prevents release of the compound from the pH-dependent HPMCAS polymer. The second component of a model suspending vehicle is a viscosity enhancer. This component is added to prevent rapid settling of the suspension. In this case 0.5% methocellulose was selected as it is a common suspending agent. Other pharmaceutically acceptable potential viscosity enhancing agents could include other cellulosic polymers or other polymers such as povidone or co-povidone. The third component is a surfactant which will help improve the wetting of HPMCAS. In this case 0.25% SLS was selected as a model surfactant with the surfactant amount just above the critical micelle concentration for SLS[58]. Other pharmaceutically acceptable potential surfactants could include polysorbates and poloxamers. SLS was selected, due to a simple non-polymeric structure, which is less likely to act like an anti-nucleation agent, and confound the measurements.

4. Spray Drying Processing Parameters:

a.) Materials:

Analytical HPLC Grade acetone, methanol and tetrahydrofuran (Sigma-Aldrich; tetrahydrofuran inhibited with butylated hydroxytoluene to prevent peroxide formation), HPMCAS-LF (Shin-Etsu), griseofulvin (Sigma), indoprofen (Sigma), Chloropropamide (TCI-GR), neviripine (Ava Chem Scientific), celecoxib (Matrix Scientific), tolazamide (Sigma), bifonazole (MP Biomedicals), itraconazole (Spectrum), miconazole (Spectrum), indomethacin (MP Biomedicals), piroxicam (MP Biomedicals), clotrimazole (Sigma), ketoconazole (Spectrum), clofoctol (Sigma), telaprevir (Merck), efavirenz (Merck), ritonavir (Merck), aprepitant (Merck), felodipine (Ontario), torcetrapib (Merck), telmisartan (Astatech), carbamazepine (Acros), fenofibrate (Sigma), and omerprazole (Spectrum). All compounds obtained were greater than 97% purity and used as received.

b.) Preparation of the spray dried dispersions:

The drug substance and HPMCAS were dissolved in acetone, methanol or tetrahydrofuran, with preference given to acetone and methanol to avoid any safety risks

associated with spray drying from tetrahydrofuran, which is a solvent which can form peroxides upon prolonged exposure to oxygen. The mixture was stirred on a magnetic stir plate or submersed into a Branson Ultra-Sonicator until all components had dissolved. Materials were spray dried using a ProCepT Microspray Dryer with a bi-fluid nozzle. Unless there were solubility limitations, the solid loading was fixed at 40 mg of solid per milliliter of solvent, although a few compounds, such as itraconazole and telmisartan, needed further dilution to fully solubilize. Other key parameters include nozzle size (0.6 or 0.8 mm), spray rate (5-8 mL/min), outlet drying temperature (5-10 °C below solvent boiling point) and atomization air flow (3-6 L/min). In all cases the spray dried dispersion was stored overnight in a vacuum oven (30 in Hg vaccum) at room temperature to evaporate residual moisture and solvents. Additional heating was avoided due to concerns that additional heat could promote crystallization.

5. Characterization of spray dried amorphous dispersion:

Spray dried materials were characterized using powder x-ray diffraction (PXRD) to assess crystallinity, modulated differential calorimetry (mDSC) to assess crystallinity and measure the glass transition temperature of the spray dried material, thermal gravimetric analysis (TGA) to assess residual solvent/moisture, polarized light microscopy (PLM) to evaluate particle size and crystallinity, high performance liquid chromatography (HPLC) to evaluate purity and potency and laser light scattering (LLS) to assess particle size and distribution.

PXRD measurements were taken with a Phillips XPERT instrument. Samples were scanned continuously from 0-40 2θ over 1 hour using a tension of 45 kV and a current of 40 mA. Key optics parameters include: a PW3373/10 CuLFF DK164254 tube, a 240 mm beam radius, a 6° take-off angle and a1.54 Å wavelength. A sample PXRD scan for an Itraconazole amorphous dispersion is shown in Figure 3. The full characterization data set for each of the 24 model compounds appears in Appendix 1.

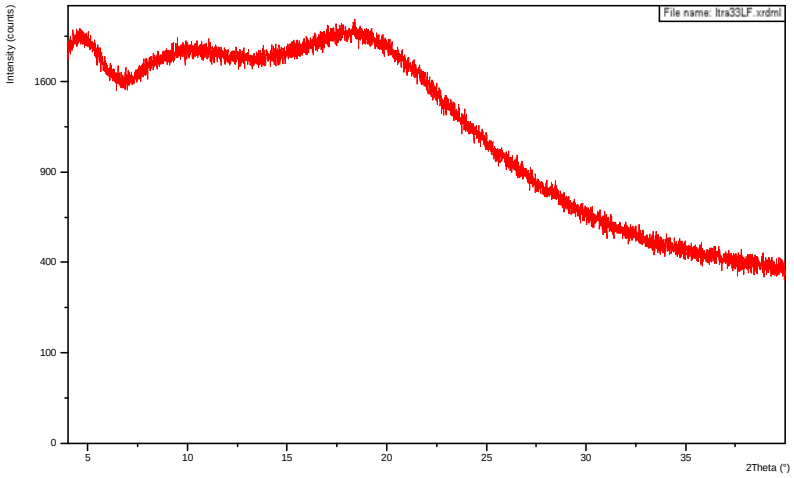

Figure 3. PXRD scan for Itraconazole 33.3% Drug Loading in HPMCAS. Note the lack of crystalline reflections and the presence of an amorphous halo.

Modulated DSC measurements were taken to assess phase uniformity and the glass transition temperature of each amorphous material. Approximately 3-5 mg of sample was loaded into a hermetically sealed pan with a pin hole in the top. The sample was loaded onto a TA Instruments Q2000 DSC and was heated from 35 to 170 °C with a modulation amplitude of 0.5 °C, a modulation period of 60 sec, and a ramp rate of 2 °C/min. A sample mDSC scan is shown for an Itraconazole amorphous solid dispersion in Figure 4. The full characterization data set for each of the 24 model compounds appears in Appendix 1.

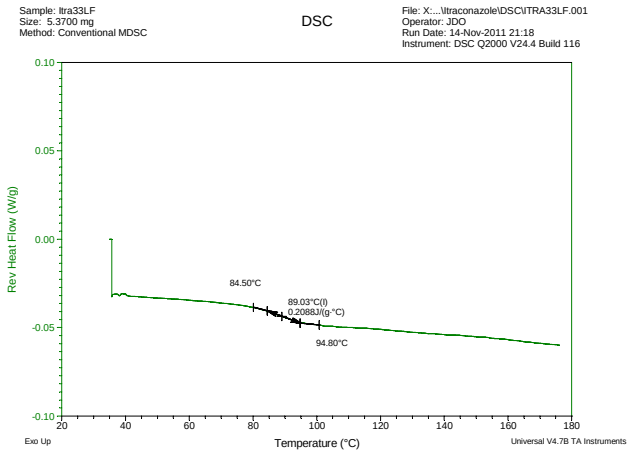

Figure 4. A modulated DSC trace for 33.3% Itraconazole/66.7% HPMCAS w/w % spray dried dispersion. Note the existence of a single Tg suggesting a single amorphous phase. Note that the Tg of HPMCAS-L is 118 to 120 °C[55].

Polarized light microscopy samples were analyzed using a Nikon Eclipse ME600 under a 20x objective utilizing cross-polarizering filters and image capture capability to look for particle size, shape, morphology and birefringence. A PLM image for an Itraconazole amorphous dispersion is shown in Figure 5. The full characterization data set for each of the 24 model compounds appears in Appendix 1.

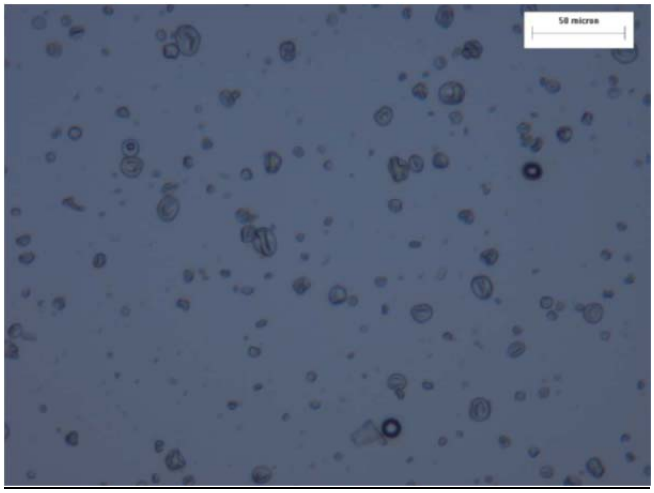

Figure 5. Polarized microscopy image of 33.3% Itraconazole/66.7% HPMCAS w/w % spray dried dispersion. Note spherical/raison-like morphology and lack of birefringence under cross polarized light.

TGA was conducted for select amorphous dispersions to attempt to gain a typical residual solvents and moisture range. Samples were loaded onto a TA Instruments Q5000 and heated from room temperature to 170 °C at 20 °C/min. The full characterization data set appears in Appendix 1.

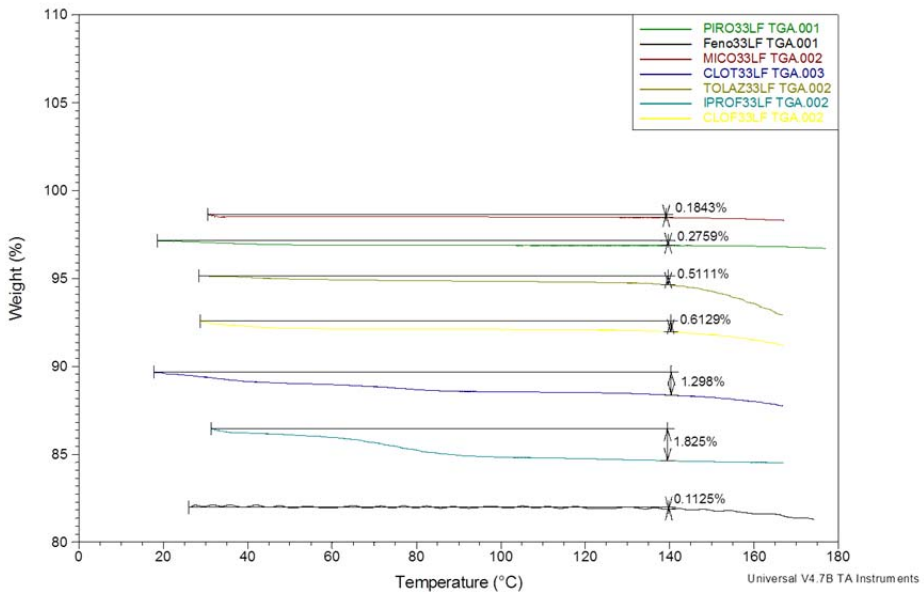

Figure 6. TGA data for spray dried amorphous dispersions (from top to bottom) of Piroxicam, Fenofibrate, Miconazole, Clotrimazole, Tolazamide, Indoprofen and Clofoctol in HPMCAS-LF at 33.3% DL.

HPLC was conducted for numerous amorphous dispersions to verify correct drug loading. Samples were diluted in 75:25 MeCN:water approximately to 0.1-0.2 mg/mL. Samples were then analyzed on a 10 minute linear gradient from 95:5 A:B to 10:90 A:B where A and B are 0.1% H_3PO_4 and MeCN respectively. Samples were analyzed verses a reference standard of the compound dissolved in 75:25 MeCN:water. HPLC analysis were conducted at 210 nm and the column compartment contained a Supelco Ascentis Express C18 (10cm x 4.6mm, 2.7 µm) column heated to 40 °C. From these studies one could conclude that an accurate potency for the amorphous dispersions had been obtained. Additional data appears in Appendix 1.

LLS studies were conducted on select samples to measure the representative particle size and distributions for spray dried amorphous dispersions prepared on the ProCepT Micro-Spray Dryer. Particle size distribution was measured with a HELOS/KF-Magic laser diffraction particle size analyzer by Sympatec. The instrument was equipped with a RODOS dry disperser and a VIBRI feeder. R1 lens with a measure range of 0.13-32.08 µm was selected for measurements. The measurement was performed under the dry dispersion mode with a dispersing pressure at 2.5

bars. Typical results from an Itraconazole amorphous dispersion are shown in Figure 7. Additional data is available in Appendix 1. This method was selected because the particle size for the spray dried dispersion was appropriate for the lens range. In addition the dispersion pressure was selected so as to prevent destruction of primary particles.

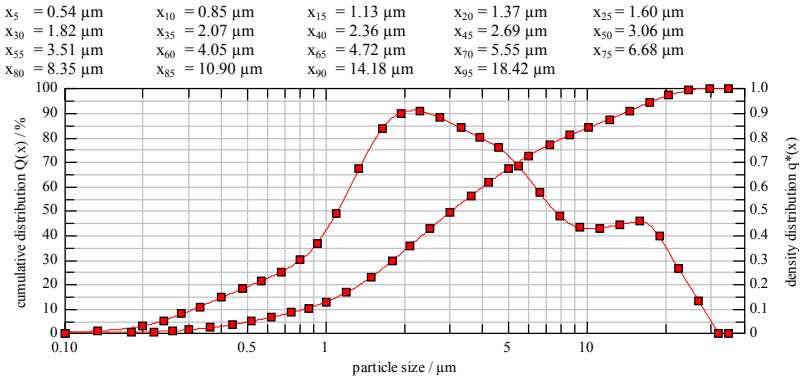

Figure 7. Laser light scattering particle size data for spray dried 33.3% Itraconazole/66.7% HPMCAS w/w %.

The particle size, of spray dried amorphous dispersions, can be sensitive to spray drying parameters and to the scale of the spray drying operation, thus it is important to make these measurements to ensure the material prepared for suspension physical stability studies is within a consistent range.

6. Suspension physical stability (onset of crystallization) studies:

Suspensions of the amorphous spray dried dispersions were prepared by suspending 120 mg of material in 2 mL of platform vehicle (i.e., 60 mg/mL amorphous dispersion; 20 mg/mL drug; 100 mg/kg drug when dosed at 5 mL/kg). This model dose/concentration would be a pharmaceutically relevant dose for either a toxicology or pharmacology animal study. The exact onset of crystallization is not possible to determine due to instrument sensitivity, but in the present work onset of crystallization was bracketed by determining a time point where crystallization was not observed and a time point where crystallization was confirmed. These experiments used two orthogonal techniques, PXRD and PLM.

Figure 8 shows an example of the experimental data for Bifonazole (See Appendix 2 for the full data set). The physical stability data from the 24 model amorphous dispersions is compiled in Figure 9. Note that within Figure 9 model amorphous dispersions have been color coded. The amorphous dispersions which showed signs of crystallization within 20 minutes, have been color coded red, as it would not be possible to dose these amorphous dispersions without risk of crystallization. Three hours was selected as a reasonable time for preparation and dosing of numerous animals on a pharmacology or toxicology study. Activities to support a study would include formulation preparation, drawing the formulation into syringes, and administering the formulation to each sample subject. It is acknowledged that a faster or slower time may occur depending upon the study design and number of groups involved. The amorphous dispersions which did not show signs of crystallization within 3 hours were color coded green, as these amorphous dispersions would have a physical stability window which would be sufficient for dosing in a preclinical setting. Amorphous dispersions which had more than 20 minutes of physical stability, but less than 3 hours of physical stability, were color coded orange. Also, note that due to the delineation of the data into 3 groups, selection of 2 hours versus 4 hours would not change the categorization of molecules.

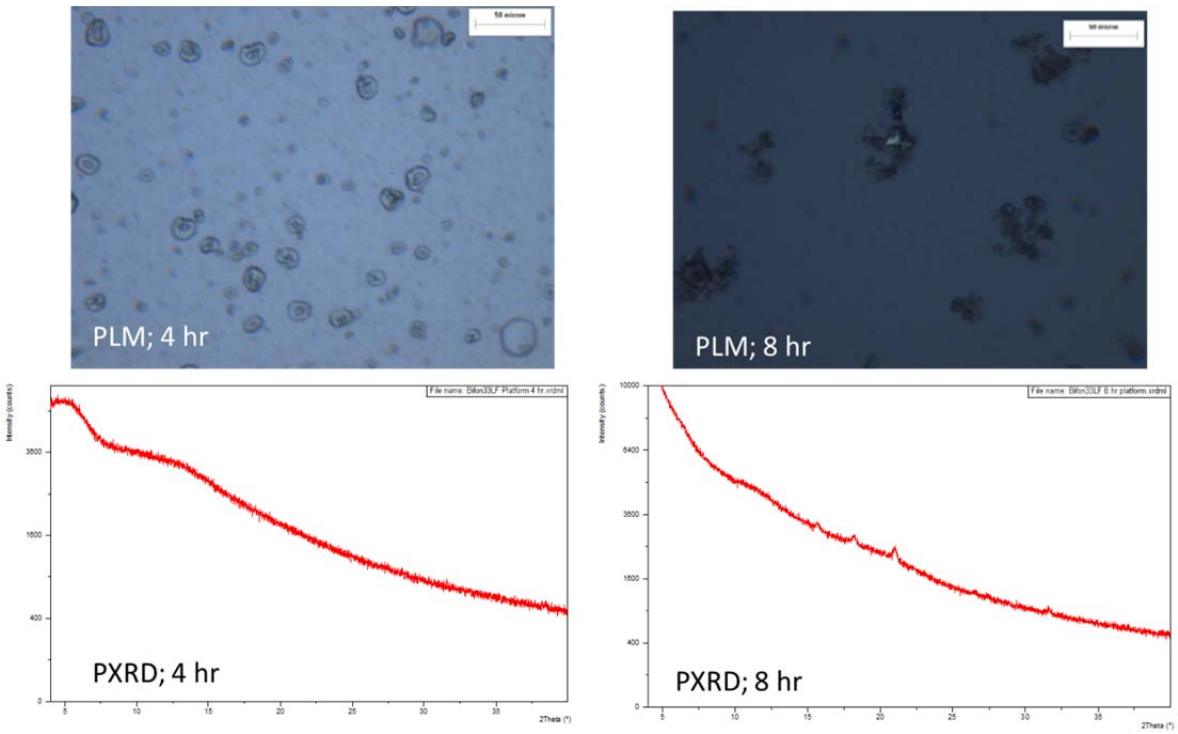

Figure 8. Comparison of Bifonazole prepared as 33.3% active spray dried amorphous solid dispersions in HPMCAS-LF and suspended in 0.5% methocellulose + 0.25% SLS + 5 mM HCl at 4 and 8 hour time points by PXRD and PLM.

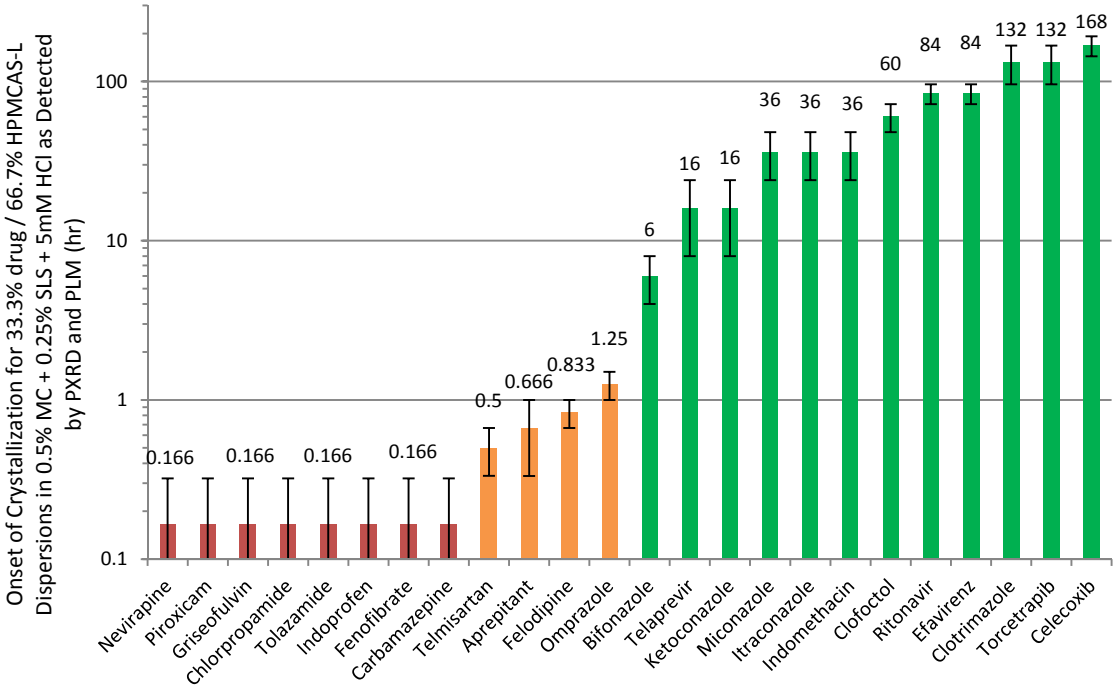

Figure 9. Onset of crystallization (in hours) summary of 24 model compounds prepared as 33.3% active spray dried amorphous solid dispersions in HPMCAS-LF and suspended in 0.5% methocellulose + 0.25% SLS + 5 mM HCl. Note the red color coding denoting a crystallization time of less than 20 minutes, the orange color coding for crystallization time between 20 minutes and 3 hours and the green color coding denoting a crystallization time of greater than 3 hours.

Chapter 3: Uni-variate Analysis of Molecular Descriptors:

Chapter 3 focuses on comparing the previously generated amorphous suspension crystallization data with the tabulated descriptors (See Tables 1, 2 and3) of each of the 24 model compounds. Initially comparisons are made between the physical stability data and structural descriptors for each compound. This is followed by a comparison of the physical stability data with thermal descriptors for each model compound. Lastly, the physical stability data is compared to hydrophilicity parameters. From these comparisons it is clear that one descriptor alone is not sufficiently predictive of the tendency of these compounds to crystallize as amorphous suspensions, and additional multi-variate analysis will be required in Chapter 4.

Structural Descriptors:

The molecular weight, number of rotatable bonds, and number of hydrogen bond donating and accepting groups for each molecule were determined from the structure of each model molecule. Table 1 contains the structural descriptors of the 24 model compounds.

Table 1. Structural descriptors of the 24 model compounds.

Model Compound	Molecular Weight	Number of Rotatable Bonds	Number of H-Donors	Number of H-Acceptors
Nevirapine	267	1	1	3
Griseofulvin	353	3	0	6
Indoprofen	281	3	1	4
Chlorpropamide	277	3	2	3
Tolazamide	311	3	2	4
Piroxicam	331	5	2	6
Bifonazole	310	4	0	1
Clofoctol	365	5	1	1
Celecoxib	381	3	1	1
Itraconazole	706	11	0	7
Miconazole	416	6	0	2
Ketoconazole	531	7	0	5
Clotrimazole	345	4	0	1
Indomethacin	358	4	1	4
Telaprevir	680	14	4	8
Efavirenz	316	3	1	2
Ritonavir	721	18	4	6
Aprepitant	534	8	2	5
Felodipine	384	6	1	3
Torcetrapib	600	10	0	6
Telmisartan	515	7	1	4
Carbamazepine	236	0	1	1
Fenofibrate	361	7	0	3
Omeprazole	345	5	1	5

Thermal Descriptors:

The melting temperature, enthalpy of fusion and entropy of fusion of each compound was determined via either a literature search (See Appendix 3 for reference data) or via DSC analysis (Approximately 3-5 mg of sample was loaded into a hermetically sealed pan with a pin hole in the top. The sample was analyzed with a TA Instruments Q2000 DSC and was heated from room temperature to 300 °C with a ramp rate of 10 °C/min). The Gibbs free energy of each compound was determined using the Hoffman equation (equation 3).

The glass transition temperature of each drug substance and spray dried dispersion was determined via either a literature search (See Appendix 3 for reference data) or via DSC analysis (Approximately 3-5 mg of sample was filled into a hermetically sealed pan with a pin hole in the top. The sample was analyzed with a TA Instruments Q2000 DSC and was heated from 35 to 170 °C with a modulation amplitude of 0.5 °C, a modulation interval of 60 sec, and a ramp rate of 2 °C/min).

The crystallization classification for cyclic DSC experiments was determined by either a literature search (See Appendix 3 for reference data), or by cyclic DSC (Approximately 3-5 mg of sample was weighed into a hermetically sealed pan with a pin hole in the top. The sample was analyzed with a TA Instruments Q2000 DSC and was heated from room temperature to 5 °C above the melting temperature with a ramp rate of 10 °C/min. The sample was then held isothermal for 2 minutes. The sample was then cooled to 25 °C at 10 °C/min. The sample was then heated to the melting temperature at 10 °C/min). A drawback with this method is the possibility of chemical degradation during the analysis. Due to the sample size, 24 model compounds, detailed chemical stability analysis was not conducted.

Table 2 contains the thermal descriptors of the 24 model compounds.

Table 2. Thermal descriptors of the 24 model compounds.

Model Compound	Melting Temp. (deg C)	Enthalpy Fusion (kJ/mol)	Entropy Fusion (kJ/K*mol)	Hoffman Delta G (kJ/mol)	Tg, Drug (deg C)	Tm/Tg, Drug	Tg,dry Dispersion (deg C)	Cyclic DSC Class
Nevirapine	246	39.5	0.076	10.6	76	1.49	80	1
Griseofulvin	218	39.1	0.079	10.4	89	1.36	88	1
Indoprofen	212	36.0	0.074	9.54	50	1.5	70	1
Chlorpropamide	124	27.4	0.069	6.34	16	1.37	90	1
Tolazamide	172	43.4	0.098	11.1	18	1.53	73	2
Piroxicam	240	34.5	0.067	9.25	62	1.53	80	3
Bifonazole	151	39.2	0.092	9.69	17	1.46	88	2
Clofoctol	88	35.1	0.097	6.98	-4	1.34	89	2
Celecoxib	163	37.4	0.086	9.44	58	1.32	72	2
Itraconazole	168	57.6	0.129	14.6	58	1.33	89	3
Miconazole	160	32.7	0.091	6.43	1	1.58	81	3
Ketoconazole	150	52.9	0.125	13.1	45	1.33	95	3
Clotrimazole	145	31.8	0.076	7.7	30	1.38	86	3
Indomethacin	161	37.6	0.086	9.46	45	1.36	73	3
Telaprevir	239	56.5	0.110	15.1	71	1.49	106	3
Efavirenz	137	15.6	0.038	3.74	38	1.32	82	3
Ritonavir	121	60.4	0.153	13.86	50	1.22	81	3
Aprepitant	254	49.2	0.093	13.20	89	1.46	99	2
Felodipine	145	31.0	0.074	7.57	45	1.31	77	3
Torcetrapib	90	30.8	0.085	6.20	22.4	1.23	100	3
Telmisartan	269	52.9	0.098	14.3	128	1.35	109	3
Carbamazepine	190	25.5	0.055	6.65	61	1.39	69	1
Fenofibrate	80	33.0	0.093	6.24	-19	1.39	79	3
Omeprazole	159	26.6	0.062	6.67	45	1.36	71	3

Hydrophilicity Descriptors:

Here the term hydrophilicity descriptor is defined as descriptors which involve the interaction of a model compound with water. Descriptors include aqueous solubility, Log P and pKa were determined via a literature search (See Appendix 3 for reference data).

The solubility in the platform vehicle (0.5% methocellulose + 0.25% SLS + 5 mM HCl) was determined by stirring excess crystalline drug with the vehicle for 48 hours at 25 °C. Given the number of samples required for testing, 48 hours was approximated to represent the equilibrium solubility (although attainment of equilibrium was not verified in the studies).

Samples were then filtered through 0.22 μm PTFE filters. The filtrate was then analyzed by HPLC using the same method described in Chapter 2.

The General Solubility Equation for each compound was determined by using equation 6, where $S_{Crystalline}$ is the crystalline solubility and *Tm* is the melting temperature[59].

$$Log\left(S_{Crystalline}\right) = 0.5 - 0.01 \times \left(Tm - 25\right) - LogP \qquad (6)$$

Moisture sorption isotherms were taken of each model spray dried amorphous dispersion. Approximately 5 mg of the amorphous dispersion was loaded onto a TA Instruments Q5000 TGA. Samples were dried at 60 °C for 1 hour followed by a ramp up, and ramp down, in humidity (10 to 90 to 10% RH). Each sample was held at a given relative humidity until there was less than 0.01% weight change over 5 minutes.

The $T_{g,dispersion,100\%RH}$ was calculated using the equation (7). This equation was derived from work done by Marsac[60] and Andronis[61]. The $T_{g,dispersion,100\%RH}$ was calculated, rather than measured, due to the inherent difficulty of measuring this value without a sample undergoing crystallization or phase transformation.

$$T_{g,dispersion,100\%RH} = T_{g,dispersion,dry} - 10\ °C \times \text{extrapolated \% wt. gain @ 100\% RH} \qquad (7)$$

Table 3 contains the hydrophilicity descriptors of the 24 model compounds.

Table 3. Hydrophilicity properties of the 24 model compounds.

Model Compound	Log P	pKa	Water Solubility (mg/mL)	General Solubility Equation (mg/mL)	Vehicle Solubility (mg/mL)	% Wt. Gain at 90% RH	$T_{g,dispersion,100\%RH}$
Nevirapine	2.5	2.8	0.0007	0.016	0.443	6.2	1
Griseofulvin	0.7	x	0.0086	2.61	0.859	5.5	15.5
Indoprofen	2.8	5.1	-	0.019	0.031	6.7	8
Chlorpropamide	1.8	4.3	0.157	1.42	0.215	5.6	20
Tolazamide	1.4	3.6	0.308	1.33	0.153	5.7	5
Piroxicam	0.6	1.8, 5.1	0.143	1.86	0.250	4.3	20
Bifonazole	4.7	6.7	0.0025	0.0012	0.453	2.6	52
Clofoctol	8.2	x	0.0022	0.000001	0.02	6.2	48
Celecoxib	4.3	11.1	0.0033	0.0025	0.093	4.2	17
Itraconazole	7.3	3.7	0.0009	0.000004	0.011	4.5	33
Miconazole	5.1	6.7	0.0007	0.0026	0.721	3.1	42
Ketoconazole	3.5	2.9	0.0001	0.029	1.84	5.0	25
Clotrimazole	5.2	6.6	0.0147	0.0004	0.997	2.9	50
Indomethacin	3.6	4.5	0.0009	0.012	0.044	5.0	11
Telaprevir	4.0	11.9	0.0047	0.001326	-	6.4	26
Efavirenz	4.6	12.5	0.0082	0.001777	-	4.4	31
Ritonavir	5.6	2.8	0.0013	0.000628	-	6.1	9
Aprepitant	4.5	9.7	0.019	0.000274	-	6.3	27
Felodipine	3.9	5.4	0.0009	0.009646	-	4.8	17
Torcetrapib	7.8	-	-	1.47E-05	-	5.3	30
Telmisartan	6	3.5, 4.1, 6.0	0.004	6.95E-06	-	4.7	57
Carbamazepine	2.7	x	0.17	0.033336	-	4.8	5
Fenofibrate	4.8	x	0.25	0.005099	-	4.4	24
Omeprazole	2.4	4.0	0.357	0.212725	-	6.0	10

Uni-variate analysis of the descriptors data set for the 24 model compounds:

Initially uni-variate analysis of the data set was conducted to compare how the amorphous suspension crystallization data correlated with the possible descriptors. Description of this analysis is broken up between the structural, thermal and hydrophilicity parameters.

a.) Structural Descriptors:

Uni-variate analysis was attempted for the various structural descriptors including molecular weight, number of rotatable bonds and number of hydrogen bond donating and accepting groups. The plots of these data are shown in Figures 11, 12, 13 and 14. In addition, Figures 15, 16 and 17 show the normalized (by molecular weight) data for number of rotatable bonds, hydrogen bond donor and acceptor groups.

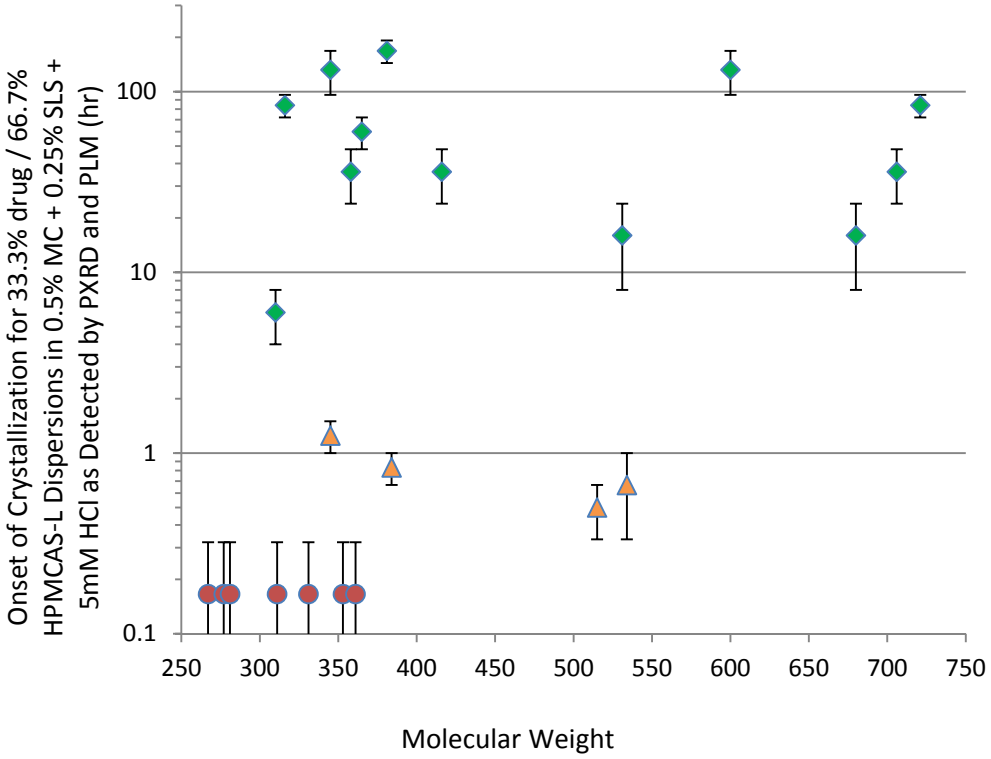

Figure 11. Molecular weight versus onset of crystallization time for 33.3% drug/66.7% HPMCAS-LF spray dried amorphous dispersions in 0.5% MC + 0.25% SLS + 5 mM HCl. Note the red circle color coding denoting a crystallization time of less than 20 minutes, the orange triangle color coding for crystallization time between 20 minutes and 3 hours, and the green diamond color coding denoting a crystallization time of greater than 3 hours.

When looking at molecular weight for the 24 model compounds, compounds with higher molecular weight values show less of a propensity to crystallize than those with lower molecular weight values. For compounds with a molecular weight >400, 6 of the 8 compound crystallize after 3 hours, 2 of the 8 compounds crystallize between 20 minutes and 3 hours, and none of the

8 compounds crystallize before 20 minutes. This parameter may be explained by the complexity of crystal nucleation or the slow diffusivity into the vehicle. For instance compounds with elevated molecular weight may have delayed crystallization kinetics in our model system, as predicted by classical nucleation theory[29,30] in Chapter 1, as it may take longer for the molecules to orient into a repeating pattern in a crystal lattice.

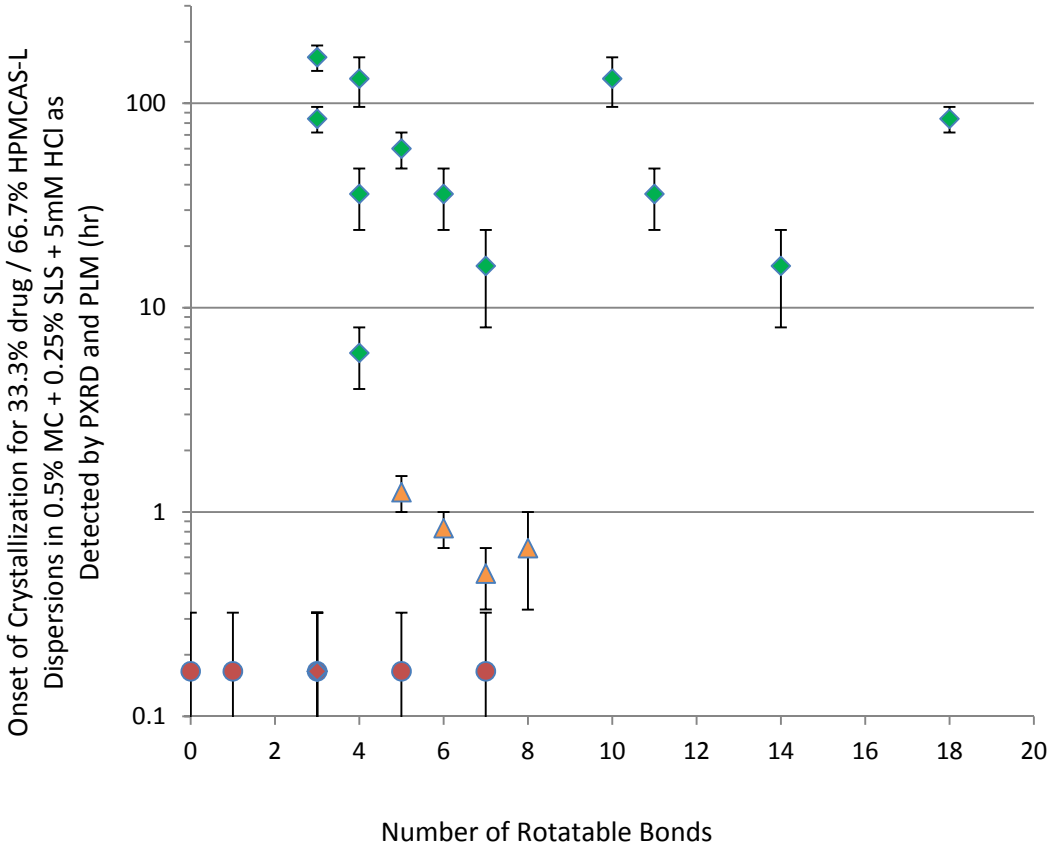

Figure 12. Number of rotatable bonds versus onset of crystallization time for 33.3% drug/66.7% HPMCAS-LF spray dried amorphous dispersions in 0.5% MC + 0.25% SLS + 5 mM HCl. Note the red circle color coding denoting a crystallization time of less than 20 minutes, the orange triangle color coding for crystallization time between 20 minutes and 3 hours, and the green diamond color coding denoting a crystallization time of greater than 3 hours.

When looking at number of rotatable bonds, for the 24 model compounds, there is considerable variability in the data. However, a trend does appear in which compounds with

values above 8 show less of a propensity to crystallize within 3 hours than those with values below 8. Like molecular weight, this parameter may elude to the complexity of crystal nucleation as outlined in Chapter 1 and predicted by classical nucleation theory. For instance compounds with an elevated number of rotatable bonds, have increased number of geometrical arrangements possible for the molecule. This increased geometrical freedom to rotate may delay crystallization kinetics in our model suspension system, as it may take longer for the molecules to line up in the correct orientation for crystallization[29,30].

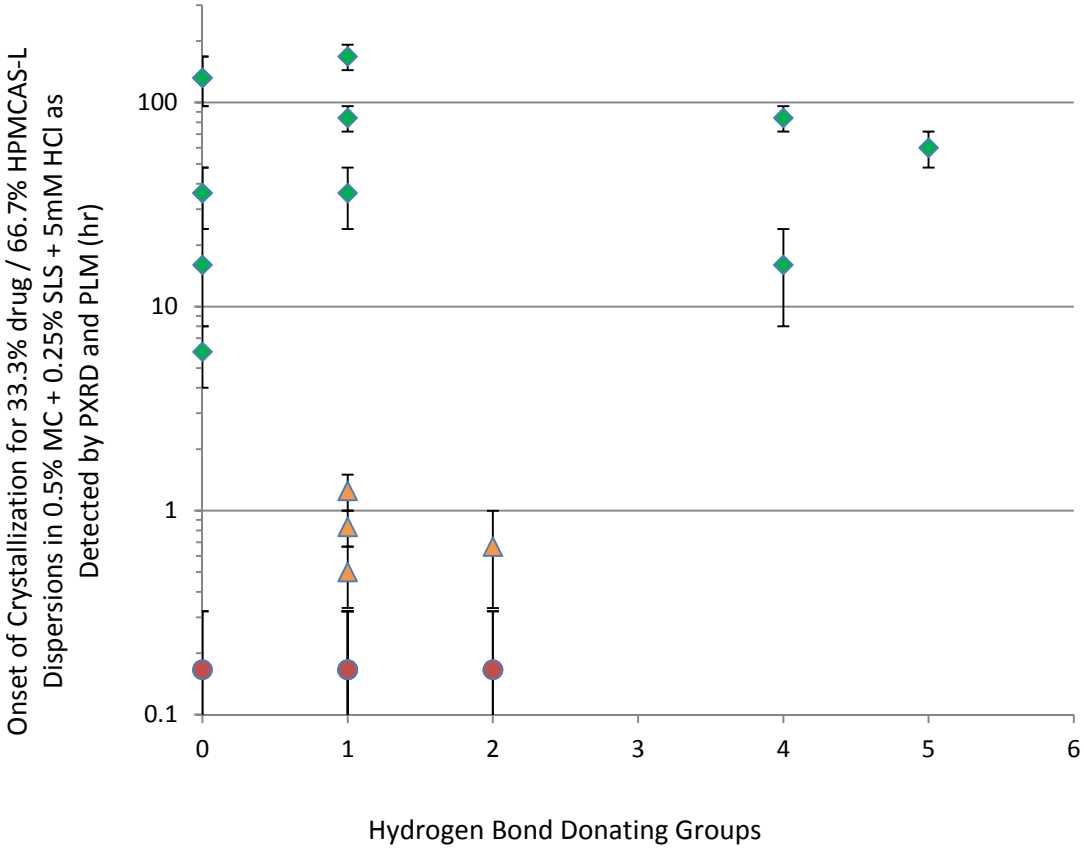

Figure 13. Number of hydrogen bond donating groups versus onset of crystallization time for 33.3% drug/66.7% HPMCAS-LF spray dried amorphous dispersions in 0.5% MC + 0.25% SLS + 5 mM HCl. Note the red circle color coding denoting a crystallization time of less than 20 minutes, the orange triangle color coding for crystallization time between 20 minutes and 3 hours, and the green diamond color coding denoting a crystallization time of greater than 3 hours.

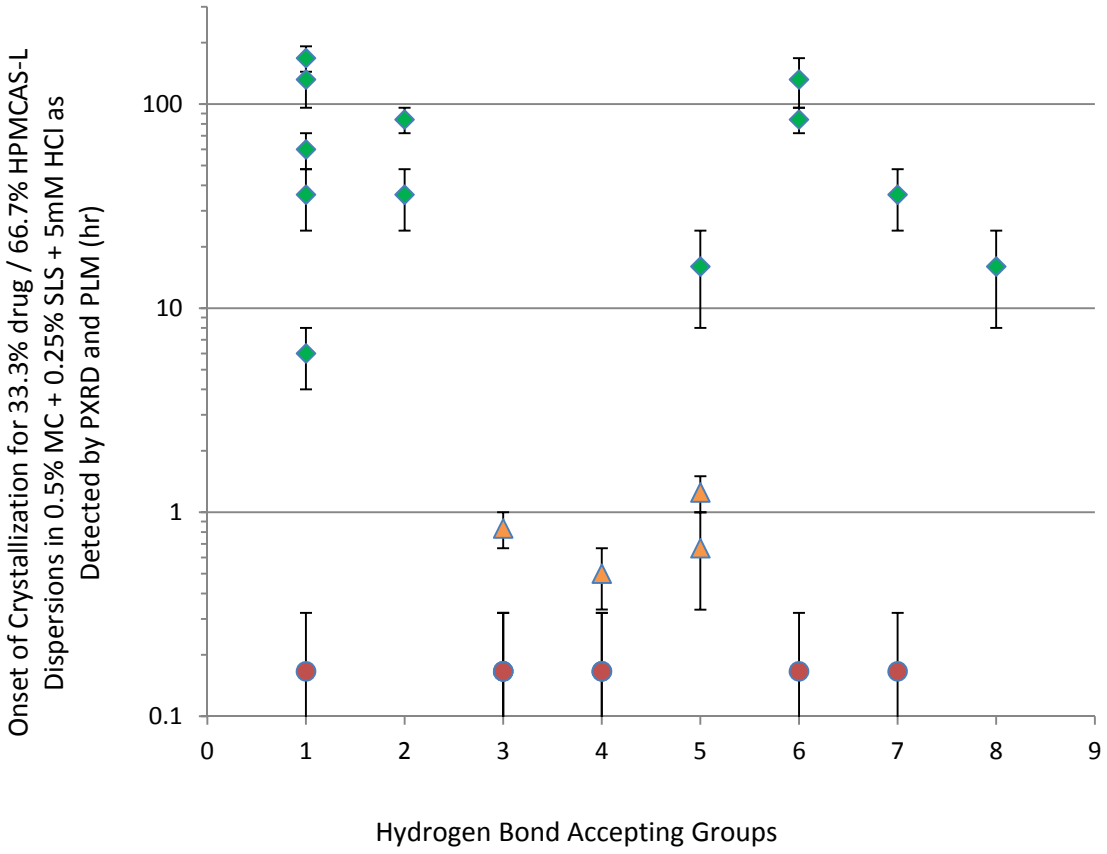

Figure 14. Number of hydrogen bond accepting groups versus onset of crystallization time for 33.3% drug/66.7% HPMCAS-LF spray dried amorphous dispersions in 0.5% MC + 0.25% SLS + 5 mM HCl. Note the red circle color coding denoting a crystallization time of less than 20 minutes, the orange triangle color coding for crystallization time between 20 minutes and 3 hours, and the green diamond color coding denoting a crystallization time of greater than 3 hours.

Figure 13 and 14 attempt to show how the number of hydrogen bond accepting groups (Figure 13) and donating groups (Figure 14) correlate with the rate at which the model suspension system crystallizes. The data shown in the figures suggests that the number of hydrogen bond accepting groups and the number of hydrogen bond donating groups plays minimal role in the crystallization kinetics of the model suspension system. However, there may be a slight trend that compounds with >4 hydrogen bond donating groups are less likely to

crystallize within 3 hours in the model suspension system, unfortunately the limited sample size prevents a firm conclusion

The number of rotational bonds/molecular weight (Figure 15), hydrogen bond accepting groups/molecular weight (Figure 16) and the hydrogen bond donating groups/molecular weight (Figure 17) were also plotted to normalize for molecular weight.

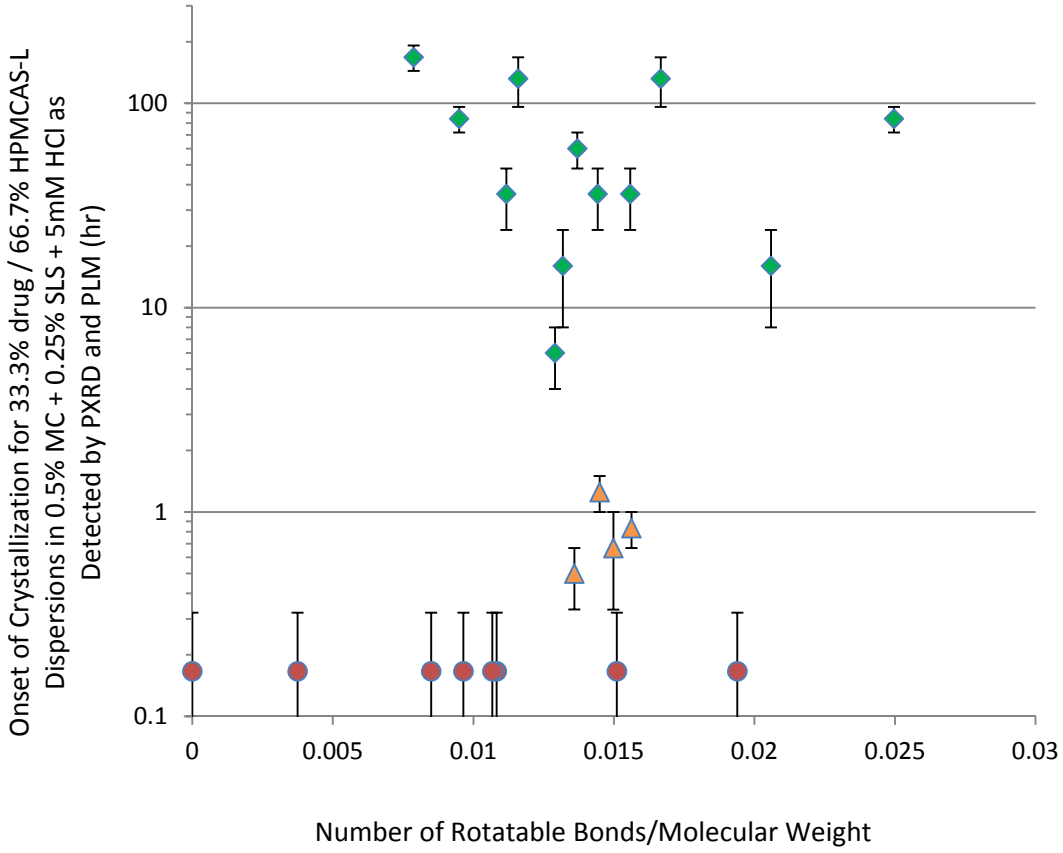

Figure 15. Number of rotatable bonds/molecular weight versus onset of crystallization time for 33.3% drug/66.7% HPMCAS-LF spray dried amorphous dispersions in 0.5% MC + 0.25% SLS + 5 mM HCl. Note the red circle color coding denoting a crystallization time of less than 20 minutes, the orange triangle color coding for crystallization time between 20 minutes and 3 hours, and the green diamond color coding denoting a crystallization time of greater than 3 hours.

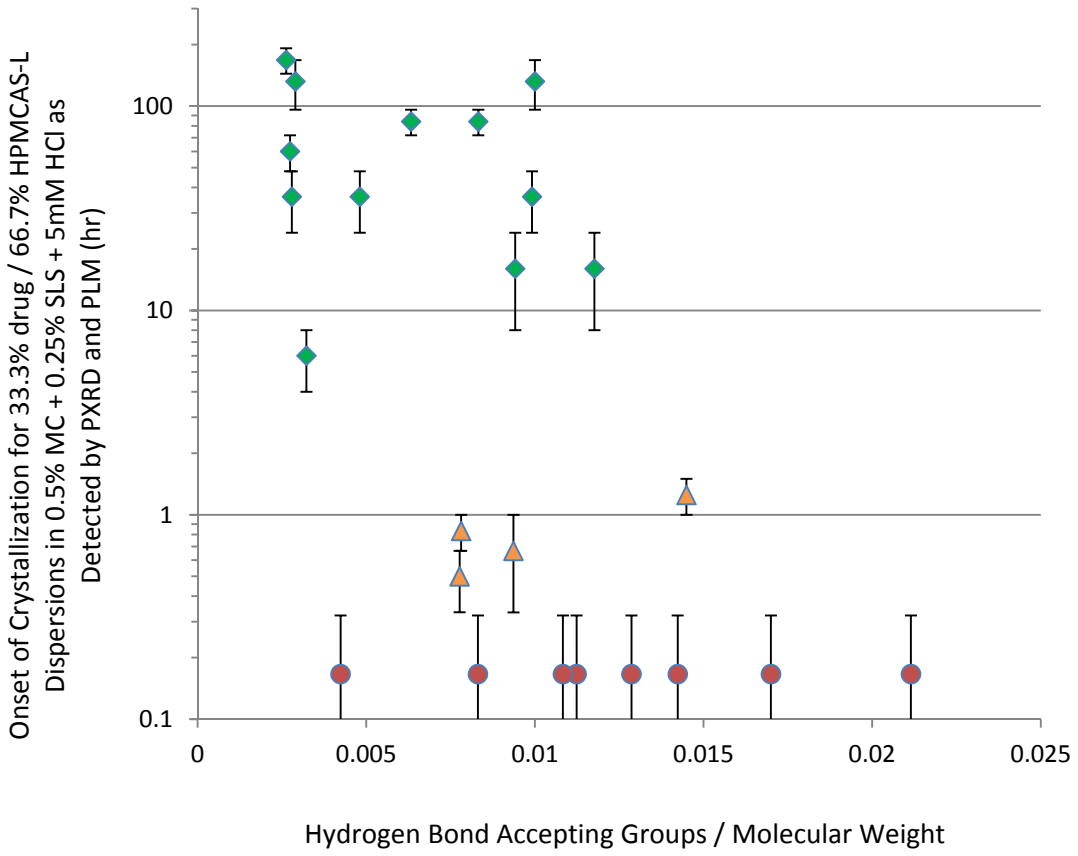

Figure 16. Number of hydrogen bond acceptors/molecular weight versus onset of crystallization time for 33.3% drug/66.7% HPMCAS-LF spray dried amorphous dispersions in 0.5% MC + 0.25% SLS + 5 mM HCl. Note the red circle color coding denoting a crystallization time of less than 20 minutes, the orange triangle color coding for crystallization time between 20 minutes and 3 hours, and the green diamond color coding denoting a crystallization time of greater than 3 hours.

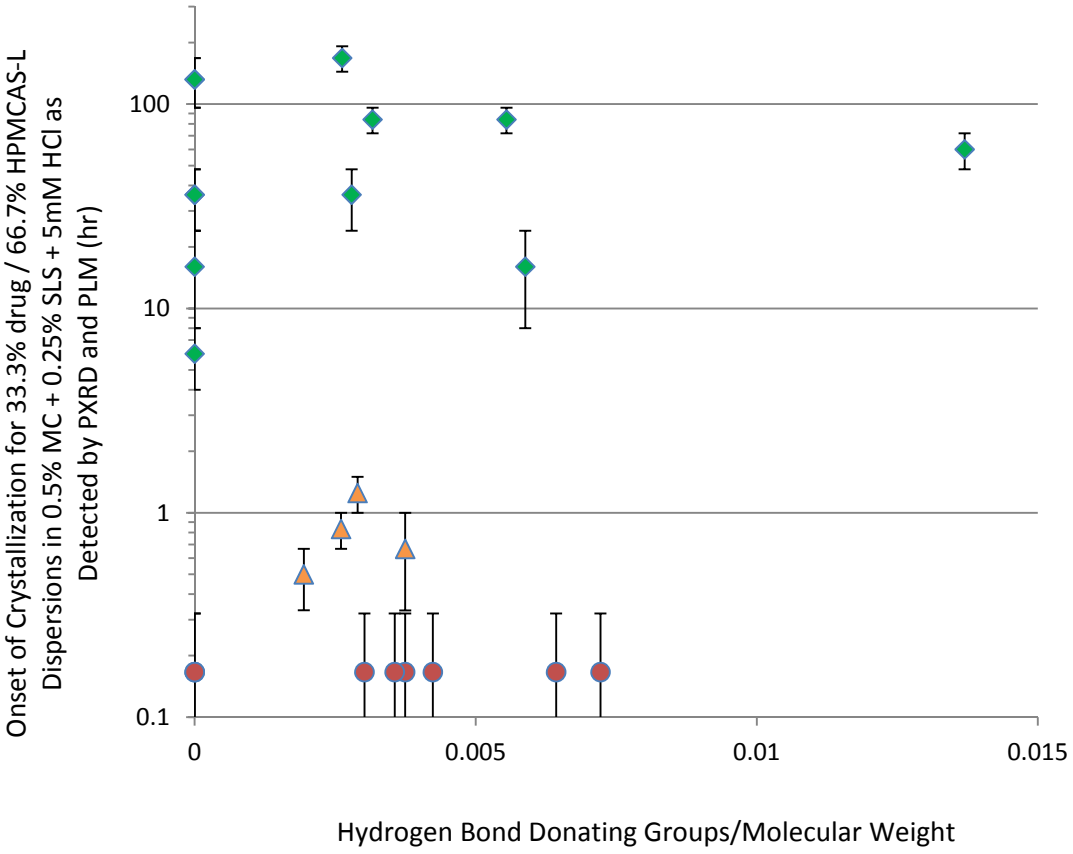

Figure 17. Number of hydrogen bond donors/molecular weight versus onset of crystallization time for 33.3% drug/66.7% HPMCAS-LF spray dried amorphous dispersions in 0.5% MC + 0.25% SLS + 5 mM HCl. Note the red circle color coding denoting a crystallization time of less than 20 minutes, the orange triangle color coding for crystallization time between 20 minutes and 3 hours, and the green diamond color coding denoting a crystallization time of greater than 3 hours.

Of the various structural descriptors, molecular weight is the most predictive parameter of physical stability. For compounds with a molecular weight >400, 6 of the 8 compound crystallize after 3 hours, 2 of the 8 compounds crystallize between 20 minutes and 3 hours, and none of the 8 compounds crystallize before 20.

b.) Thermal Descriptors:

Uni-variate analysis was attempted for the various thermal property descriptors including glass transition temperature of the model amorphous dispersion, glass transition temperature of the model drug substance, the melting temperature of the model drug substance, the entropy of fusion, enthalpy of fusion and Gibbs free energy of the model drug substance, as well as the crystallization tendency classification (as predicted by cyclic DSC) and the drug substance melting temperature/glass transition temperature ratio. The plots of these data are shown in the subsequent figures.

The glass transition temperature was first evaluated. For solid oral dosage formulations, it is relatively accepted in the literature that an elevated amorphous dispersion glass transition temperature should correlate with solid state stability[35,36,39,40]. However, for suspensions of amorphous dispersions, there is not a strong correlation between the glass transition temperature of a model compound and the solid state stability of the amorphous dispersion in suspension. However, Figure 18 does not include an adjustment for how humidity would depress the glass transition temperature.

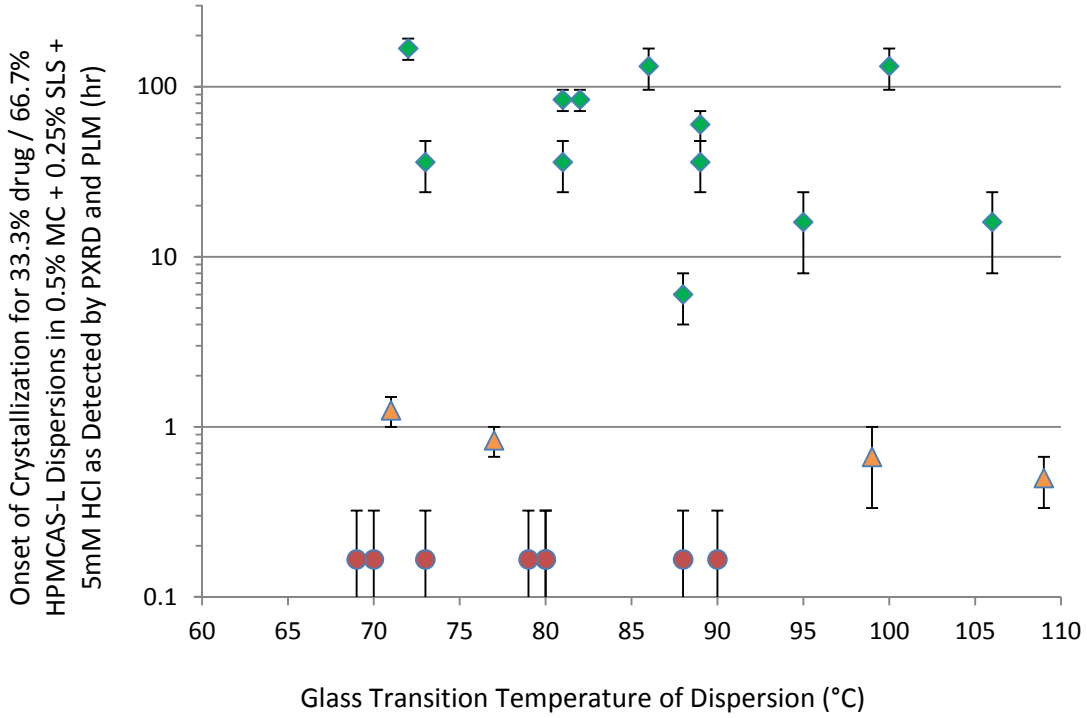

Figure 18. Amorphous dispersion glass transition temperature versus onset of crystallization time for 33.3% drug/66.7% HPMCAS-LF spray dried amorphous dispersions in 0.5% MC + 0.25% SLS + 5 mM HCl. Note the red circle color coding denoting a crystallization time of less than 20 minutes, the orange triangle color coding for crystallization time between 20 minutes and 3 hours, and the green diamond color coding denoting a crystallization time of greater than 3 hours.

A correlation between the glass transition temperature of the drug substance and the time for onset of crystallization in our model suspending system was also evaluated in Figure 19.

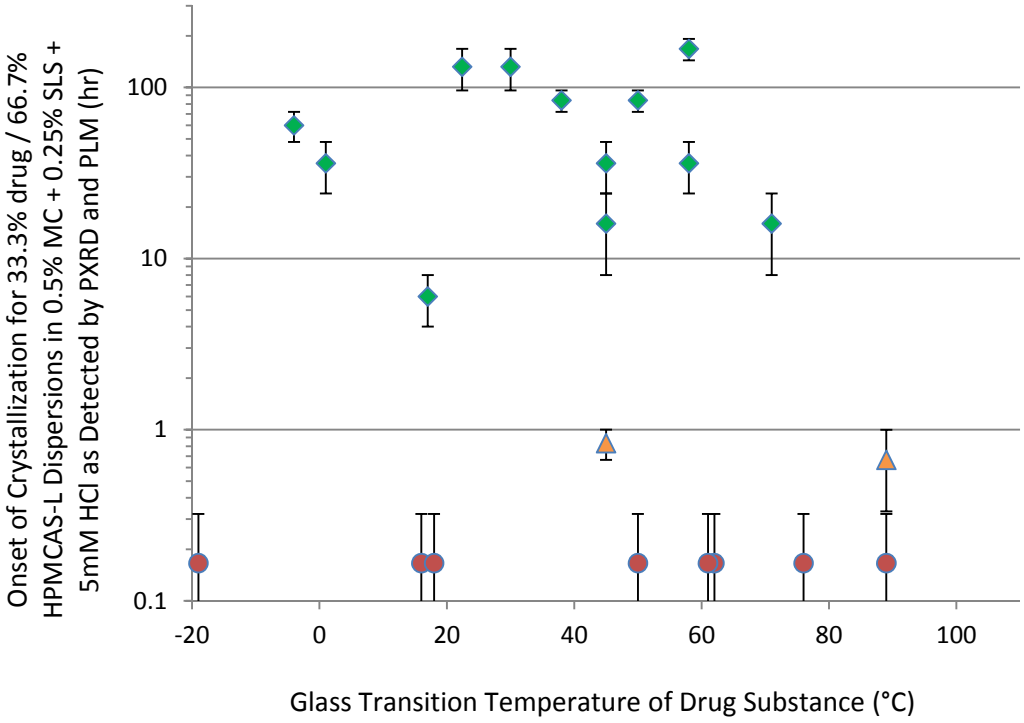

Figure 19. Drug substance glass transition temperature versus onset of crystallization time for 33.3% drug/66.7% HPMCAS-LF spray dried amorphous dispersions in 0.5% MC + 0.25% SLS + 5 mM HCl. Note the red circle color coding denoting a crystallization time of less than 20 minutes, the orange triangle color coding for crystallization time between 20 minutes and 3 hours, and the green diamond color coding denoting a crystallization time of greater than 3 hours.

Both the glass transition temperature of the amorphous dispersion and the glass transition temperature of the drug substance show lack of correlation with the onset of crystallization in our model suspension systems. This may be due to the measurements being taken under dry conditions. In the hydrophilicity section of this chapter a correction will be made for the amorphous dispersion glass transition temperature at 100% RH, and this value will show superior predictive capability and physical meaning.

The next thermal property to be evaluated was melting temperature as shown in Figure 20.

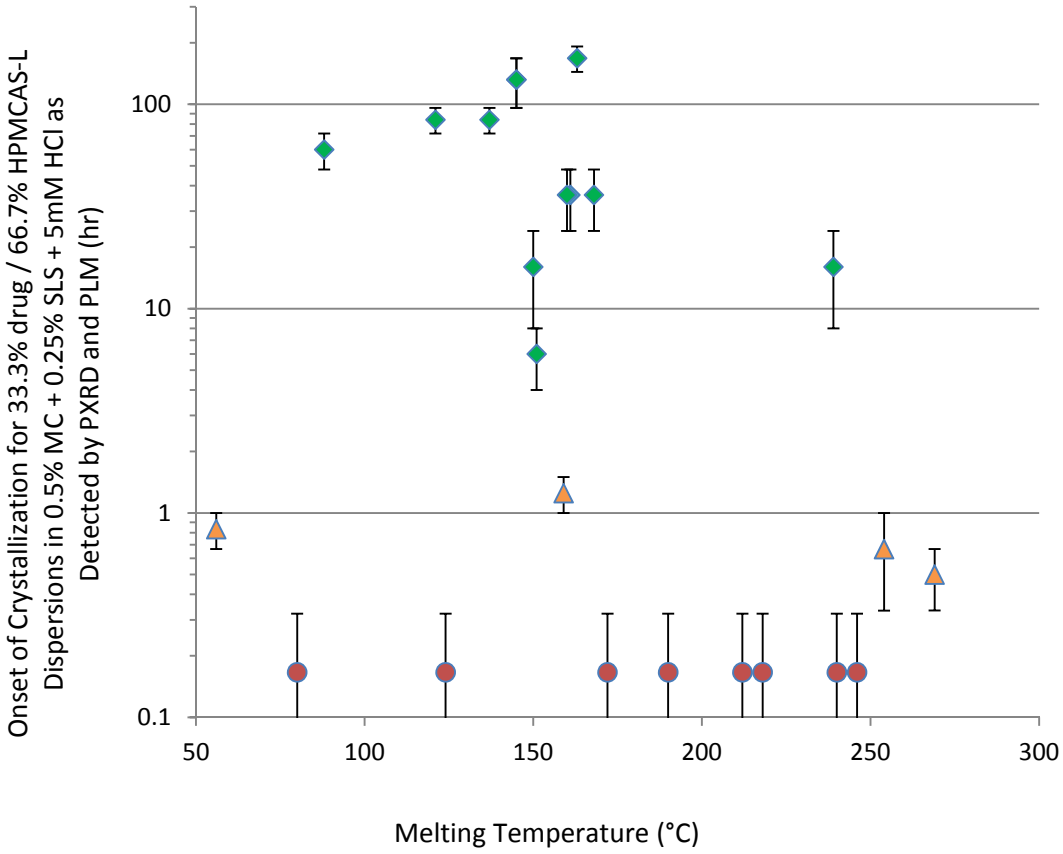

Figure 20. Melting temperature versus onset of crystallization time for 33.3% drug/66.7% HPMCAS-LF spray dried amorphous dispersions in 0.5% MC + 0.25% SLS + 5 mM HCl. Note the red circle color coding denoting a crystallization time of less than 20 minutes, the orange triangle color coding for crystallization time between 20 minutes and 3 hours, and the green diamond color coding denoting a crystallization time of greater than 3 hours.

For melting temperature, compounds with a melting temperature above 180 °C have a greater propensity to crystalize than those with melting temperatures below 180 °C (of these 8 compounds, 5 model compounds crystallize within 20 minutes, 2 compounds crystallize between 20 minutes and 3 hours, and 1 compound crystallizes after 3 hours). This parameter may serve as a surrogate to crystal lattice energy[11,48-51]. This data trend suggests that compounds with a high melting temperature have an elevated potential to crystallize in our model amorphous suspension system. This is consistent with numerous literature references which describe the

difficulty in solubilizing high melting temperature compounds and the potential for these compounds to crystallize[11,48-51]. This is also consistent with classical nucleation theory[29,30].

After determining the utility of melting temperature as a predictive parameter in predicting the rate of onset of crystallization in the model suspension system, enthalpy of fusion (Figure 21), entropy of fusion (Figure 22) and the Gibbs Free Energy via the Hoffman Equation (Figure 23) were evaluated.

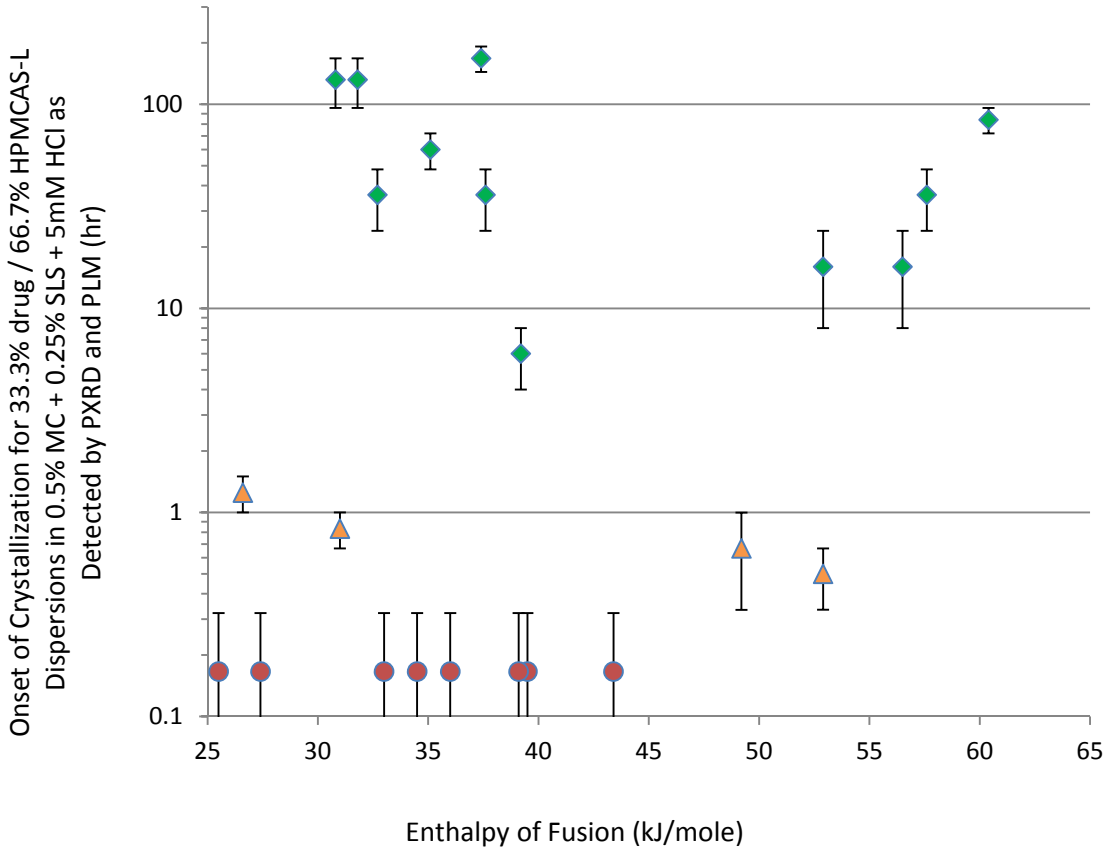

Figure 21. Enthalpy of fusion versus onset of crystallization time for 33.3% drug/66.7% HPMCAS-LF spray dried amorphous dispersions in 0.5% MC + 0.25% SLS + 5 mM HCl. Note the red circle color coding denoting a crystallization time of less than 20 minutes, the orange triangle color coding for crystallization time between 20 minutes and 3 hours, and the green diamond color coding denoting a crystallization time of greater than 3 hours.

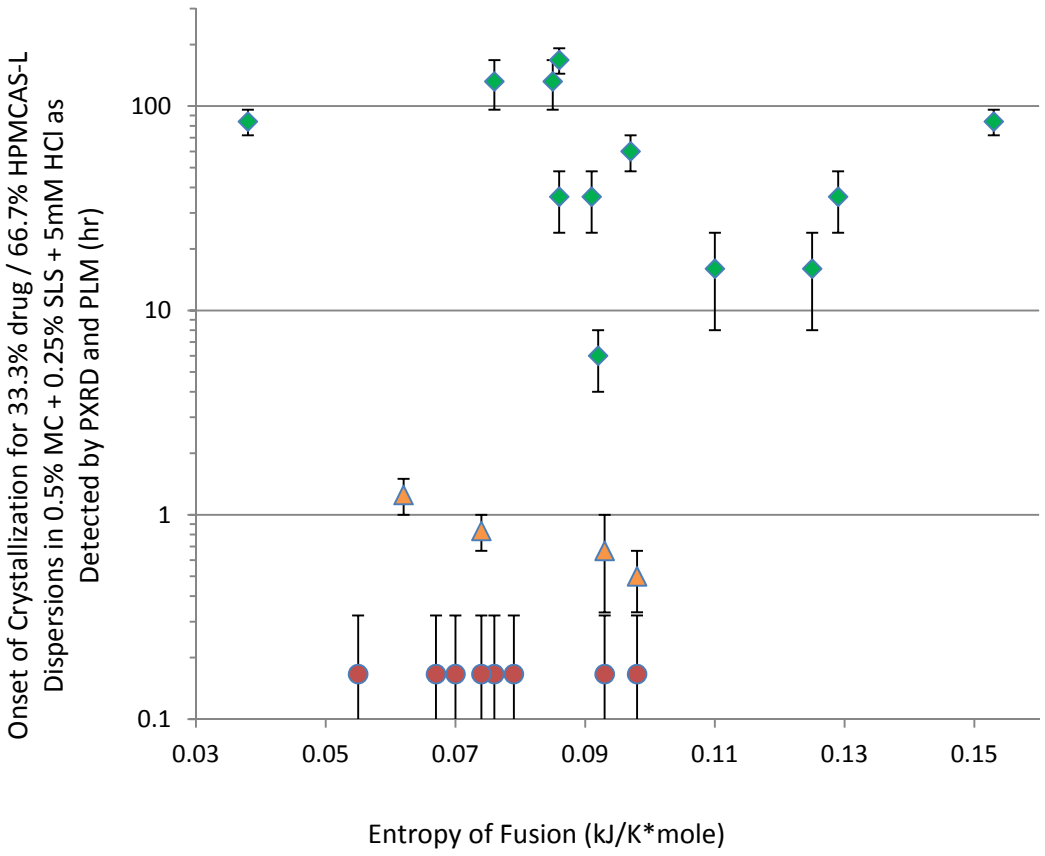

Figure 22. Entropy of fusion versus onset of crystallization time for 33.3% drug/66.7% HPMCAS-LF spray dried amorphous dispersions in 0.5% MC + 0.25% SLS + 5 mM HCl. Note the red circle color coding denoting a crystallization time of less than 20 minutes, the orange triangle color coding for crystallization time between 20 minutes and 3 hours, and the green diamond color coding denoting a crystallization time of greater than 3 hours.

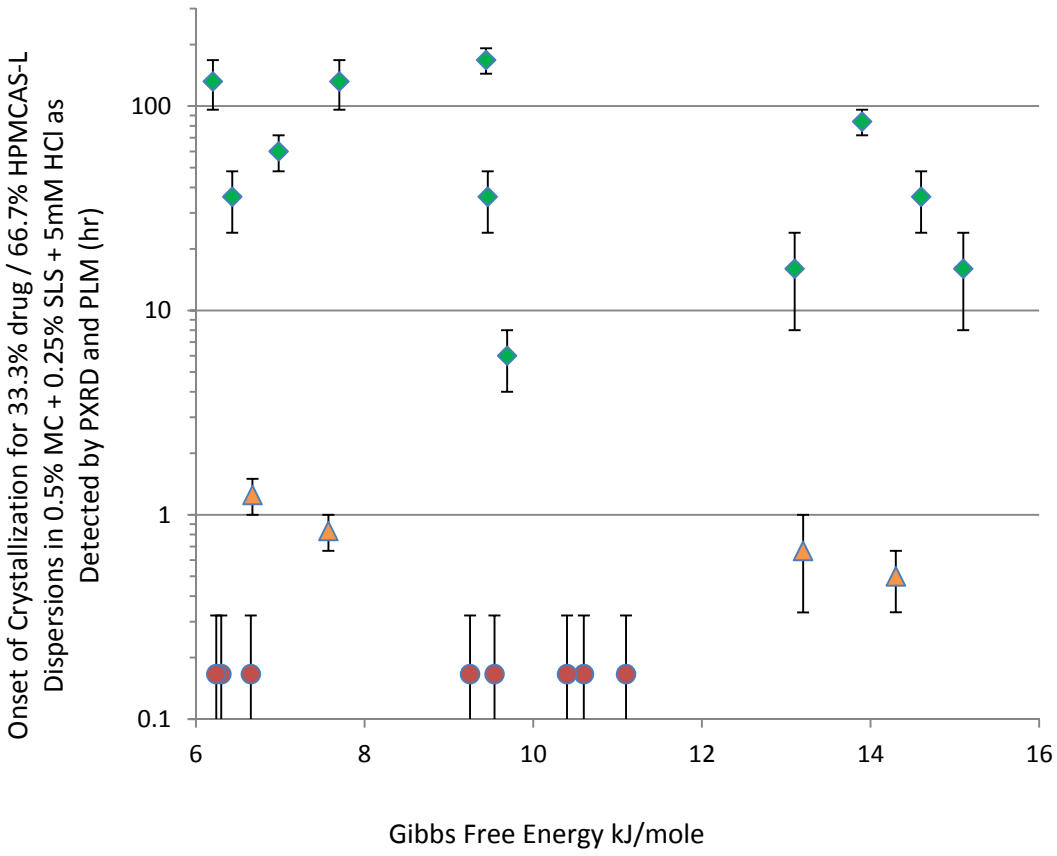

Figure 23. Gibbs Free Energy (Hoffman Equation) versus onset of crystallization time for 33.3% drug/66.7% HPMCAS-LF spray dried amorphous dispersions in 0.5% MC + 0.25% SLS + 5 mM HCl. Note the red circle color coding denoting a crystallization time of less than 20 minutes, the orange triangle color coding for crystallization time between 20 minutes and 3 hours, and the green diamond color coding denoting a crystallization time of greater than 3 hours.

Enthalpy of fusion, and Gibbs free energy (Hoffman Equation) versus onset of crystallization time figures, fail to provide additional predictive value relative to melting temperature. However, it is interesting to note that compounds with entropy of fusion values of greater than 0.1 kJ/K*mole all have delayed crystallization kinetics relative to model compounds with less crystal lattice entropy. This suggests that a crystal lattice with a high degree of entropy (propensity for disorder) would be beneficial in delaying the onset of crystallization for these model suspension systems. This logical finding is consistent with numerous literature references on classical nucleation theory[29,30].

Having established the value of melting temperature as a thermal predictive parameter for rank ordering the propensity of model compounds to crystallize in the model suspension system, it was important to evaluate whether the ratio of melting temperature to glass transition temperature (Tm/Tg) would help improve or refine the model. It has been suggested in the literature[55] that this ratio could be predictive of physical stability of amorphous systems. Figure 24 shows these data, however there is not additional predictive value relative to use of melting temperature alone. One potential explanation for this lack of correlation could stem from the difference between the glass transition temperature of a suspended amorphous dispersion (a three component system of drug substance, polymer and water) versus the glass transition temperature of the drug substance alone.

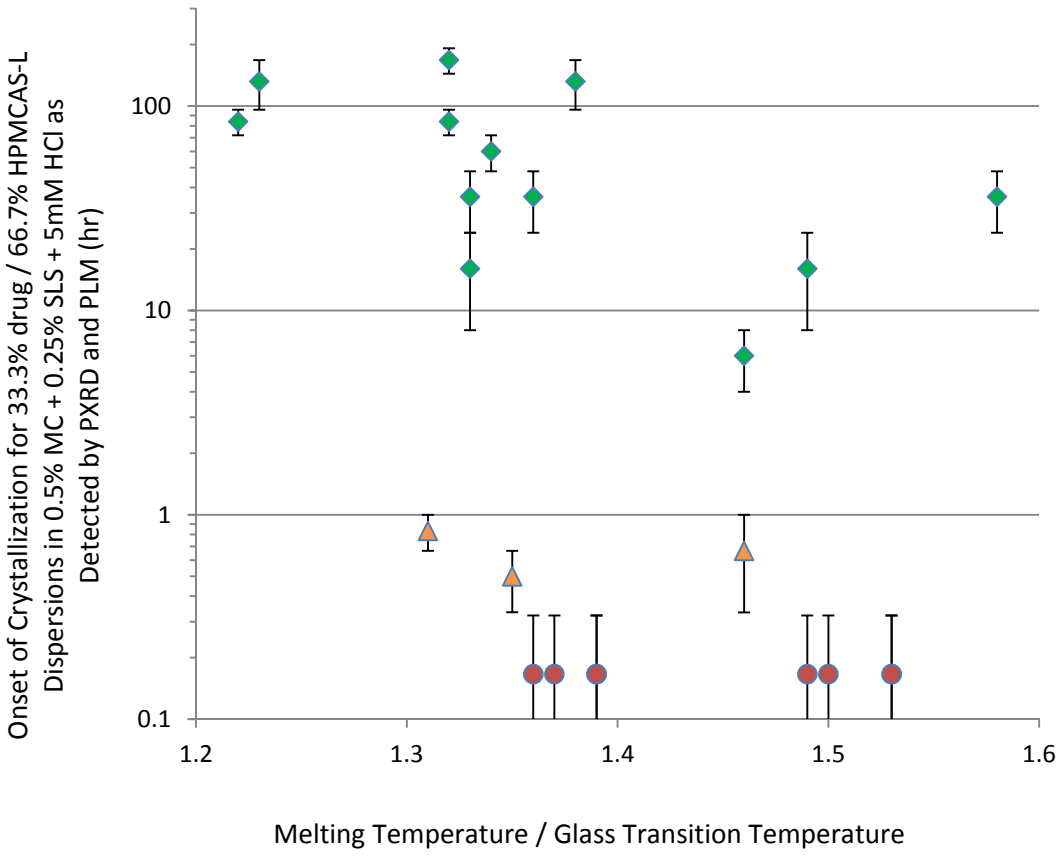

Figure 24. Ratio of melting temperature to glass transition temperature (Tm/Tg) versus onset of crystallization time for 33.3% drug/66.7% HPMCAS-LF spray dried amorphous dispersions in 0.5% MC + 0.25% SLS + 5 mM HCl. Note the red circle color coding denoting a crystallization time of less than 20 minutes, the orange triangle color coding for crystallization time between 20 minutes and 3 hours, and the green diamond color coding denoting a crystallization time of greater than 3 hours.

In addition to the thermal models shown previously in this thesis, cyclic DSC, as originally described by Baird and Taylor has become widely used for rank ordering the crystallization tendency of pharmaceutical compounds[62]. Figure 25 describes the cyclic DSC process. First, the sample is heated in the DSC to beyond the melting temperature of the compound and held isothermal for several minutes to allow the model compound to fully melt. The compound is then cooled at a controlled rate to room temperature. If the compound undergoes crystallization during the cooling process, the compound would be classified as a

strong crystallizer/class I compound. After cooling to room temperature the compound is the reheated at a controlled rate to above the melting temperature of the compound. If the compound crystallizes during this reheating phase of the cycle, the compound is classified as a moderate crystallizer/class II compound. If the compound fails to crystallize during this process, the compound is classified as a weak crystallizer/class III compound. This process is outlined in Figure 25.

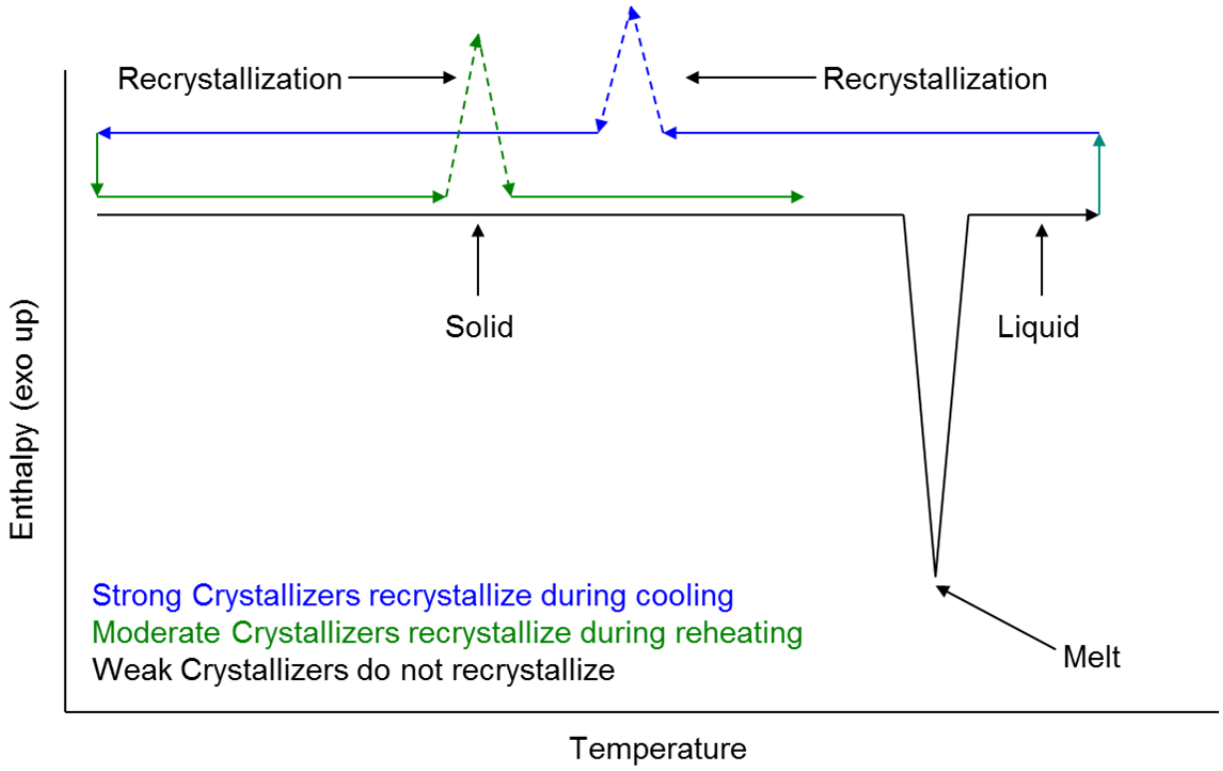

Figure 25. A cyclic DSC diagram describing how compounds are classified into strong, moderate and weak crystallizing compounds.

Each of the 24 model compounds was classified as a class I, II or III compound via cyclic DSC experiments. For the strong crystallizers, this model shows all compounds crystallize within 3 hours in the model suspension conditions. However, the model fails to predict the number of class II and class III compounds that crystallize in the model suspension system. This inability of the model to predict which class II and class III compounds crystallize could be explained in three different ways, likely stemming from the dry (lack of moisture) nature of this

model. This predictive deficiency could be due to the inability of the model to account for the potential of the drug to leach out of the amorphous dispersion particle and into the bulk suspending media. Once dissolved in the bulk suspending media, the compound has considerably more molecular mobility than is present in the DSC pan. In addition, this could be due to the inability of the model to account for interactions with moisture such as anti-solvent effects or potential to form hydrates. Lastly, several compounds may undergo thermal degradation due to the stress of the heat/cool/heat cycle. This could lead to sample impurities, which could either serve as crystallization inhibitors, or could undergo their own thermal events which could be misinterpreted[62].

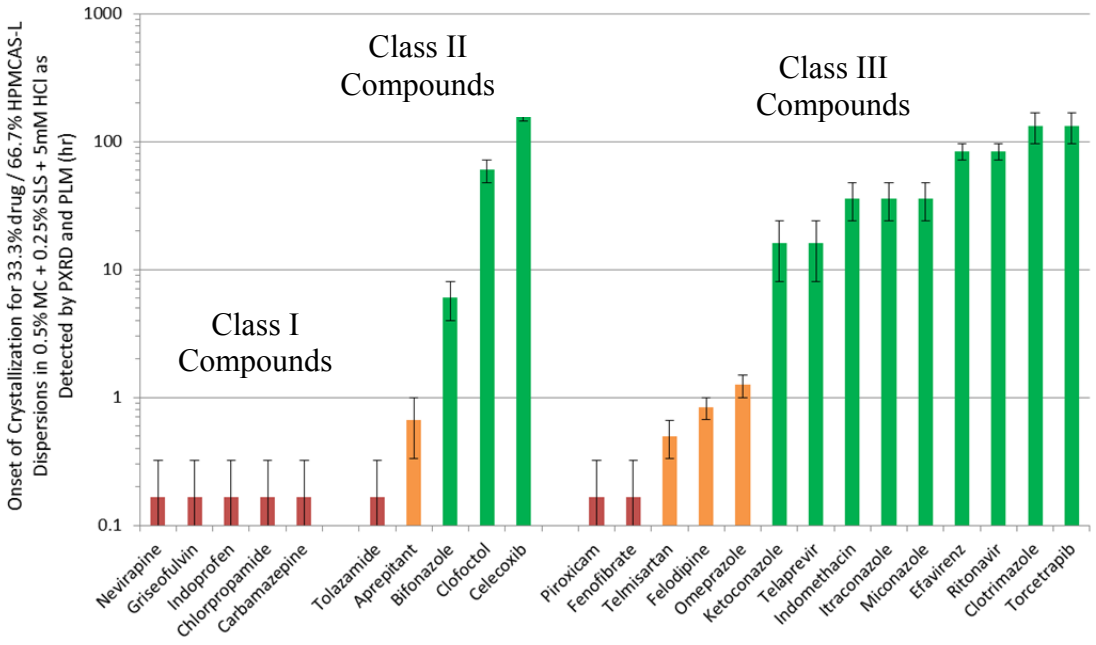

Figure 26. Cyclic DSC class as a predictive tool for crystallization of 33.3% drug/66.7% HPMCAS-LF spray dried amorphous dispersions in 0.5% MC + 0.25% SLS + 5 mM HCl. Note the red color coding denoting a crystallization time of less than 20 minutes, the orange color coding for crystallization time between 20 minutes and 3 hours, and the green color coding denoting a crystallization time of greater than 3 hours.

After detailed uni-variate analysis of the thermal descriptors including glass transition temperature of the model amorphous dispersion, glass transition temperature of the model drug

substance, the melting temperature of the model drug, the entropy of fusion, enthalpy of fusion and Gibbs free energy of the model drug substance, as well as the cyclic DSC classification and the drug substance melting temperature/glass transition temperature ratio, it was determined that melting temperature and entropy of fusion provide the greatest utility in predicting which compounds which will crystallize in the model suspension system. Melting temperature provides the most utility for two reasons. First, this is a relatively easy experimental parameter to determine and is readily available in the drug discovery space, assuming crystalline material is available. Second, the clear delineation of compounds above and below 180 °C shows the critical risk of crystallization which stems from high melting temperature compounds. Entropy of fusion helps predict which compounds will have delayed crystallization rates despite having a high melting temperature, or which compounds may have accelerated crystallization rates despite having a low melting temperature.

c.) Hydrophilicity Descriptors:

Uni-variate analysis was attempted for the various hydrophilicity descriptors including Log P, water solubility, the general solubility equation, platform vehicle solubility, and moisture uptake at 90% humidity. The upcoming figures display these correlations.

Log P was evaluated as a property that would describe the lipophilicity of each model compound (Figure 27).

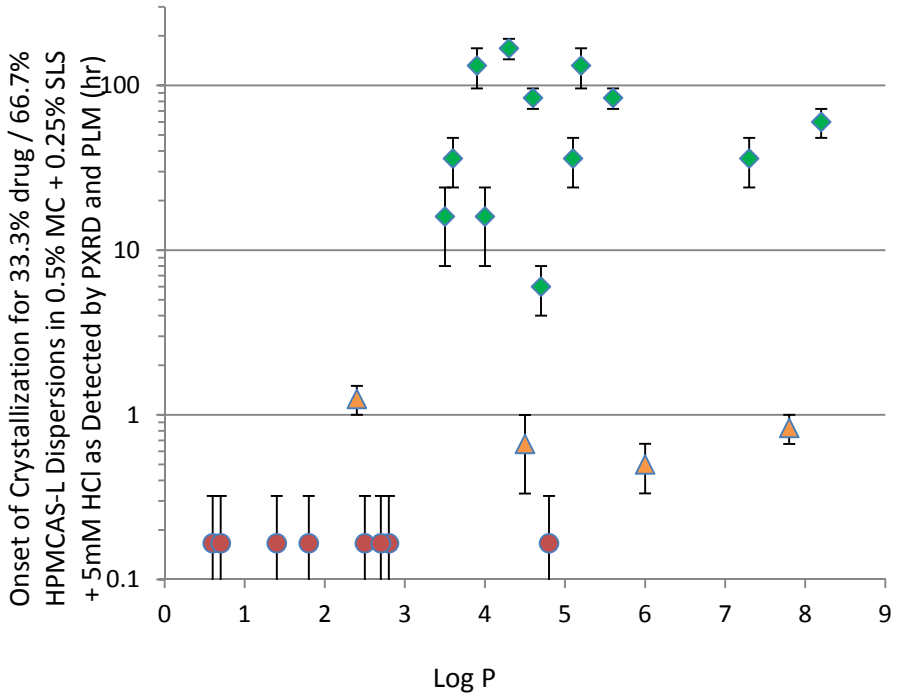

Figure 27. Log P versus onset of crystallization time for 33.3% drug/66.7% HPMCAS-LF spray dried amorphous dispersions in 0.5% MC + 0.25% SLS + 5 mM HCl. Note the red circle color coding denoting a crystallization time of less than 20 minutes, the orange triangle color coding for crystallization time between 20 minutes and 3 hours, and the green diamond color coding denoting a crystallization time of greater than 3 hours.

Compounds with a Log P above 3 show a reduced time to crystallize in our model amorphous suspension system than do compounds with a Log P below 3. This parameter may infer interactions with the suspending media. If the primary crystallization mechanism first requires dissolution into the bulk suspending media (Failure Mode 1), a largely aqueous/polar environment, than it may be hypothesized that this rate of dissolution/leaching may be delayed for more compounds with a higher Log P.

Water solubility for the model compounds may be a critical parameter as dissolution into the bulk suspending media may be required for the crystallization mechanism for these model suspensions. To this end, a calculated water solubility, from the general solubility equation, and literature (See Appendix 3 for reference data) water solubility numbers for each of the 24 model

compounds were obtained. The plots for these solubility values versus crystallization kinetics for each model suspension appear in Figures 28 and 29.

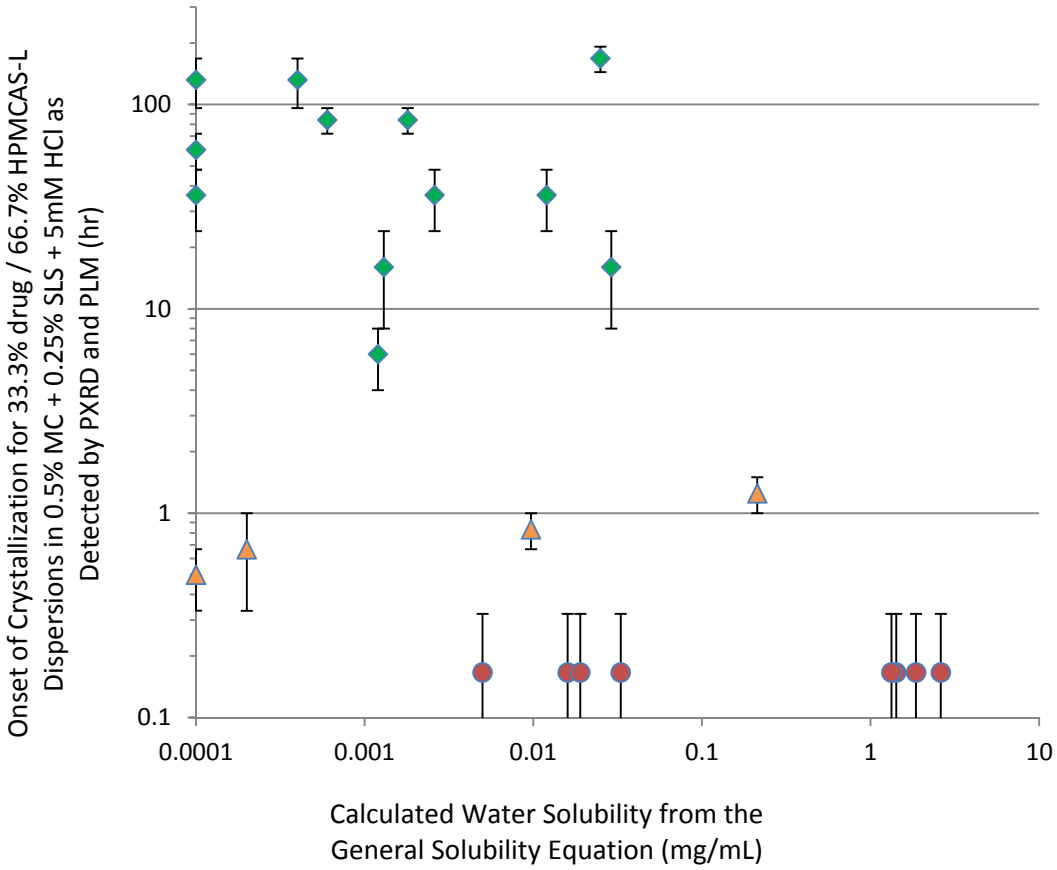

Figure 28. Calculated water solubility (GSE) versus onset of crystallization time for 33.3% drug/66.7% HPMCAS-LF spray dried amorphous dispersions in 0.5% MC + 0.25% SLS + 5 mM HCl. Note the red circle color coding denoting a crystallization time of less than 20 minutes, the orange triangle color coding for crystallization time between 20 minutes and 3 hours, and the green diamond color coding denoting a crystallization time of greater than 3 hours.

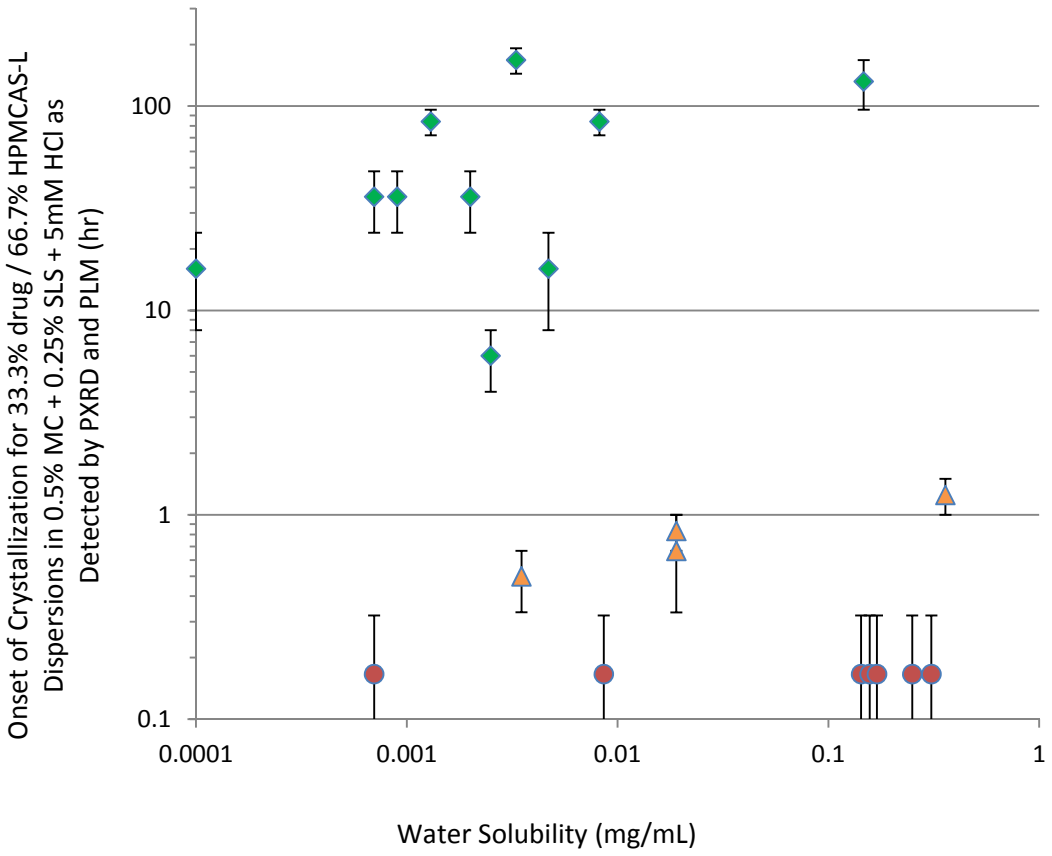

Figure 29. Water solubility (mg/mL) versus onset of crystallization time for 33.3% drug/66.7% HPMCAS-LF spray dried amorphous dispersions in 0.5% methocellulose + 0.25% SLS + 5 mM HCl. Note the red circle color coding denoting a crystallization time of less than 20 minutes, the orange triangle color coding for crystallization time between 20 minutes and 3 hours, and the green diamond color coding denoting a crystallization time of greater than 3 hours.

There is limited correlation between the calculated or literature water solubility and the propensity for each model compound to crystallize in the model amorphous suspension system. However, a trend can be observed, where compounds with solubility values greater than 0.1 mg/mL have an increased propensity to crystallize. This may be due to an enhanced dissolution rate from the amorphous dispersion, in which compound must first dissolve out of the suspended amorphous spray dried dispersion and into the bulk suspending vehicle prior to crystallization (failure mode 1). Attempts at improving the correlation between the amorphous suspension physical stability and solubility measurements were made by measuring the equilibrium

solubility of each compound in the platform suspending vehicle (Figure 30). Unfortunately this fails to improve the correlation between solubility and suspension physical stability.

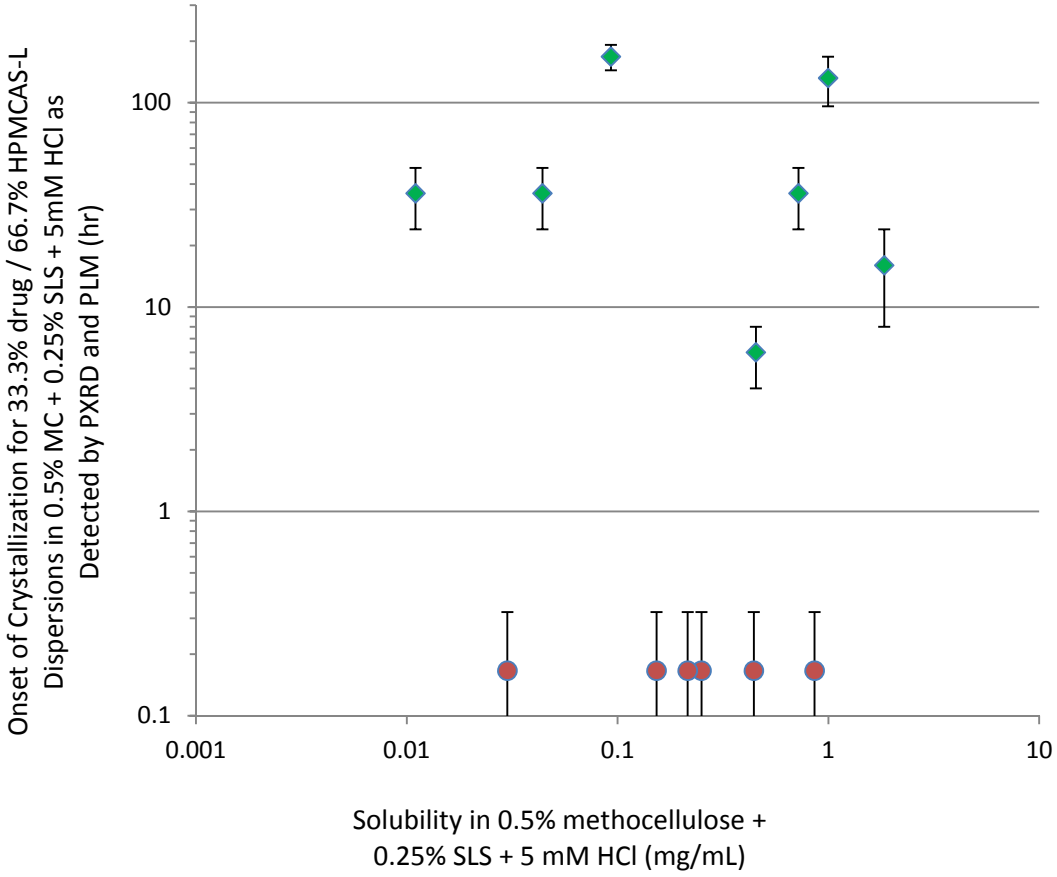

Figure 30. Platform vehicle solubility (mg/mL; 48 hr/25 °C) versus onset of crystallization time for 33.3% drug/66.7% HPMCAS-LF spray dried amorphous dispersions in 0.5% MC + 0.25% SLS + 5 mM HCl. Note the red circle color coding denoting a crystallization time of less than 20 minutes, the orange triangle color coding for crystallization time between 20 minutes and 3 hours, and the green diamond color coding denoting a crystallization time of greater than 3 hours.

Given that the suspending medium (0.5% methocellulose + 0.25% SLS + 5 mM HCl) is acidified with HCl, and the suspended polymer (HPMCAS-LF) is enteric with an apparent pKa of 5.0[55], it is vital to consider whether the ionization state (pKa) of each model compound is predictive of suspension physical stability in the model system. Table 4 compares the pKa and

Ionization state to onset of crystallization time for the model system. However, note the lack of correlation between pKa or ionization state and rate of crystallization.

Table 4. pKa and ionization state versus physical stability for each model amorphous dispersion. Note the red color coding denoting a crystallization time of less than 20 minutes, the orange color coding for crystallization time between 20 minutes and 3 hours, and the green color coding denoting a crystallization time of greater than 3 hours.

Acid/ Base Classification	Model Compound	Crystal Rate Category	pKa	Ionization
Zwitterion	Piroxicam	< 20 minutes	1.8, 5.1	partially
Weak Base	Nevirapine	< 20 minutes	2.8	partially
	Ritonavir	> 3 hours	2.8	partially
	Ketoconazole	> 3 hours	2.9	partially
	Tolazamide	< 20 minutes	3.6	partially
	Itraconazole	> 3 hours	3.7	partially
	Omeprazole	20 min - 3 hours	4	unionized
	Chlorpropamide	< 20 minutes	4.3	unionized
	Felodipine	20 min - 3 hours	5.4	unionized
	Clotrimazole	> 3 hours	6.6	unionized
	Bifonazole	> 3 hours	6.7	unionized
	Miconazole	> 3 hours	6.7	unionized
	Aprepitant	20 min - 3 hours	9.7	unionized
	Celecoxib	> 3 hours	11.1	unionized
	Telaprevir	> 3 hours	11.9	unionized
	Efavirenz	> 3 hours	12.5	unionized
Weak Acid	Indomethacin	> 3 hours	4.5	unionized
	Indoprofen	< 20 minutes	5.8	unionized
	Telmisartan	20 min - 3 hours	3.5	unionized
Neutral	Griseofulvin	< 20 minutes	x	unionized
	Torcetrapib	> 3 hours	x	unionized
	Clofoctol	> 3 hours	x	unionized
	Carbamazepine	< 20 minutes	x	unionized
	Fenofibrate	< 20 minutes	x	unionized

Another factor to consider, in regards to amorphous materials and interactions with moisture, is the hygroscopicity of each amorphous dispersion. The 24 model amorphous dispersions can be rank ordered in hygroscopicity by determining the peak amount of moisture

uptake of each of the amorphous dispersions after undergoing a moisture sorption/desorption isotherm (details appear in chapter 2). An example moisture sorption isotherm appears below for a 33.3% Aprepitant/66.7% HPMCAS-LF spray dried amorphous solid dispersion. The compilation plot of moisture uptake versus suspension physical stability appears in Figure 31.

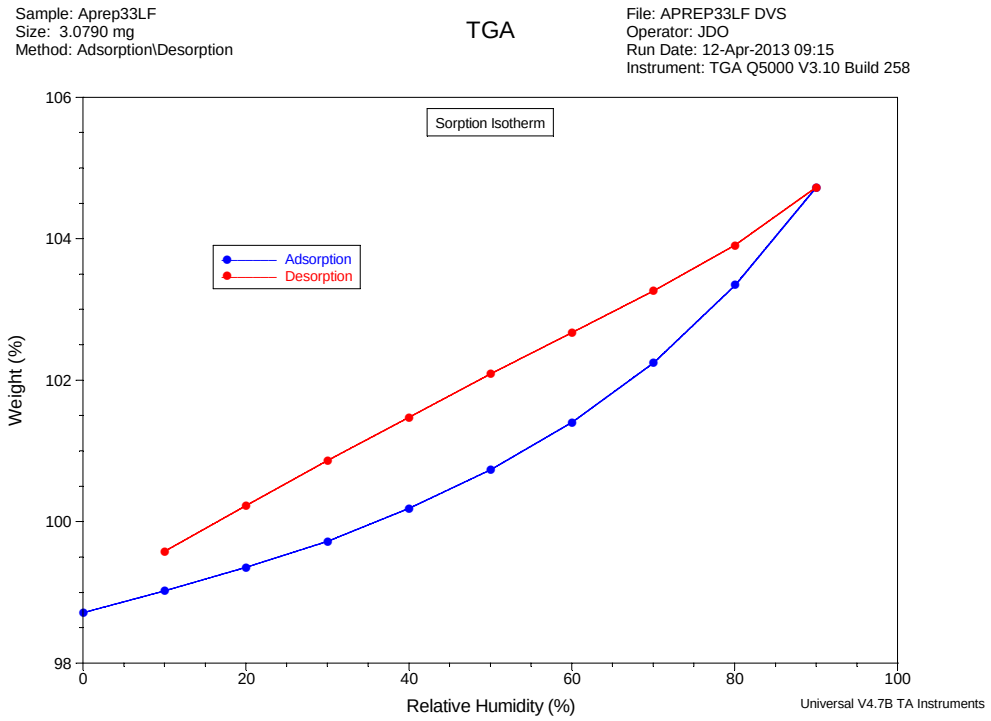

Figure 31. Moisture sorption isotherm (25 °C) for a spray dried amorphous dispersion of 33.3% Aprepitant/66.7% HPMCAS-LF

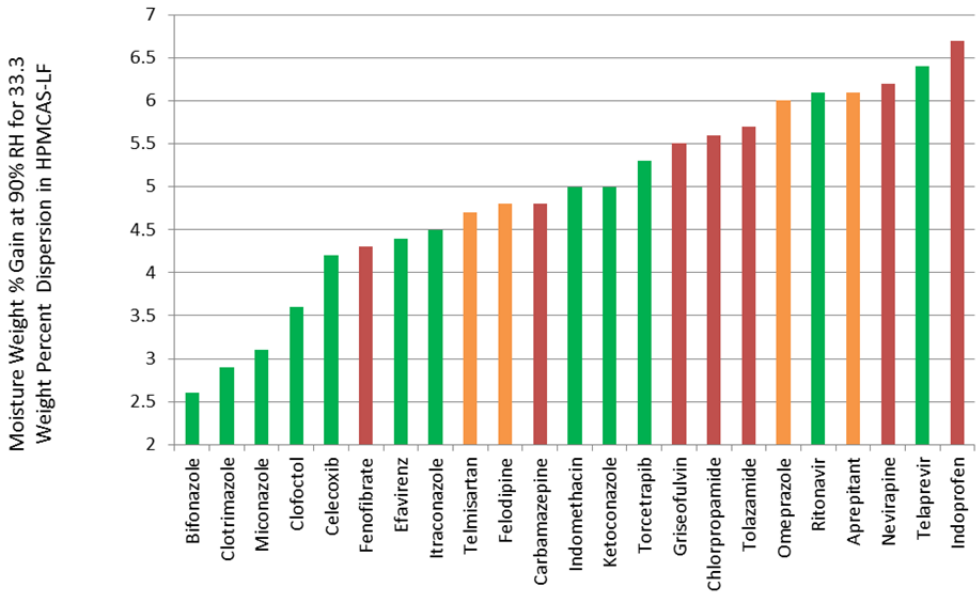

Figure 32. Moisure weight percent gain at 25 °C/90% RH for 33.3% wt active amorphous dispersions in HPMCAS-LF. Note the red color coding denoting a crystallization time of less than 20 minutes, the orange color coding for crystallization time between 20 minutes and 3 hours, and the green color coding denoting a crystallization time of greater than 3 hours.

There is a trend between the hygroscopity of the amorphous dispersion and the physical stability of the model system. For amorphous dispersions in which the weight gain is less than 5.5%, 10 amorphous dispersions have onset of crystallization times >3 hours, 2 have times between 20 minutes and 3 hours, and only 2 have onset of crystallization times less than 20 minutes.

The value of the hygroscopicity data increases when it is used with the amorphous dispersion glass transition temperature to calculate the $T_{g,dispersion,100\%RH}$. This parameter has significant predictive value (Figure 33). As the $T_{g,dispersion,100\%RH}$ rises above 30 °C, the material can be assumed to be in the glassy state at room temperature. In this case 7 of the 8 compounds show onset of crystallization times which exceed 3 hours and only 1 compound shows an onset of crystallization time which is between 20 minutes and 3 hours. No compounds show onset of crystallization times below 20 minutes. It can be hypothesized that both failure mode 1 and 2 would show a decreased rate of crystallization as $T_{g,dispersion,100\%RH}$ rises above 30 °C. In failure mode 1, the dissolution of drug from the glass into the bulk could be hypothesized to be slower

than that of a super cooled liquid. For failure mode 2, the crystallization in the amorphous dispersion particle would be slower for a glass than a super cooled liquid.

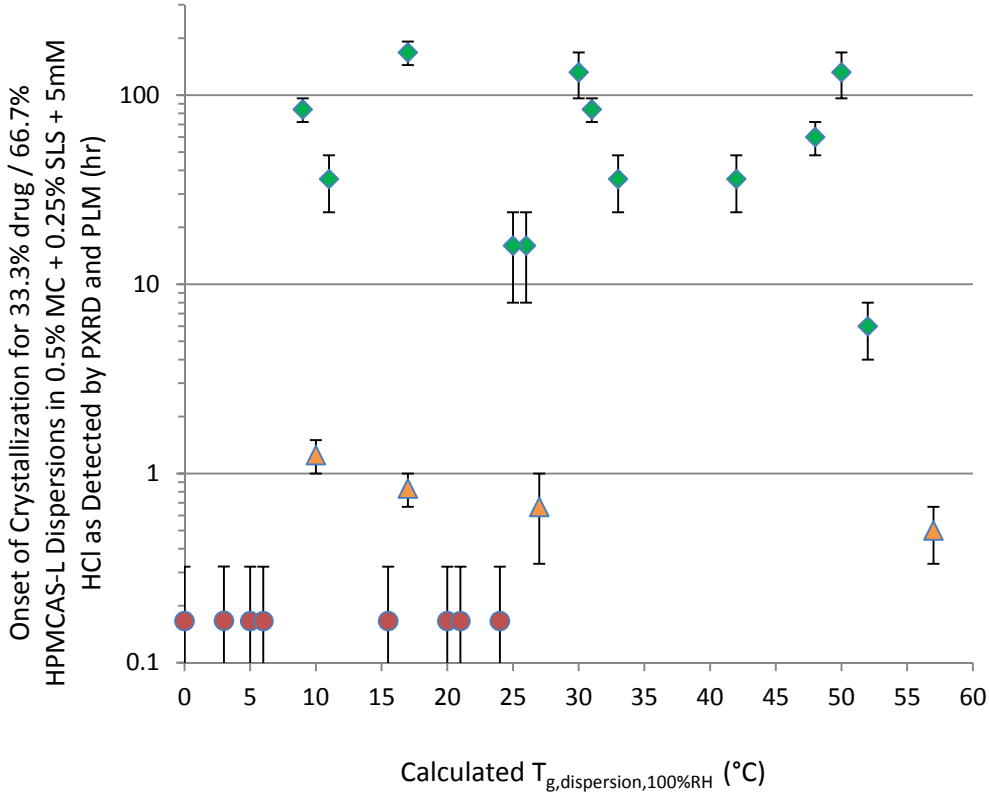

Figure 33. $T_{g,dispersion,100\%RH}$ (°C) versus onset of crystallization time for 33.3% drug/66.7% HPMCAS-LF spray dried amorphous dispersions in 0.5% MC + 0.25% SLS + 5 mM HCl. Note the red circle color coding denoting a crystallization time of less than 20 minutes, the orange triangle color coding for crystallization time between 20 minutes and 3 hours, and the green diamond color coding denoting a crystallization time of greater than 3 hours.

Chapter 4: Multi-variate Analysis of Descriptors

*This chapter focuses on the value of building a multi-variate model to predict the amorphous suspension physical stability of a spray dried amorphous dispersion based upon the physicochemical properties of the selected model compound. From this a 2-tiered model emerges in which first, the model considers the humidity adjusted glass transition temperature of the amorphous dispersion ($T_{g,dispersion,100\%\ RH}$). For compounds where $T_{g,dispersion,100\%\ RH}$ is >30 °C the amorphous dispersion is in a glassy state and is protected from crystallization within 3 hours of preparation. For compounds where $T_{g,dispersion,100\%\ RH}$ is <30 °C the amorphous dispersion is a super cooled liquid at room temperature and is not kinetically protected from rapid crystallization. For these compounds analysis of melting temperature/ entropy of fusion (must be <5500 K^2*mol/KJ to be predicted stable) and molecular weight x LogP (must be >1000 to be predicted stable) can be used to successfully predict a 3 hour shelf-life. The resulting decision tree is outlined in Figure 1.*

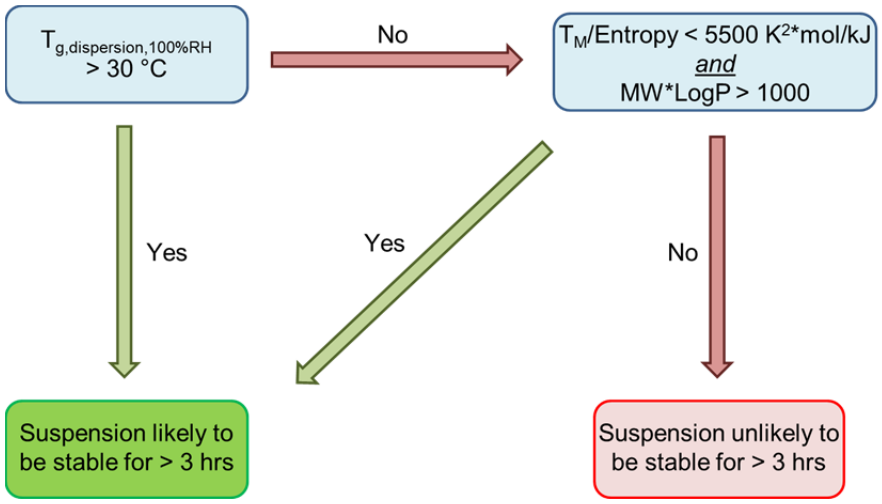

Figure 1. Decision tree for assessing the physical stability of a model compound spray dried to form an amorphous dispersion at 33.3% drug load in HPMCAS and suspended in 0.5% methocellulose + 0.25% SLS + 5 mM HCl.

Uni-variate analysis of the available data suggests there is a relationship between physicochemical descriptors of each of the model molecules and the rate of crystallization in the

model amorphous suspension system. However, there is the opportunity to combine these descriptors in two dimensional, three dimensional and even multi-dimensional models.

Five parameters, from uni-variate analysis, which show trends with suspension crystallization rates are melting temperature, entropy of fusion, Log P, molecular weight and $T_{g,dispersion,100\%\ RH}$.

First, these results suggest that amorphous dispersions in the glassy state ($T_{g,dispersion,100\%\ RH}$ < 30°C; Figure 33) are more stable than those which are super cooled liquids ($T_{g,dispersion,100\%\ RH}$ >30°C; Figure 33). Next, it becomes evident that compounds in the super cooled liquid state are more likely to nucleate and crystallize, by either failure mode 1 or failure mode 2, if they are small (<400 dalton; Figure 11), lipophilic (Log P <3; Figure 27), high melting temperature (> 180 °C; Figure 20), low entropy of fusion (<0.08 kJ/K*mole; Figure 22) compounds, which is consistent with classical nucleation theory[29,30].

Several figures can be constructed considering 2-4 of these parameters (melting temperature, entropy of fusion, lipophilicity and molecular weight) for the molecules in the super cooled liquid state. A simplistic 2-D diagram is a melting temperature versus Log P diagram. These parameters were selected because they showed a predictive trend in the uni-variate analysis.

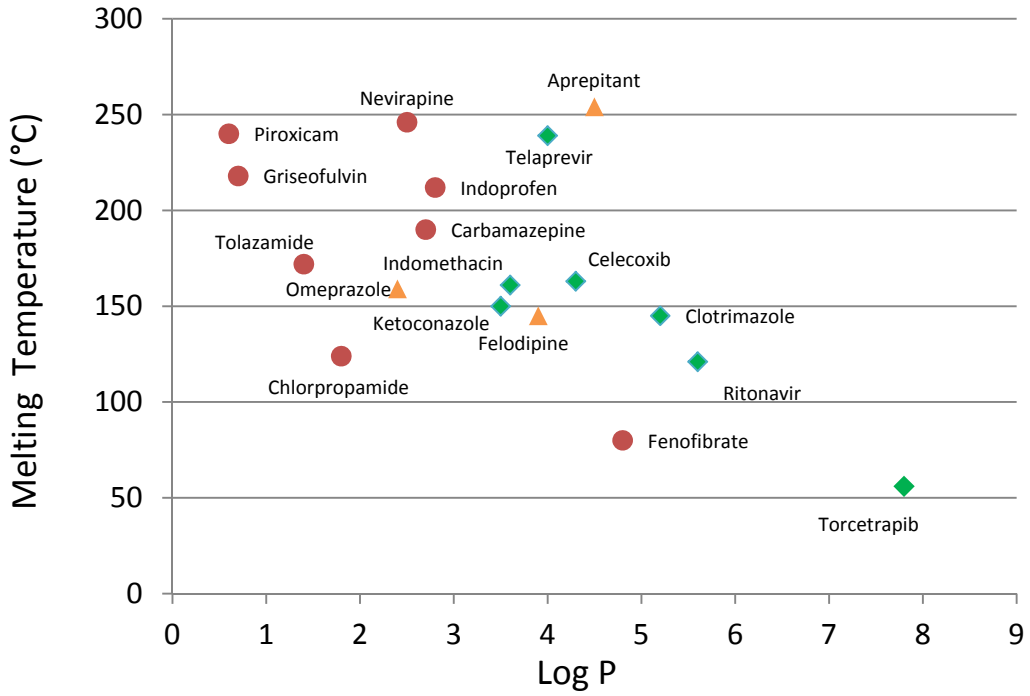

Figure 34. Melting temperature and Log P versus onset of crystallization time for 33.3% drug/66.7% HPMCAS-LF spray dried amorphous dispersions in 0.5% MC + 0.25% SLS + 5 mM HCl. Note the red circle color coding denoting a crystallization time of less than 20 minutes, the orange triangle color coding for crystallization time between 20 minutes and 3 hours, and the green diamond color coding denoting a crystallization time of greater than 3 hours.

While Figure 34 illustrates the importance of melting temperature and Log P on the crystallization rate of amorphous suspensions, and differentiates rapid crystallizing compounds (top left) and slow crystallizing compounds (bottom right), it over estimates the crystallization potential for Telaprevir and Aprepitant, which are high entropy of fusion compounds. This model also underestimates the importance of the low entropy of fusion for Felodipine, Fenofibrate and Omeprazole. Once the Y-Axis is converted to melting temperature/entropy of fusion versus Log P Figure 35 is generated.

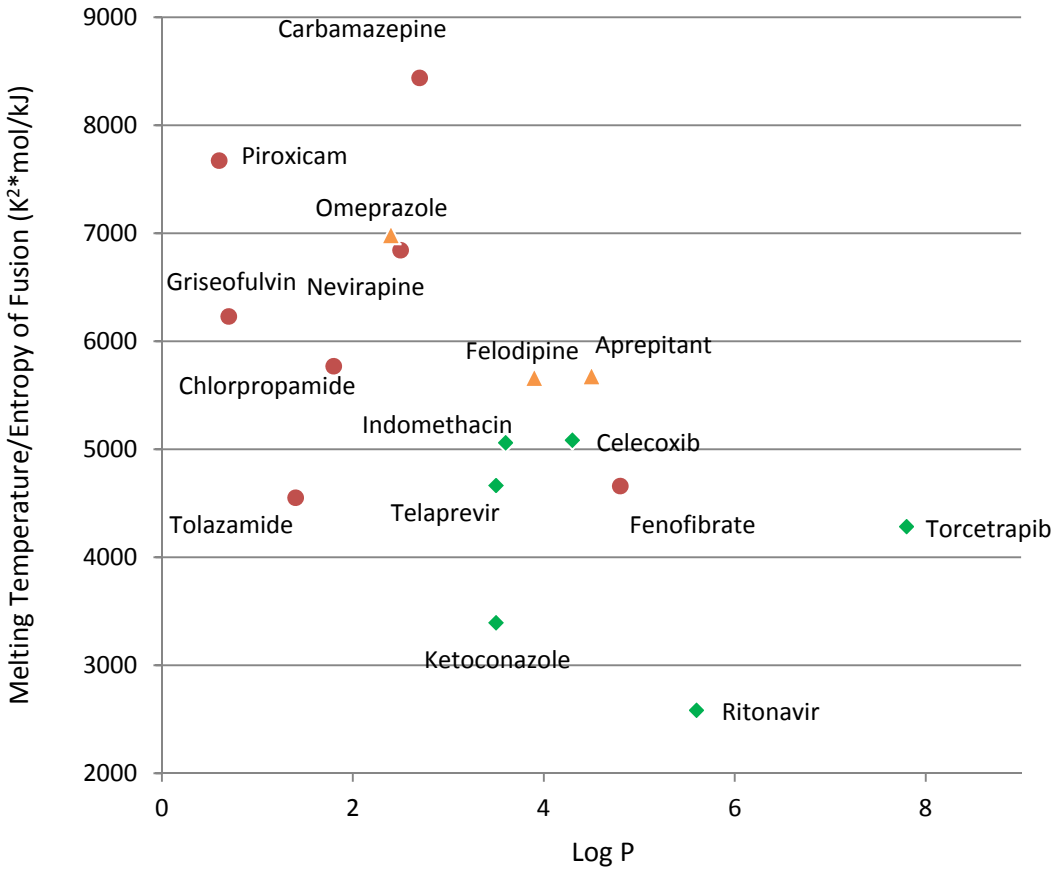

Figure 35. Melting temperature/entropy of fusion and Log P versus onset of crystallization time for 33.3% drug/66.7% HPMCAS-LF spray dried amorphous dispersions in 0.5% MC + 0.25% SLS + 5 mM HCl. Note the red circle color coding denoting a crystallization time of less than 20 minutes, the orange triangle color coding for crystallization time between 20 minutes and 3 hours, and the green diamond color coding denoting a crystallization time of greater than 3 hours.

In the plot shown in Figure 35 melting temperature, entropy of fusion and Log P are incorporated into the model. However, this model fails to incorporate the importance of molecular weight on crystallization rate. This can be accomplished by converting the x-axis into Log P x Molecular Weight as shown in Figure 36.

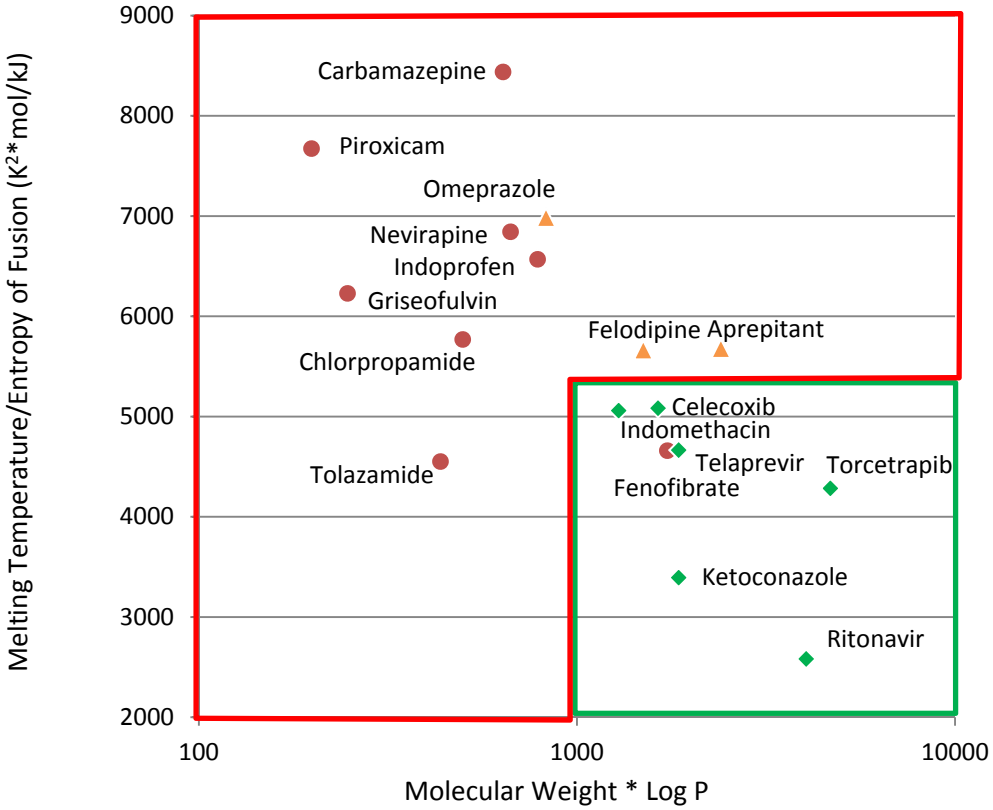

Figure 36. Melting temperature/entropy of fusion vs. molecular weight x Log P versus onset of crystallization time for 33.3% drug/66.7% HPMCAS-LF spray dried amorphous dispersions in 0.5% MC + 0.25% SLS + 5 mM HCl. Note the red circle color coding denoting a crystallization time of less than 20 minutes, the orange triangle color coding for crystallization time between 20 minutes and 3 hours, and the green diamond color coding denoting a crystallization time of greater than 3 hours.

Figure 36 is able to capture 4 critical descriptors (melting temperature, entropy of fusion, molecular weight and Log P) of nucleation onto one 2-D plot. Compounds in the upper left hand corner will rapidly crystalline (< 3 hours) in the model system, as these compound are characterized by a high melting temperature, low entropy of fusion, low Log P and low molecular weight. Compounds in the lower right hand corner will be slower (> 3 hours) to crystallize in the model system because these compounds are characterized by a low melting temperature, a high entropy of fusion, a high Log P and a high molecular weight. From these data, a region of Figure 36, in which melting temperature/entropy of fusion is < 5500 K^2mol/kJ

and Molecular Weight x Log P is > 1000 can be established as a 'physical stability zone' in which compounds are likely to have greater than 3 hours of physical stability within the model system.

A two tiered model in which the calculated glass transition temperature of the amorphous dispersion at 100% RH ($T_{g,dispersion,100\%\ RH}$), to differentiate amorphous dispersions in the glassy state from the super cooled liquid state is first considered, and the melting temperature/ entropy of fusion versus the molecular weight x Log P for the compounds in the super cooled liquid state is considered next, and this model will correctly predict the relative physical stability of 22 of the 24 model compounds. This two staged approach can be thought of as first applying theory related to amorphous systems and the glass transition to determine whether the material is in a glassy or super cooled liquid state, followed by evaluating descriptors which are relevant to classical nucleation theory for those amorphous dispersions which are in the super cooled liquid state.

Two outliers emerge in the data analysis. The first outlier is Telmisartan. Telmisartan has a high $T_{g,dispersion,100\%\ RH}$ of 57 °C, which one would predict to be stable in suspension. However, the melting temperature of Telmisartan is 269 °C, and the melting temperature/entropy of fusion for Telmisartan is 5542 K^2mol/kJ, which suggests that any drug substance, which is able to partition into the bulk suspending vehicle, as per failure mode 1, would rapidly crystallize. This strong driving force for crystallization is the likely reason that Telmisartan appears in the moderate crystallization rate group (20 minutes – 3 hours) despite having a $T_{g,dispersion,100\%\ RH}$ of 57 °C.

The second outlier in the analysis is Fenofibrate. Fenofibrate would be predicted to have a crystallization time > 3 hours based upon the melting temperature/entropy of fusion vs. Log P x molecular weight 2-D plot. However, Fenofibrate crystallizes in less than 20 minutes. The leading hypothesis for this result centers around the symmetry plane that divides Fenofibrate (Figure 37).

Figure 37. Structure of Fenofibrate

The current model fails to incorporate shape or symmetry of a molecule. Therefore, the model may under predict the crystallization rate of molecules which are linear with a symmetry plane, and may rapidly assemble into a crystal lattice.

Chapter 5: Conclusions

Suspensions of spray dried amorphous dispersions are a valuable tool for enhancing the exposure of poorly soluble compounds in preclinical animal models. However, limitations in drug supply and time/cost of manufacture in the drug discovery space make it desirable to predict the probability of obtaining a stable (free from detectable crystallization) suspension prior to synthesis, scale-up and processing of a candidate compound.

A model system was prepared for 24 model compounds and interrogated for the onset of crystallization. The crystallization kinetics for each system were monitored and compared to physicochemical descriptors for each model compound.

A 2-tiered multivariate model was assembled. This model first considers the calculated glass transition temperature of the amorphous dispersion at 100% RH ($T_{g,dispersion,100\%\ RH}$) to, delineate amorphous dispersions in the glassy state from the super cooled liquid state, and assumes amorphous dispersions in the glassy state will have a physical stability greater than 3 hours in the model system. Second, the model considers the melting temperature/entropy of fusion versus the molecular weight * Log P for the compounds in the super cooled liquid state. From this 2-D plot a physical stability zone where melting temperature/entropy of fusion is < 5500 K^2mol/kJ and molecular weight x Log P is > 1000 is estabilished.

This model is useful in its simplicity and its ability to correctly predict the physical physical stability of 22 out of 24 of the model compounds evaluated. The model also ties empirical physical physical stability data back to literature on amorphous materials and the importance of glass transition temperature and to classical nucleation theory.

Future opportunities exist to expand upon this research. While a platform dispersion polymer, drug loading and vehicle were held constant in this work, additional work could be conducted to probe the impact of these parameters on the kinetics of crystallization for suspensions of amorphous dispersions.

References:

1. R. K. Borchardt, EH; Hageman, MJ; Thakker, DR; Stevens JL.(2006) Optimizing the drug like properties of leads in drug discovery. Springer**:** 151-166.
2. Venkatesh, S. and R. A. Lipper (2000). "Role of the development scientist in compound lead selection and optimization." Journal of Pharmaceutical Sciences **89**(2): 145-154.
3. Brouwers, J., M. E. Brewster, et al. (2009). "Supersaturating Drug Delivery Systems: The Answer to Solubility-Limited Oral Bioavailability?" Journal of Pharmaceutical Sciences **98**(8): 2549-2572.
4. Engers, D., J. Teng, et al. (2008). Screening and animal bioavailability studies on itraconazole amorphous dispersions. AAPS Annual Meeting. Atlanta, Georgia.
5. Frank, K. J., U. Westedt, et al. (2012). "The amorphous solid dispersion of the poorly soluble ABT-102 forms nano/microparticulate structures in aqueous medium: Impact on solubility." International Journal of Nanomedicine **7**: 5757-5768.
6. Goldberg, A. H., M. Gibaldi, et al. (1966). "Increasing dissolution rates and gastrointestinal absorption of drugs via solid solutions and eutectic mixtures III: Experimental evaluation of griseofulvin—succinic acid solid solution." Journal of Pharmaceutical Sciences **55**(5): 487-492.
7. Leuner, C. and J. Dressman (2000). "Improving drug solubility for oral delivery using solid dispersions." European Journal of Pharmaceutics and Biopharmaceutics **50**(1): 47-60.
8. Raina, S. A., G. G. Z. Zhang, et al. "Enhancements and Limits in Drug Membrane Transport Using Supersaturated Solutions of Poorly Water-Soluble Drugs." Journal of Pharmaceutical Sciences: n/a-n/a.
9. Serajuddin, A. T. M. (1999). "Solid dispersion of poorly water-soluble drugs: Early promises, subsequent problems, and recent breakthroughs." Journal of Pharmaceutical Sciences **88**(10): 1058-1066.
10. Vasconcelos, T., B. Sarmento, et al. (2007). "Solid dispersions as strategy to improve oral bioavailability of poor water soluble drugs." Drug Discovery Today **12**(23-24): 1068-1075.
11. Hancock, B. C. and M. Parks (2000). "What is the true solubility advantage for amorphous pharmaceuticals?" Pharmaceutical Research **17**(4): 397-404.
12. Alonzo, D., G. Z. Zhang, et al. "Understanding the Behavior of Amorphous Pharmaceutical Systems during Dissolution." Pharmaceutical Research **27**(4): 608-618.
13. Corrigan, O. I. (1985). "Mechanisms of dissolution of fast release solid dispersions." Drug Development and Industrial Pharmacy **11**(2-3): 697-724.
14. Craig, D. Q. M. (2002). "The mechanisms of drug release from solid dispersions in water-soluble polymers." International Journal of Pharmaceutics **231**(2): 131-144.
15. Konno, H., T. Handa, et al. (2008). "Effect of polymer type on the dissolution profile of amorphous solid dispersions containing felodipine." European Journal of Pharmaceutics and Biopharmaceutics **70**(2): 493-499.
16. Aisha, A. F. A., Z. Ismail, et al. (2012). "Solid dispersions of α-mangostin improve its aqueous solubility through self-assembly of nanomicelles." Journal of Pharmaceutical Sciences **101**(2): 815-825.
17. Ilevbare, G. A., H. Liu, et al. "Impact of Polymers on Crystal Growth Rate of Structurally Diverse Compounds from Aqueous Solution." Molecular Pharmaceutics **10**(6): 2381-2393.
18. Ilevbare, G. A., H. Liu, et al. (2012). "Maintaining supersaturation in aqueous drug solutions: Impact of different polymers on induction times." Crystal Growth and Design **13**(2): 740-751.
19. Ilevbare, G. A. and L. S. Taylor (2013). "Liquid-liquid phase separation in highly supersaturated aqueous solutions of poorly water-soluble drugs: Implications for solubility enhancing formulations
20. Mahlin, D., J. Berggren, et al. (2004). "Moisture-induced surface crystallization of spray-dried amorphous lactose particles studied by atomic force microscopy." Journal of Pharmaceutical Sciences **93**(1): 29-37.
21. Mahlin, D., J. Berggren, et al. (2006). "The influence of PVP incorporation on moisture-induced surface crystallization of amorphous spray-dried lactose particles." International Journal of Pharmaceutics **321**(1-2): 78-85.
22. Marsac, P. J., A. C. F. Rumondor, et al. (2010). "Effect of Temperature and Moisture on the Miscibility of Amorphous Dispersions of Felodipine and Poly(vinyl pyrrolidone)." Journal of Pharmaceutical Sciences **99**(1): 169-185.
23. Marsac, P. J., S. L. Shamblin, et al. (2006). "Theoretical and practical approaches for prediction of drug-polymer miscibility and solubility." Pharmaceutical Research **23**(10): 2417-2426.
24. Rumondor, A. C. F. and L. S. Taylor (2010). "Effect of Polymer Hygroscopicity on the Phase Behavior of Amorphous Solid Dispersions in the Presence of Moisture." Molecular Pharmaceutics **7**(2): 477-490.

25. Poirier-Brulez, F., G. Roudaut, et al. (2006). "Influence of sucrose and water content on molecular mobility in starch-based glasses as assessed through structure and secondary relaxation." Biopolymers **81**(2): 63-73.
26. Rumondor, A. C. F., H. Wikstroem, et al. (2011). "Understanding the Tendency of Amorphous Solid Dispersions to Undergo Amorphous-Amorphous Phase Separation in the Presence of Absorbed Moisture." Aaps Pharmscitech **12**(4): 1209-1219.
27. Alonzo, D. E., Y. Gao, et al. (2011). "Dissolution and precipitation behavior of amorphous solid dispersions." Journal of Pharmaceutical Sciences **100**(8): 3316-3331.
28. Alonzo, D. E., S. Raina, et al. (2012). "Characterizing the impact of Hydroxypropyl methyl cellulose on the growth and nucleation kinetics of felodipine from supersaturated solutions." Crystal Growth and Design **12**(3): 1538-1547.
29. Erdemir, D., A. Y. Lee, et al. (2009). "Nucleation of Crystals from Solution: Classical and Two-Step Models." Accounts of Chemical Research **42**(5): 621-629.
30. Garside, J. E. A. (2002). Measurement of Crystal Growth and Nucleation Rates, IChemE.
31. Lindfors, L., S. ForssÃ©n, et al. (2008). "Nucleation and crystal growth in supersaturated solutions of a model drug." Journal of Colloid and Interface Science **325**(2): 404-413.
32. Sarode, A. L., P. Wang, et al. "Supersaturation, nucleation, and crystal growth during single- and biphasic dissolution of amorphous solid dispersions: Polymer effects and implications for oral bioavailability enhancement of poorly water soluble drugs." European Journal of Pharmaceutics and Biopharmaceutics(0).
33. Schuth, F. (2001). "Nucleation and crystallization of solids from solution." Current Opinion in Solid State and Materials Science **5**(5): 389-395.
34. van der Leeden, M. C., D. Kashchiev, et al. (1993). "Effect of additives on nucleation rate, crystal growth rate and induction time in precipitation." Journal of Crystal Growth **130**(1â€“2): 221-232.
35. Hancock, B. C. and S. L. Shamblin (2001). "Molecular mobility of amorphous pharmaceuticals determined using differential scanning calorimetry." Thermochimica Acta **380**(2): 95-107.
36. Qian, F., J. Huang, et al. (2010). "Is a distinctive single T-g a reliable indicator for the homogeneity of amorphous solid dispersion?" International Journal of Pharmaceutics **395**(1-2): 232-235.
37. Shah, B., V. K. Kakumanu, et al. (2006). "Analytical techniques for quantification of amorphous/crystalline phases in pharmaceutical solids." Journal of Pharmaceutical Sciences **95**(8): 1641-1665.
38. Surana, R. and R. Suryanarayanan (2000). "Quantitation of crystallinity in substantially amorphous pharmaceuticals and study of crystallization kinetics by X-ray powder diffractometry." Powder Diffraction **15**(1): 2-6.
39. Wu, T. and L. Yu (2006). "Origin of enhanced crystal growth kinetics near T-g probed with indomethacin polymorphs." Journal of Physical Chemistry B **110**(32): 15694-15699.
40. Bhugra, C. and M. J. Pikal (2008). "Role of thermodynamic, molecular, and kinetic factors in crystallization from the amorphous state." Journal of Pharmaceutical Sciences **97**(4): 1329-1349.
41. Hoffman., J. D. (1958). "Thermodynamic driving force in nucleation and growth processes. ." J. Chem. Phys. **29**: 1192-1193.
42. Greco, S., J.-R. Authelin, et al. (2012). "A Practical Method to Predict Physical Stability of Amorphous Solid Dispersions." Pharmaceutical Research **29**(10): 2792-2805.
43. Newman, A., G. Knipp, et al. (2012). "Assessing the performance of amorphous solid dispersions." Journal of Pharmaceutical Sciences **101**(4): 1355-1377.
44. Kaneniwa, N. and N. Watari (1978). "Dissolution of slightly soluble drugs. IV. Effects of particle size of sulfonamides on in vitro dissolution rate and in vivo absorption rate, and their relation to solubility." Chemical and Pharmaceutical Bulletin **26**(3): 813-826.
45. Fincher, J. H. (1968). "Particle size of drugs and its relationship to absorption and activity." Journal of Pharmaceutical Sciences **57**(11): 1825-1835.
46. Hintz, R. J. and K. C. Johnson (1989). "The effect of particle size distribution on dissolution rate and oral absorption." International Journal of Pharmaceutics **51**(1): 9-17.
47. Waterman, K. C. and S. C. Sutton (2003). "A computational model for particle size influence on drug absorption during controlled-release colonic delivery." Journal of Controlled Release **86**(2â€“3): 293-304.
48. Murdande, S. B., M. J. Pikal, et al. (2010). "Solubility Advantage of Amorphous Pharmaceuticals: I. A Thermodynamic Analysis." Journal of Pharmaceutical Sciences **99**(3): 1254-1264.
49. Murdande, S. B., M. J. Pikal, et al. (2010). "Solubility Advantage of Amorphous Pharmaceuticals: II. Application of Quantitative Thermodynamic Relationships for Prediction of Solubility Enhancement in Structurally Diverse Insoluble Pharmaceuticals." Pharmaceutical Research **27**(12): 2704-2714.

50. Murdande, S. B., M. J. Pikal, et al. (2011). "Aqueous solubility of crystalline and amorphous drugs: Challenges in measurement." Pharmaceutical Development and Technology **16**(3): 187-200.
51. Murdande, S. B., M. J. Pikal, et al. (2011). "Solubility Advantage of Amorphous Pharmaceuticals, Part 3: Is Maximum Solubility Advantage Experimentally Attainable and Sustainable?" Journal of Pharmaceutical Sciences **100**(10): 4349-4356.
52. Moser J, Broyles J, Liu L, et al. (2008). "Enhancing bioavailability of poorly soluble drugs using spray dried solid dispersions Part I" Am Pharm Rev (11): 70-71
53. Zbicinski I, Strumillo C, Delag A. (2002). "Drying kinetics and particle residence time in spray drying" Drying Technology (20): 1751 – 1768.
54. Vehring R, Pharmaceutical Particle Engineering via Spray Drying. (2008) Pharm Res (25): 999-1022
55. Friesen, D. T., R. Shanker, et al. (2008). "Hydroxypropyl methylcellulose acetate succinate-based spray-dried dispersions: An overview." Molecular Pharmaceutics **5**(6): 1003-1019.
56. Hasegawa, A. T., M.; Suzuki, R., Miyata, T., Nakagawa, H., Sugimoto, I. (1988). "Supersaturation mechanism of drugs from solid dispersions with enteric coating agents." Chemical Pharmaceutical Bulletin **36**: 4941 - 4950
57. Sertsou, G., J. Butler, et al. (2002). "Solvent change co-precipitation with hydroxypropyl methylcellulose phthalate to improve dissolution characteristics of a poorly water-soluble drug." Journal of Pharmacy and Pharmacology **54**(8): 1041-1047.
58. Williams, R. J., Phillips, J. N., Mysels, K. J. (1955) "The critical micelle concentration of sodium lauryl sulfate at 25 °C" Trans. Faraday Soc., **51**, 728-737
59. Yalkowsky, S. H. (1999). Solubility and solubilization in aqueous media. New York, Oxford University Press.
60. Marsac, P.J., Konno, H., Taylor, L. S. (2006) "A comparison of the physical stability of amorphous felodipine and nifedipine systems". Pharm. Res., **23**, 2306-2316
61. Andronis, V., Yoshioka, M., Zografi, G. (1997) "Effects of sorbed water on the crystallization of indomethacin from the amorphous state". J. Pharm. Sci., **86**, 346-351
62. Baird, J. A., Van Eerdenbrugh B., Taylor LS. (2010). "A Classification System to Assess the Crystallization Tendency of Organic Molecules from Undercooled Melts." Journal of Pharmaceutical Sciences **99**(9): 3787-3806.
63. Freiss, B., Marciacq F., Lochard H., (2007) "Inclusion Complexes Containing Piroxicam, a Cyclodextrin and Arginine". US Patent :10/594740
64. Dixit, M., Kini, A.G., Kulkarni, P.K., (2010) "Preparation and characterization of microparticles of piroxicam by spray drying and spray chilling methods". Res Pharm Sci. **5**(2), 89–97
65. Lepek P., Sawicki W., Wlodarski K., Wojnarowska Z., Paluch M., Guzik L., (2013) "Effect of amorphization method on telmisartan solubility and the tableting process". Eur J Pharm Biopharm., **83**(1):114-21.
66. Mahua S., Perumal O.P., Panchagnula R., (2008) "Solid-State characterization of Nevirapine". Indian J Pharm Sci. **70**(5): 619–630.
67. Canadian Drugbank Online Database. www.drugbank.ca/drug
68. Lookchem Online Database. www.lookchem.com
69. Kwong A.D., Kauffman R.S., Hurter P., Mueller. P. (2011) "Discovery and development of telaprevir: an NS3-4A protease inhibitor for treating genotype 1 chronic hepatitis C virus". Nature Biotechnology (**29**), 993-1003
70. Fucella LM. (1975) Clin Pharmacol Therap. (**17**) 277

Appendix 1: Spray Dried Dispersion Characterization Data

This appendix contains the data used to characterize the spray dried dispersion prior to conducting suspension crystallization studies. Each sample of spray dried dispersion was determined to be amorphous by three orthogonal techniques, PXRD (i.e., lack of crystalline reflections), mDSC (i.e., lack of a crystalline melt) and PLM (i.e., lack of birefringence) characterization. mDSC was used to confirm that the material was single phase (i.e., appearance of one glass transition temperature).

In addition to PXRD, mDSC and PLM, select samples were analyzed by HPLC (to confirm potency), TGA (to gain insight into residual solvent/moisture) and LLS (to determine typical particle size distributions for these spray dried materials).

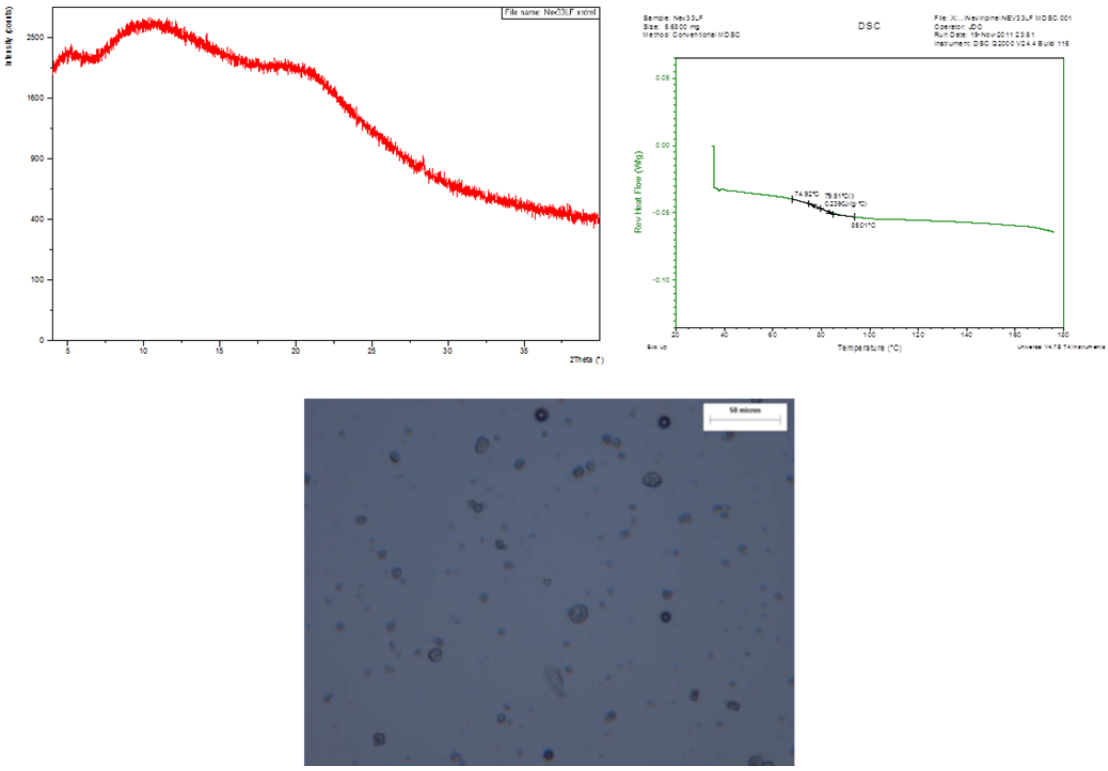

Figure 38. Characterization of spray dried 33.3% Nevirapine/66.7% HPMCAS-LF by PXRD, mDSC and PLM.

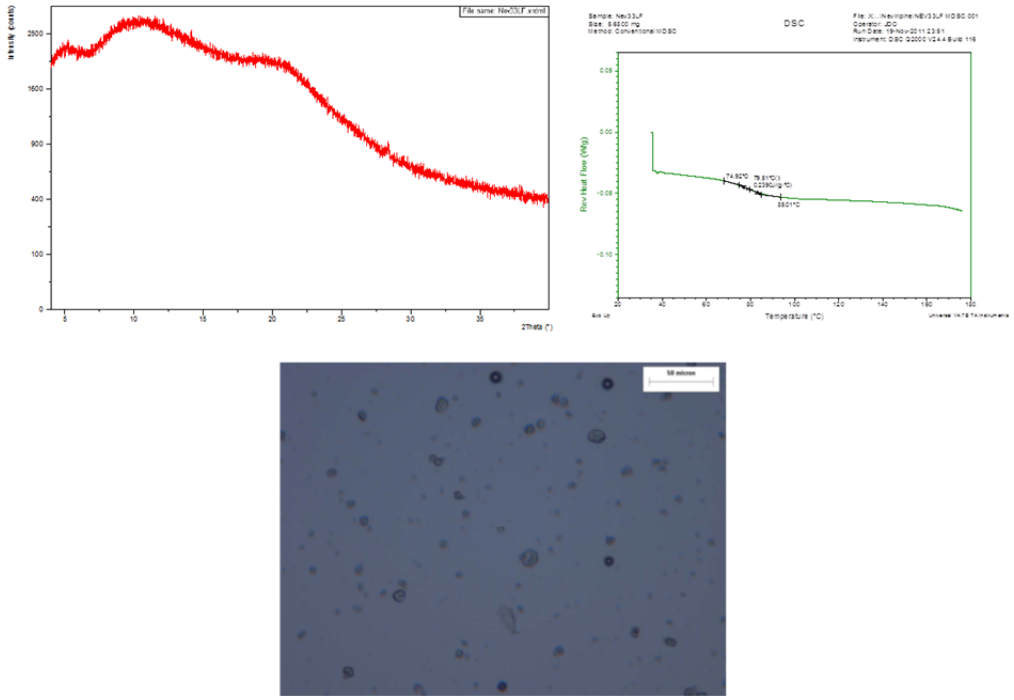

Figure 39. Characterization of spray dried 33.3% Piroxicam/66.7% HPMCAS-LF by PXRD, mDSC and PLM.

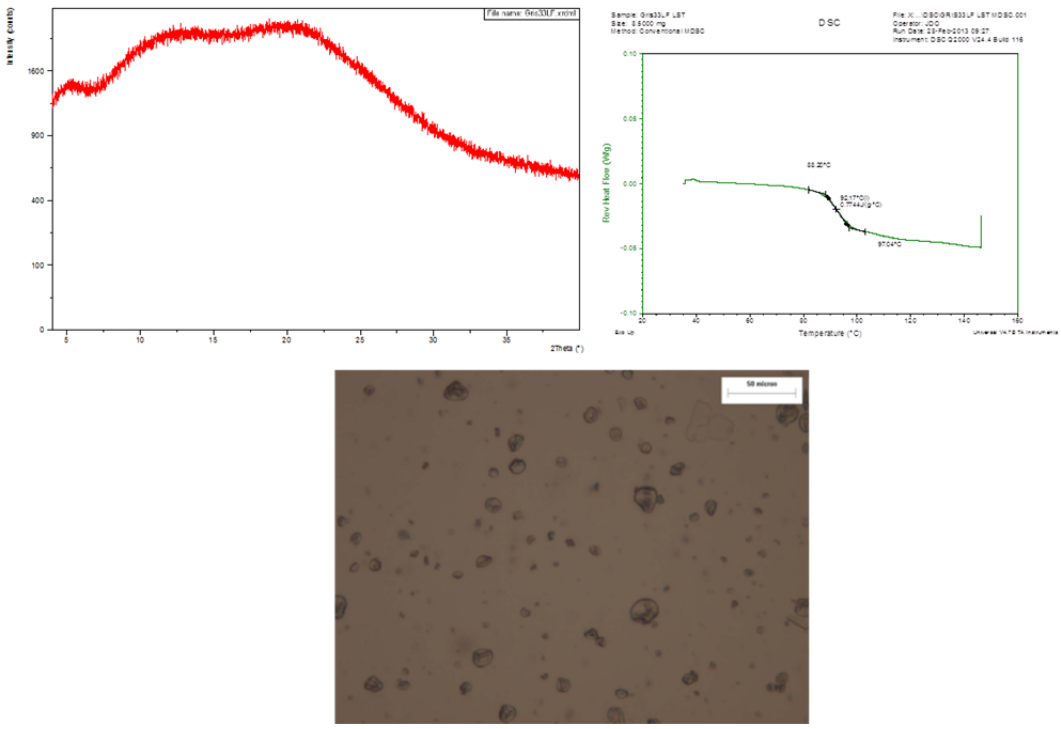

Figure 40. Characterization of spray dried 33.3% Griseofulvin/66.7% HPMCAS-LF by PXRD, mDSC and PLM.

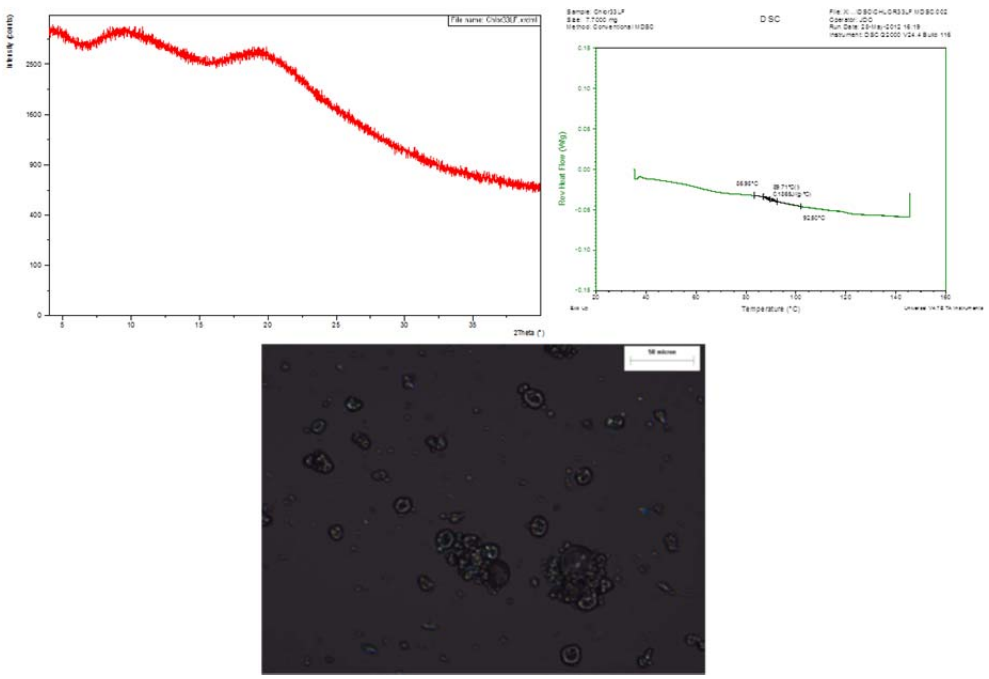

Figure 41. Characterization of spray dried 33.3% Chlorpropamide/66.7% HPMCAS-LF by PXRD, mDSC and PLM.

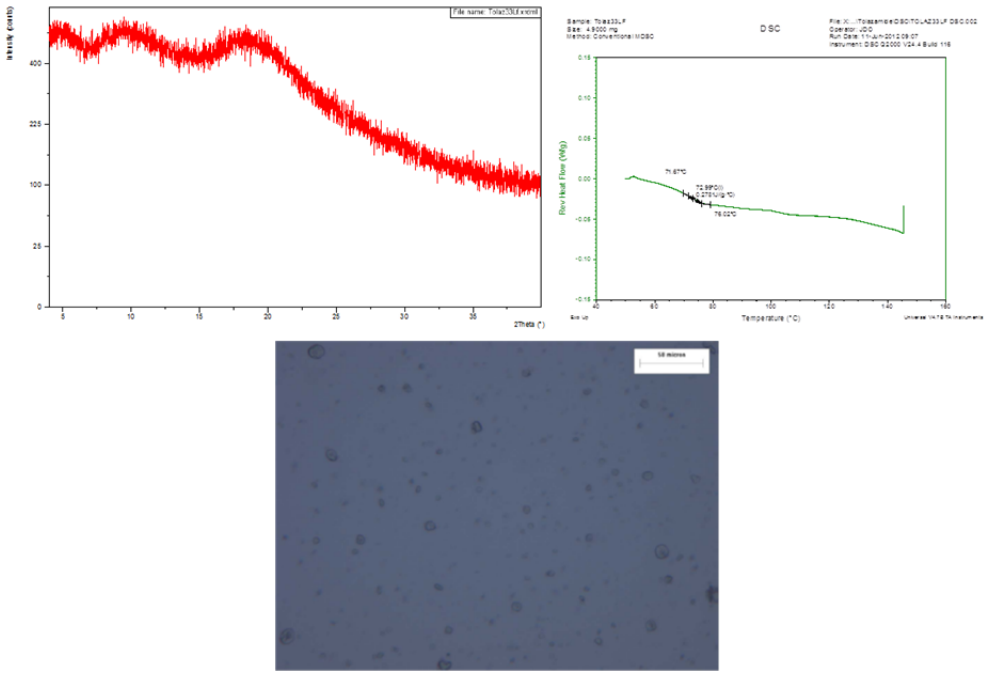

Figure 42. Characterization of spray dried 33.3% Tolazamide/66.7% HPMCAS-LF by PXRD, mDSC and PLM.

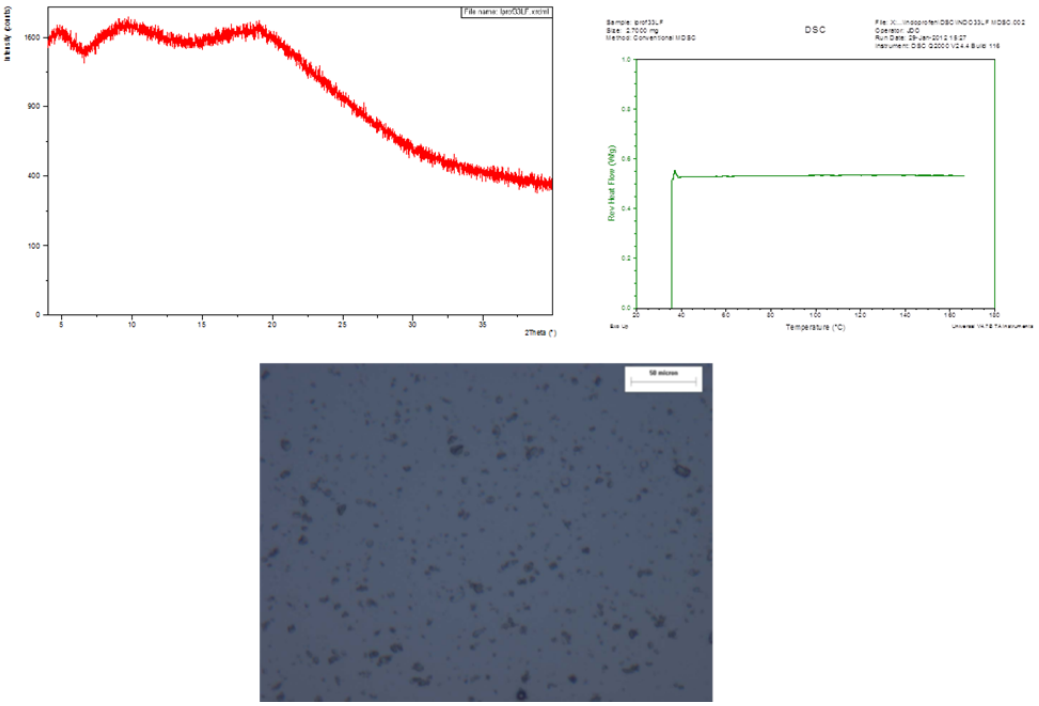

Figure 43. Characterization of spray dried 33.3% Indoprofen/66.7% HPMCAS-LF by PXRD, mDSC and PLM.

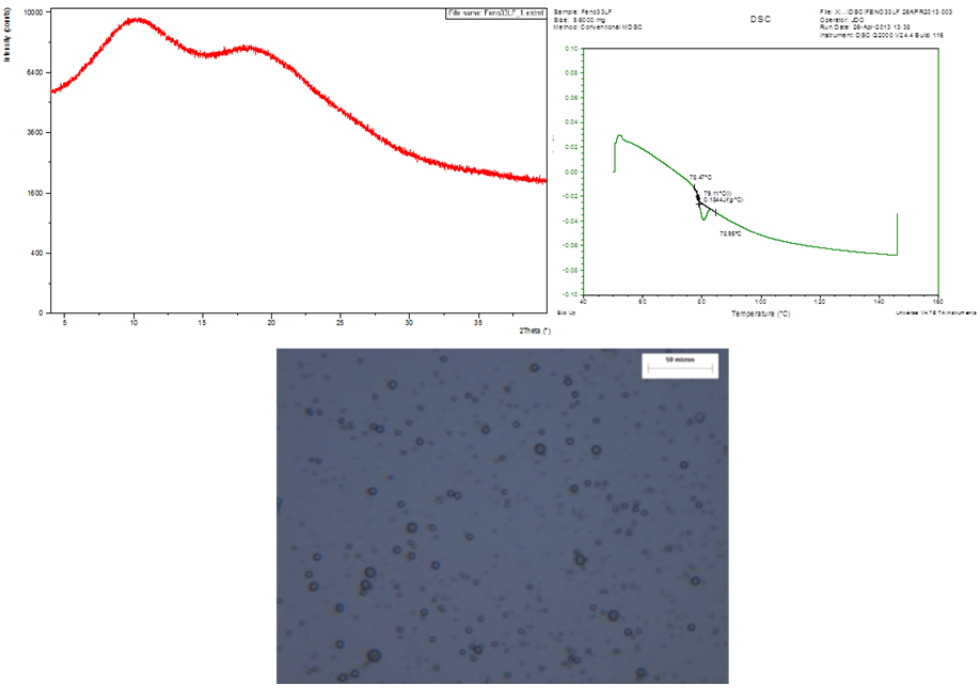

Figure 44. Characterization of spray dried 33.3% Fenofibrate/66.7% HPMCAS-LF by PXRD, mDSC and PLM.

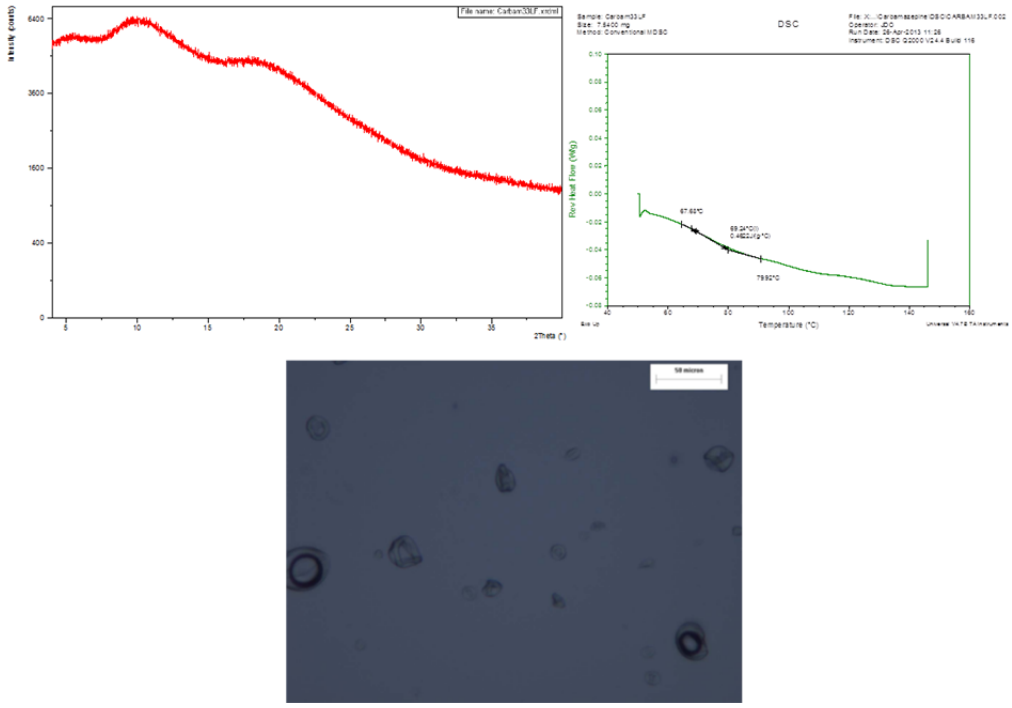

Figure 45. Characterization of spray dried 33.3% Carbamazepine/66.7% HPMCAS-LF by PXRD, mDSC and PLM.

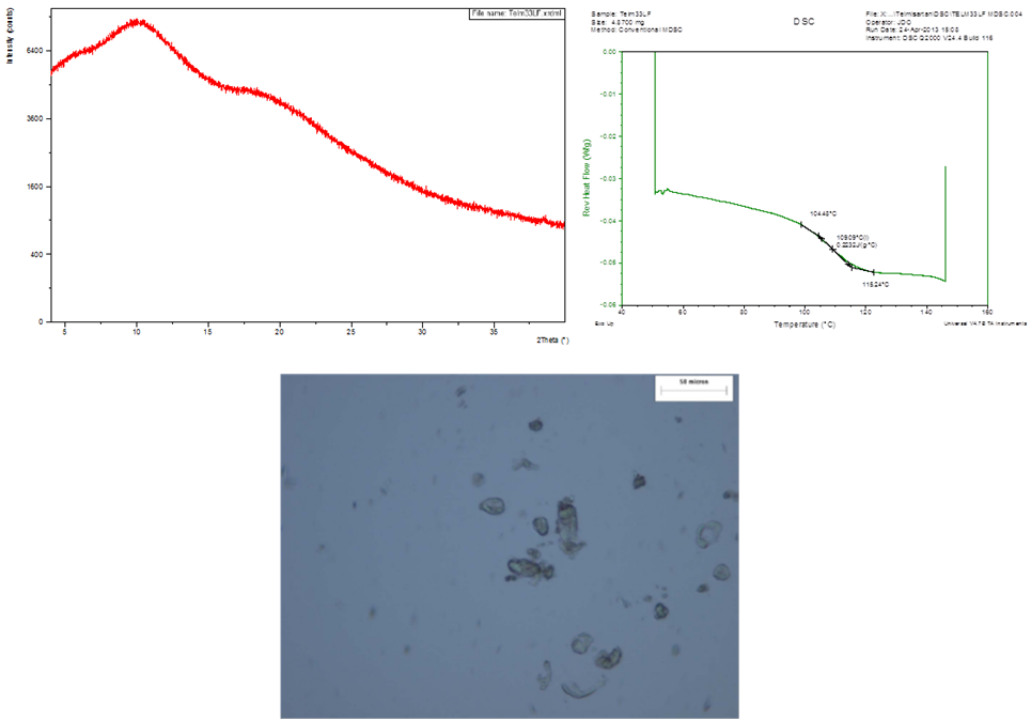

Figure 46. Characterization of spray dried 33.3% Telmisartan/66.7% HPMCAS-LF by PXRD, mDSC and PLM.

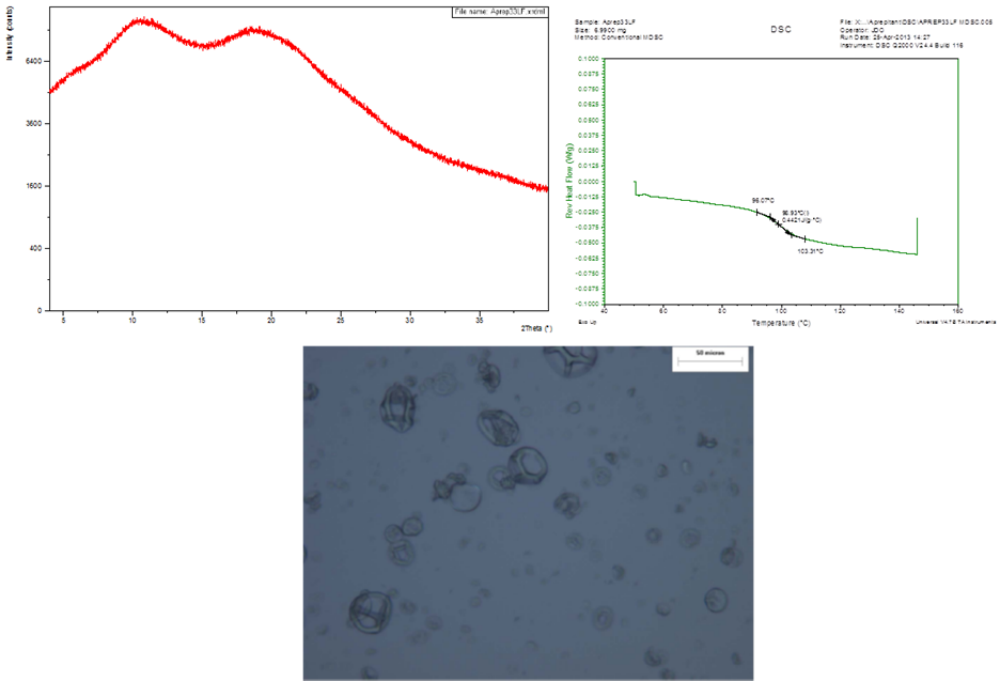

Figure 47. Characterization of spray dried 33.3% Aprepitant/66.7% HPMCAS-LF by PXRD, mDSC and PLM.

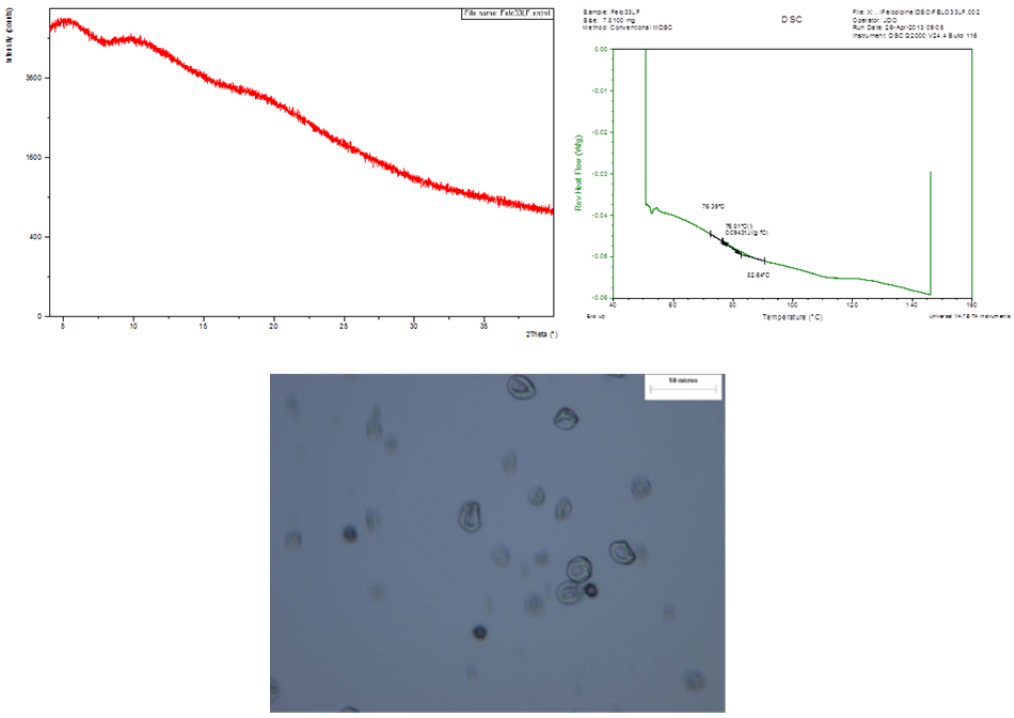

Figure 48. Characterization of spray dried 33.3% Felodipine/66.7% HPMCAS-LF by PXRD, mDSC and PLM.

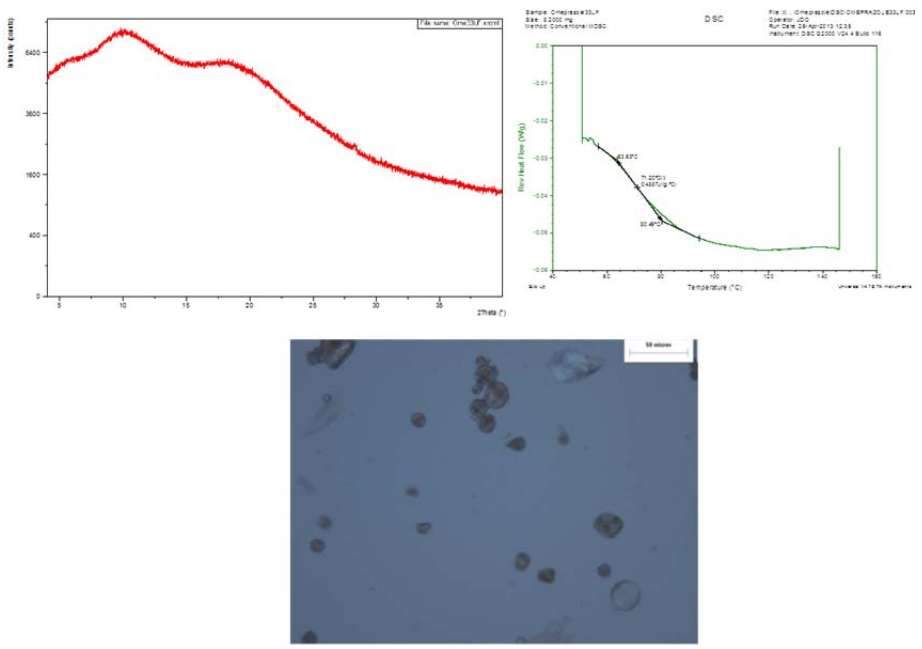

Figure 49. Characterization of spray dried 33.3% Omeprazole/66.7% HPMCAS-LF by PXRD, mDSC and PLM.

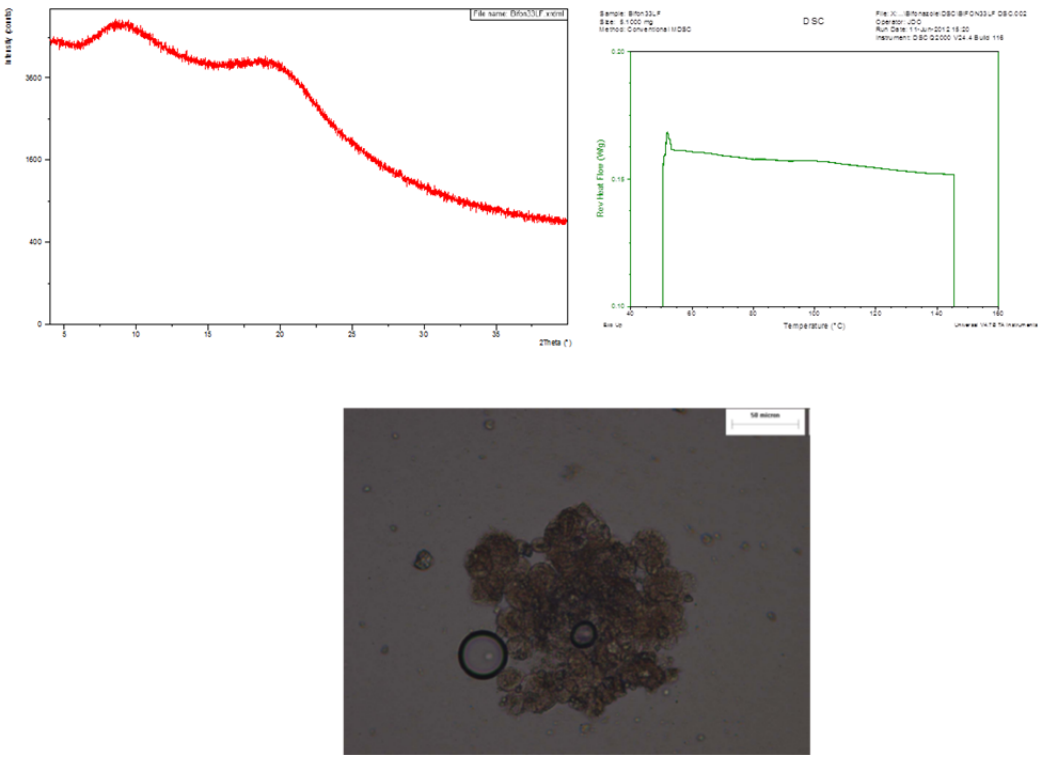

Figure 50. Characterization of spray dried 33.3% Bifonazole/66.7% HPMCAS-LF by PXRD, mDSC and PLM.

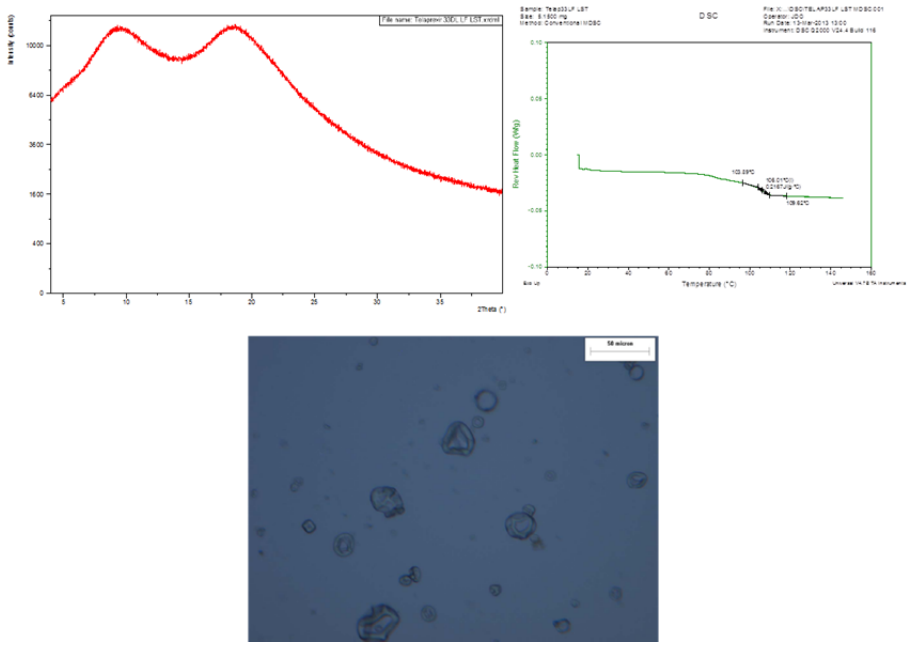

Figure 51. Characterization of spray dried 33.3% Telaprevir/66.7% HPMCAS-LF by PXRD, mDSC and PLM.

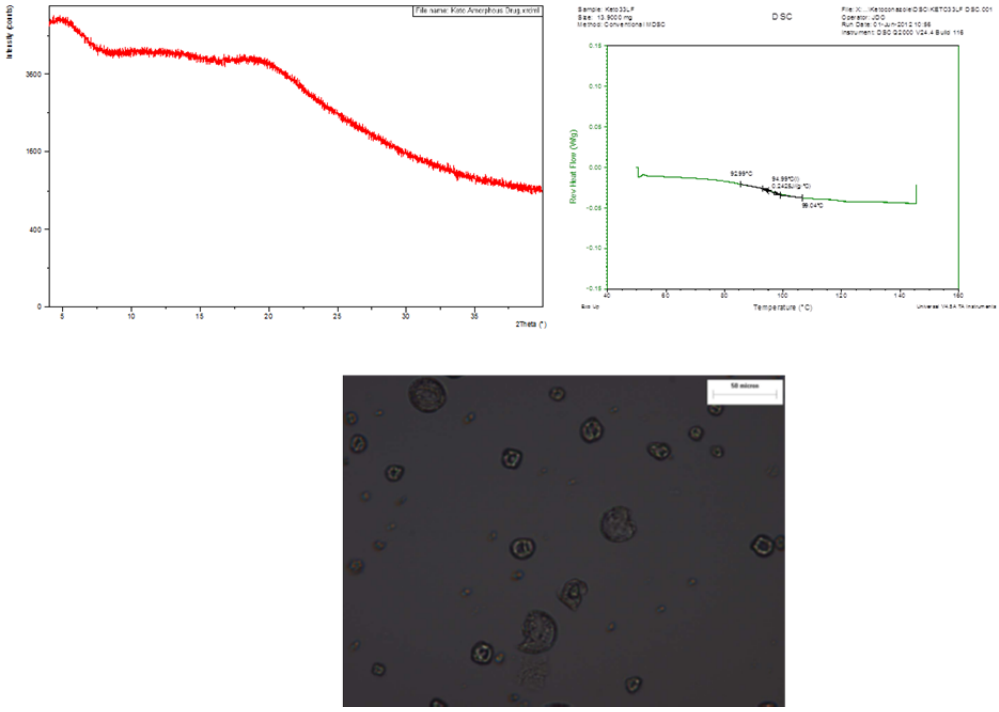

Figure 52. Characterization of spray dried 33.3% Ketoconazole/66.7% HPMCAS-LF by PXRD, mDSC and PLM.

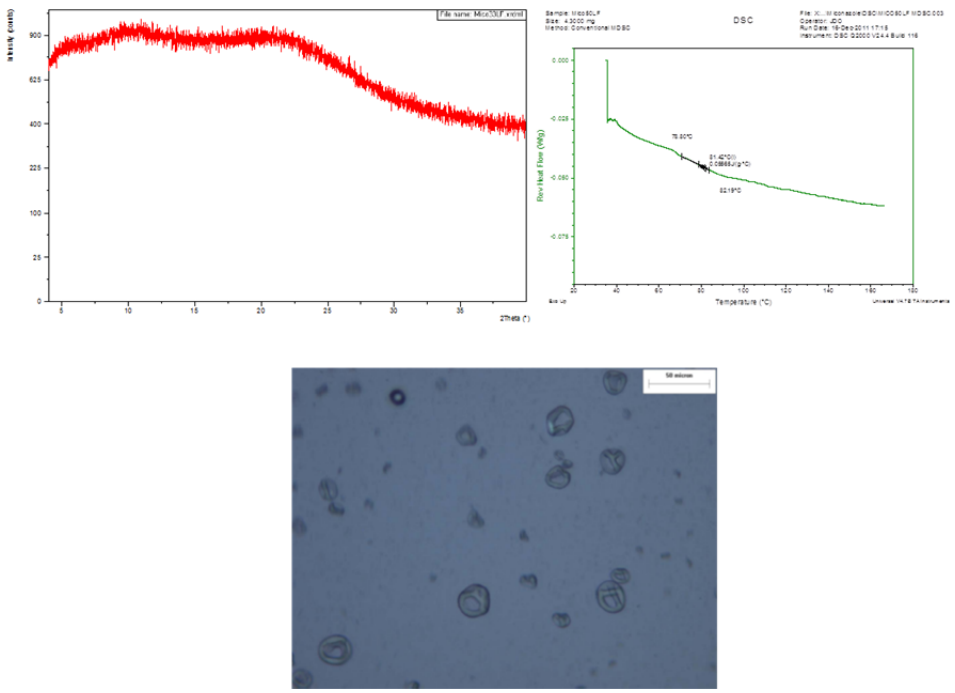

Figure 53. Characterization of spray dried 33.3% Miconazole/66.7% HPMCAS-LF by PXRD, mDSC and PLM.

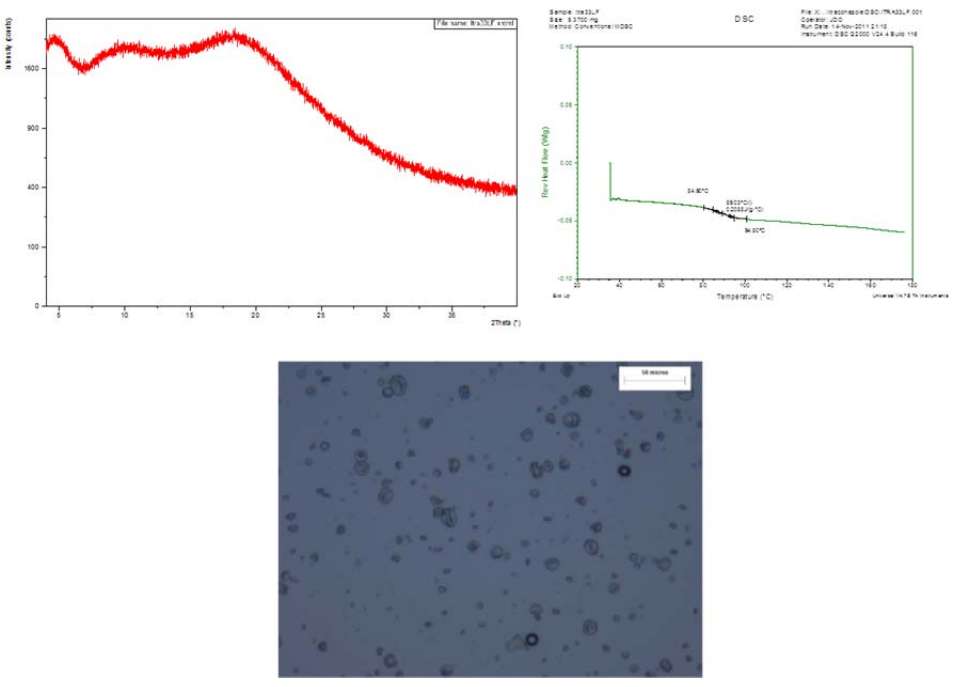

Figure 54. Characterization of spray dried 33.3% Itraconazole/66.7% HPMCAS-LF by PXRD, mDSC and PLM.

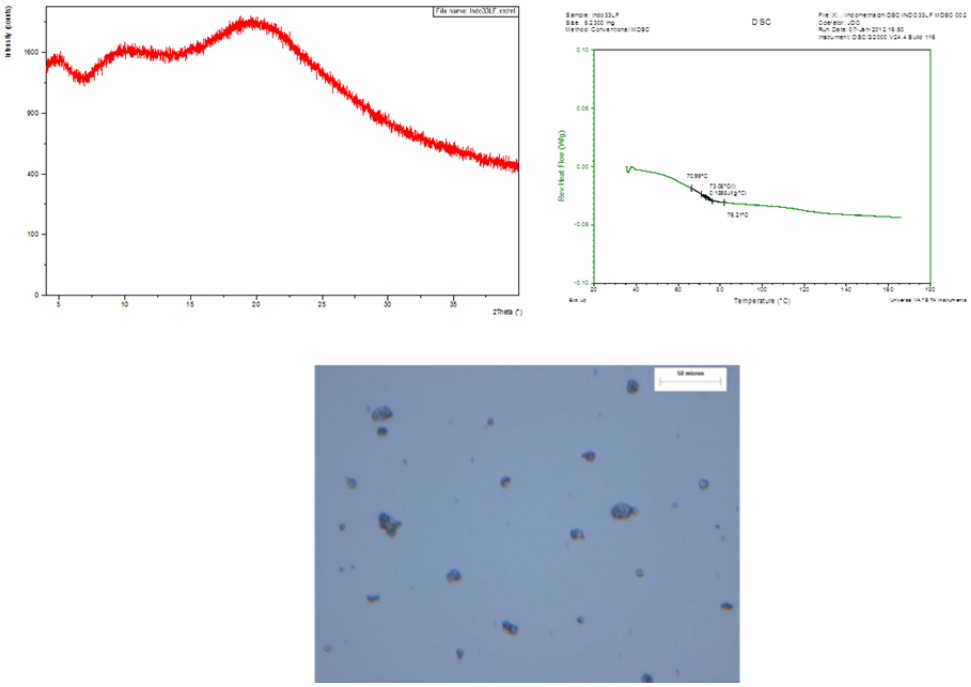

Figure 55. Characterization of spray dried 33.3% Indomethacin/66.7% HPMCAS-LF by PXRD, mDSC and PLM.

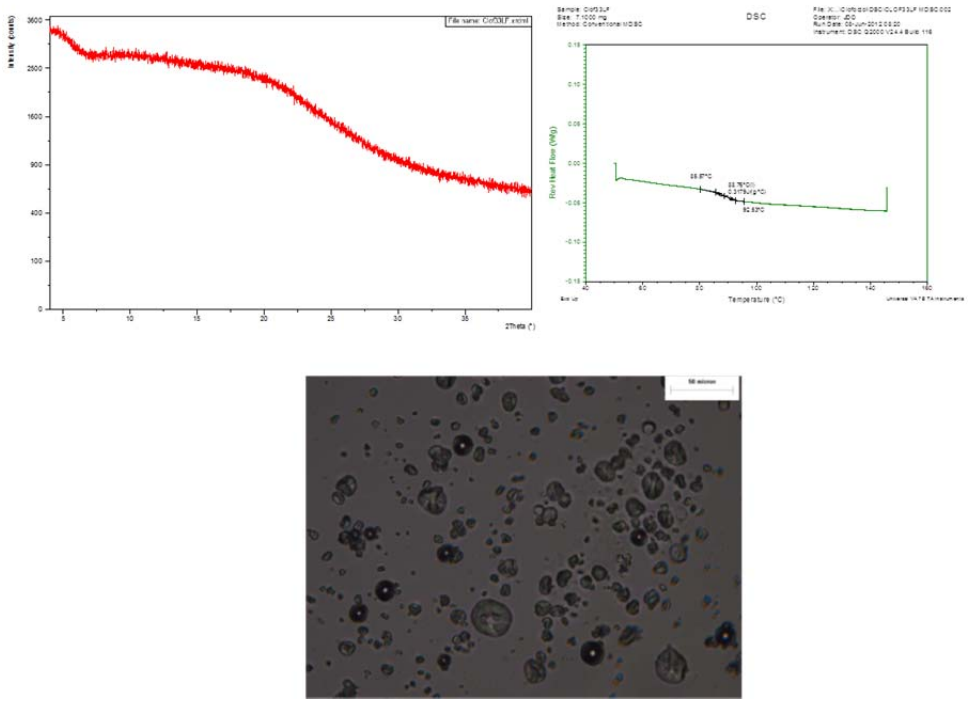

Figure 56. Characterization of spray dried 33.3% Clofoctol/66.7% HPMCAS-LF by PXRD, mDSC and PLM.

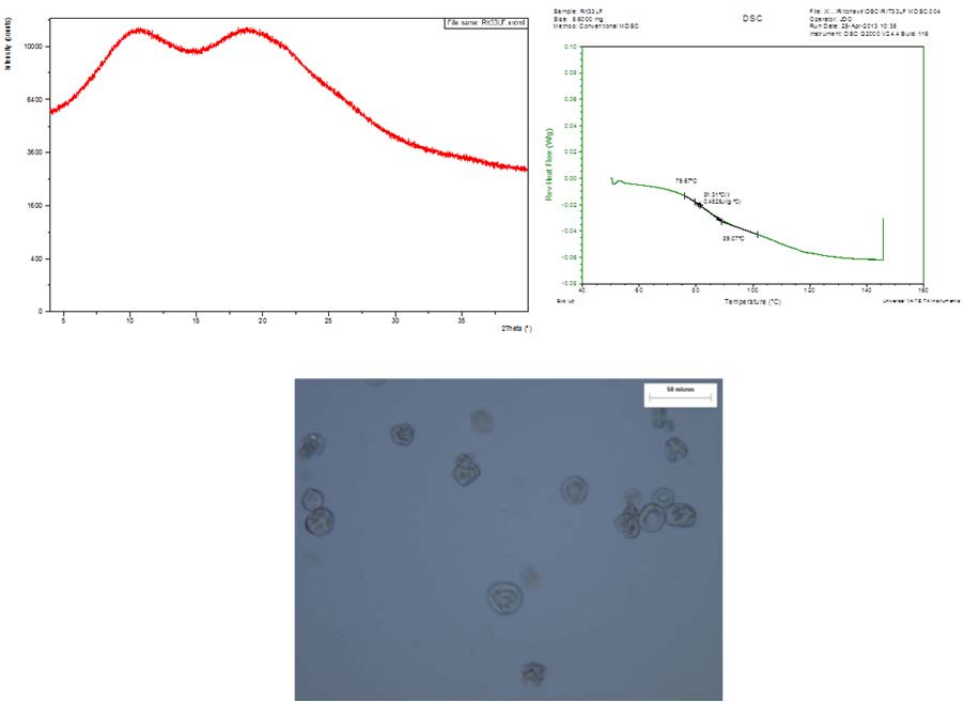

Figure 57. Characterization of spray dried 33.3% Ritonavir/66.7% HPMCAS-LF by PXRD, mDSC and PLM.

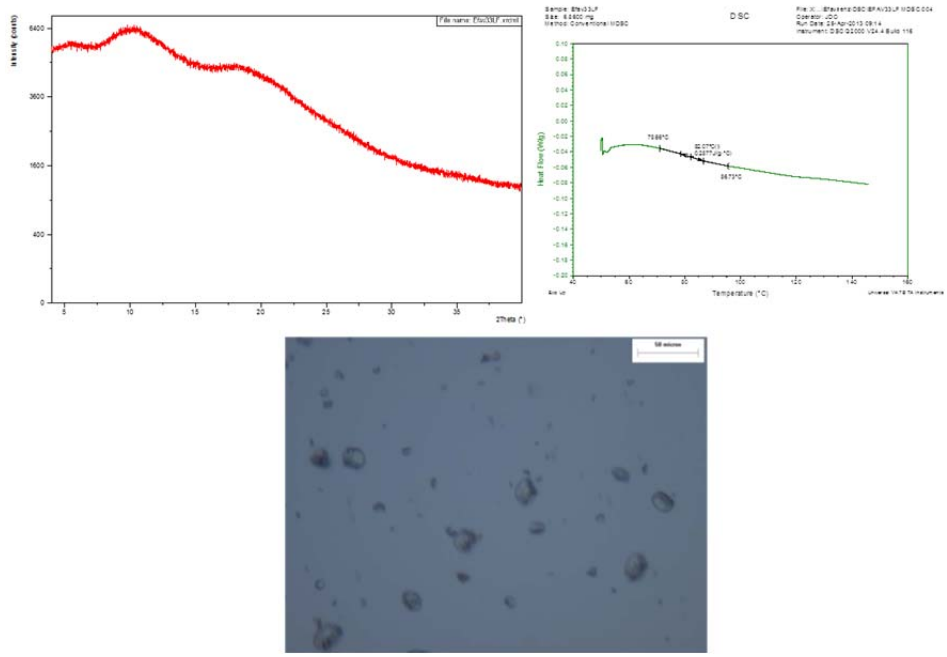

Figure 58. Characterization of spray dried 33.3% Efavirenz/66.7% HPMCAS-LF by PXRD, mDSC and PLM.

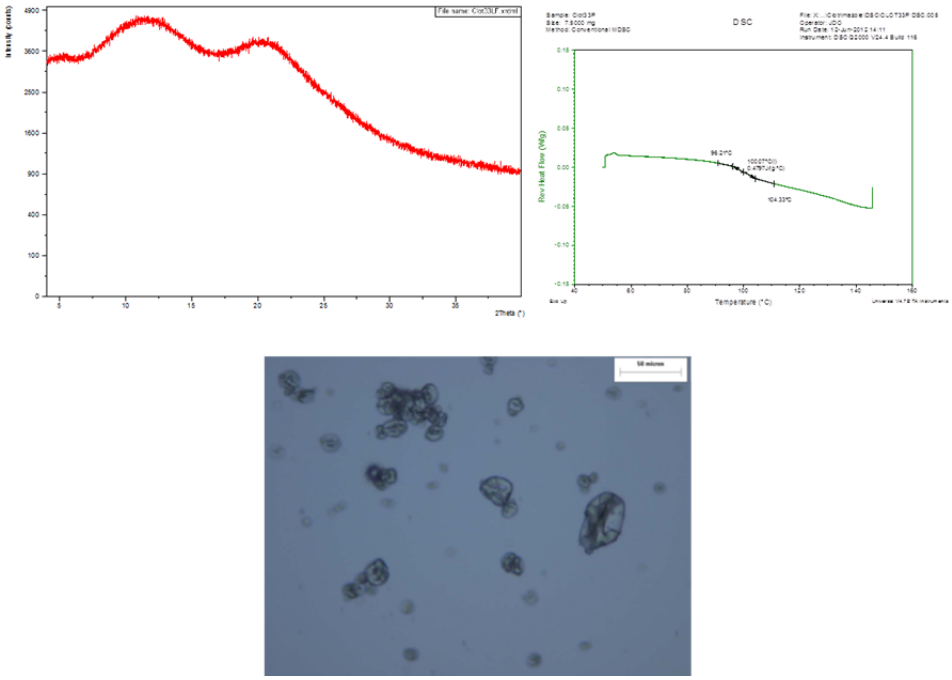

Figure 59. Characterization of spray dried 33.3% Clotrimazole/66.7% HPMCAS-LF by PXRD, mDSC and PLM.

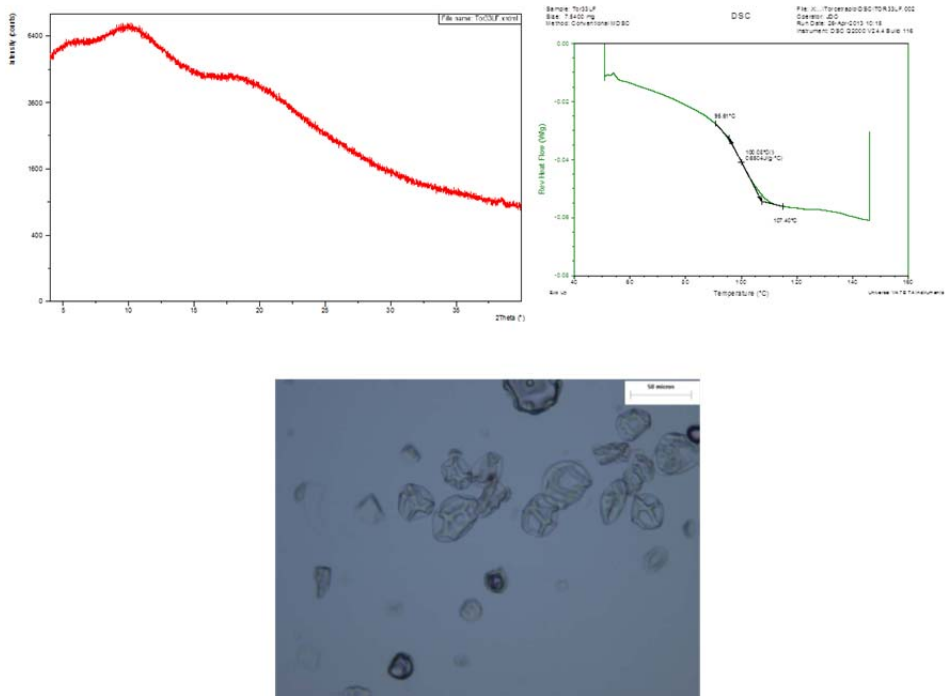

Figure 60. Characterization of spray dried 33.3% Torcetrapib/66.7% HPMCAS-LF by PXRD, mDSC and PLM.

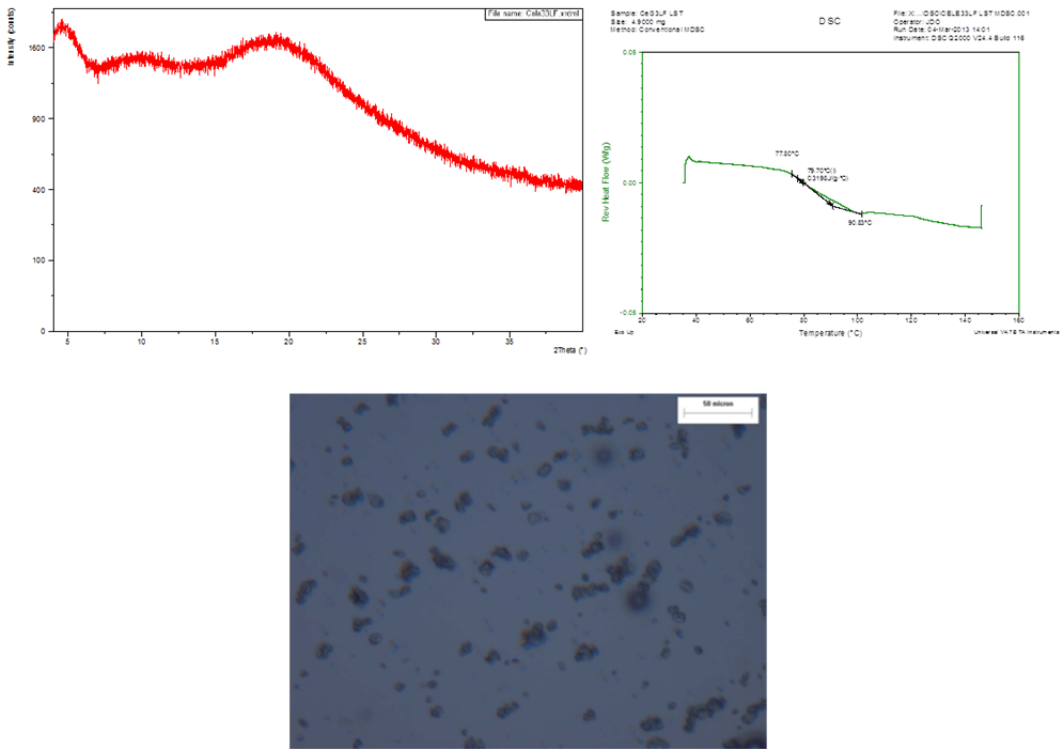

Figure 61. Characterization of spray dried 33.3% Celecoxib/66.7% HPMCAS-LF by PXRD, mDSC and PLM.

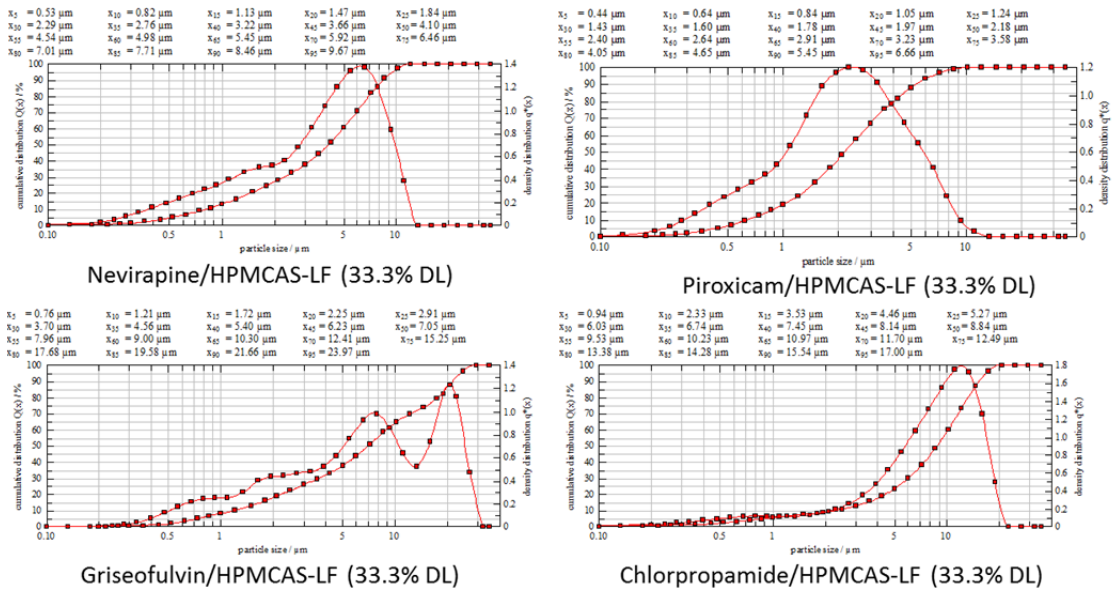

Figure 62. Particle Size data for spray dried amorphous dispersions of Nevirapine, Piroxicam, Griseofulvin and Chlorpropamide in HPMCAS-LF at 33.3% DL.

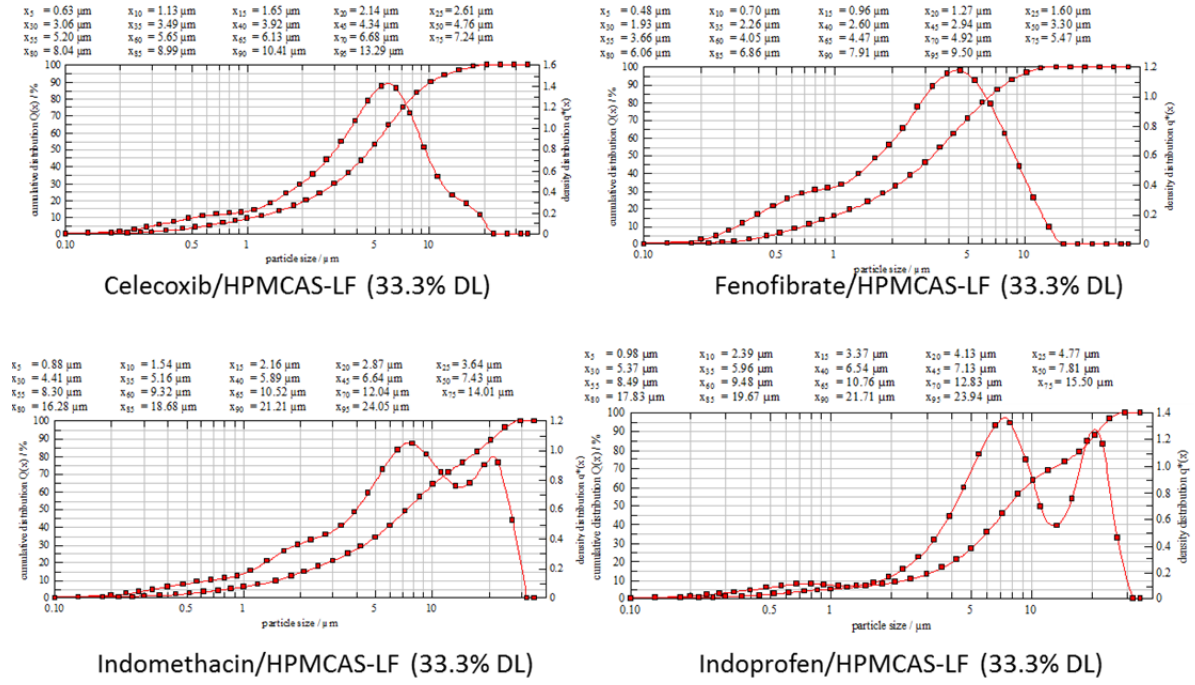

Figure 63. Particle Size data for spray dried amorphous dispersions of Celecoxib, Fenofibrate, Indomethacin, and Indoprofen in HPMCAS-LF at 33.3% DL.

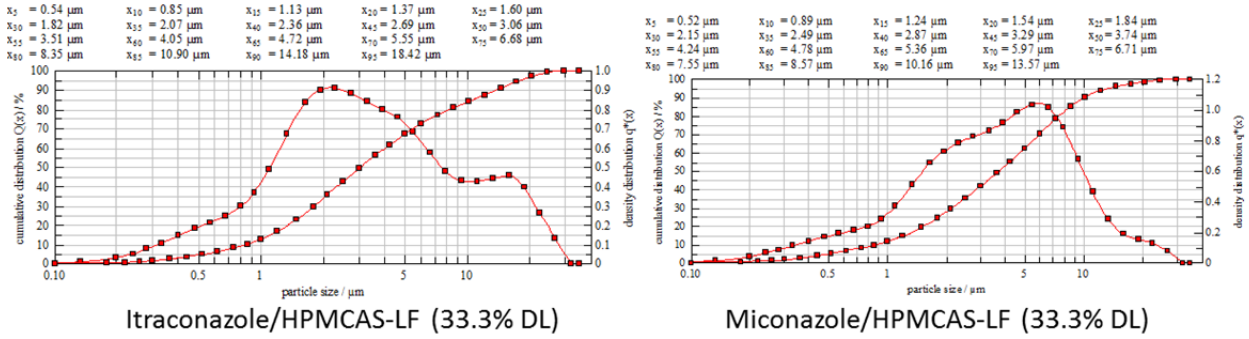

Figure 64. Particle Size data for spray dried amorphous dispersions of Itraconazole and Miconazole in HPMCAS-LF at 33.3% DL.

The particle size data from 10 representative spray dried batches (Figure 62, 63 and 64) suggest that the spray dried dispersion has a relatively narrow particle size distribution with the mean particle size typically falling between 5 and 15 µm.

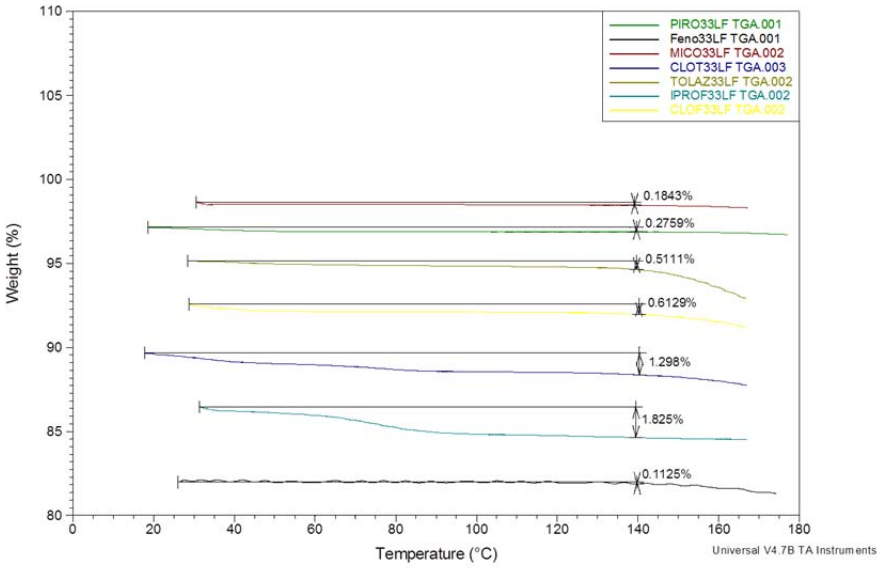

Figure 65. TGA data for spray dried amorphous dispersions of Piroxicam, Fenofibrate, Miconazole, Clotrimazole, Tolazamide, Indoprofen and Clofoctol in HPMCAS-LF at 33.3% DL.

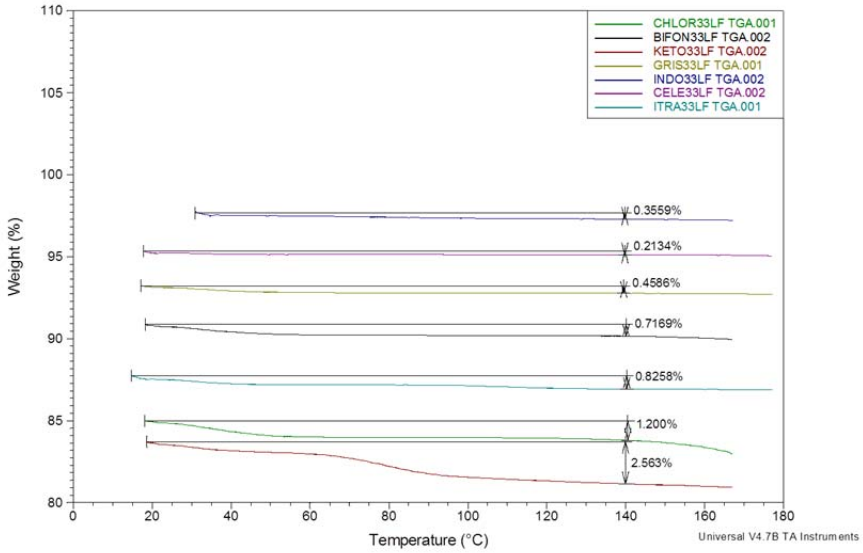

Figure 66. TGA data for spray dried amorphous dispersions of Chlorpropamide, Bifonazole, Ketoconazole, Griseofulvin, Indoprofen, Celecoxib and Intraconazole in HPMCAS-LF at 33.3% DL.

The TGA data from 14 representative spray dried batches (Figure 65 and 66) suggests that the spray dried dispersion has a relatively low levels of residual moisture/organic solvent. Levels are typically < 1.5%.

Table 5. Potency Determination for 6 Batches of Spray Dried Dispersions.

Sample	Area	ug/mL	mg	ug/mL	% Target
Celecoxib/HPMCAS-LF 33.3% DL	2462871	201.8	30.4	202.5	99.7
Fenofibrate/HPMCAS-LF 33.3% DL	1133585	143.8	42.3	140.859	102.1
Griseofulvin/HPMCAS-LF 33.3% DL	1925526	221.6	33.2	221.1	100.2
Itraconazole/HPMCAS-LF 33.3% DL	2117723	198.0	28.9	192.5	102.9
Nevirapine/HPMCAS-LF 33.3% DL	3017087	212.1	32.2	214.5	98.9
Piroxicam/HPMCAS-LF 33.3% DL	1033485	231.3	33.5	223.1	103.7

The potency data from 6 representative spray dried batches (Table 5) suggests that the spray dried dispersion typically has a potency within 2% of the target potency by weight.

Appendix 2: Amorphous Suspension Physical Stability Data

The range for the onset of crystallization of each compound was determined by PXRD and PLM. The upcoming data supports each assigned range in Figure X.

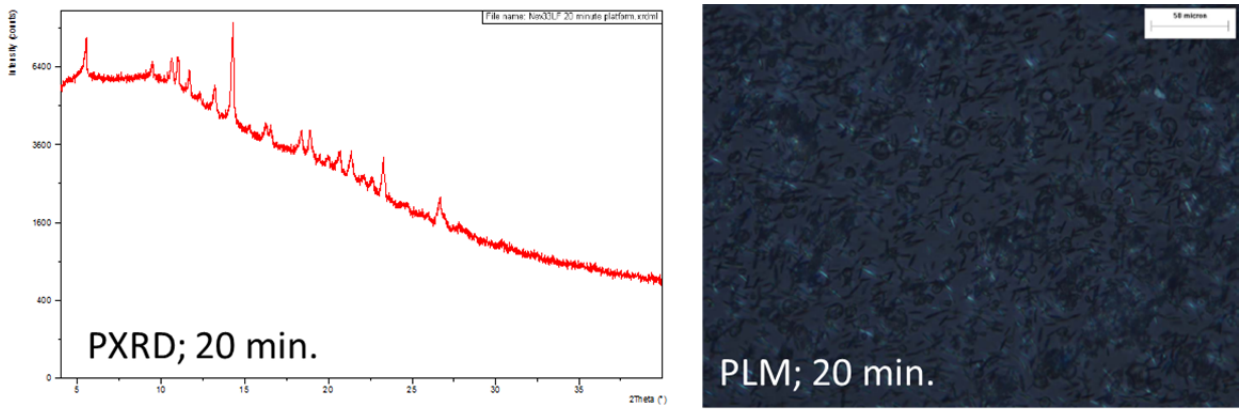

Figure 67. PXRD and PLM data for spray dried Nevirapine/HPMCAS-LF (33.3% Drug Loading) suspended in 0.5% MC + 0.25% SLS + 5 mM HCl after 20 minutes.

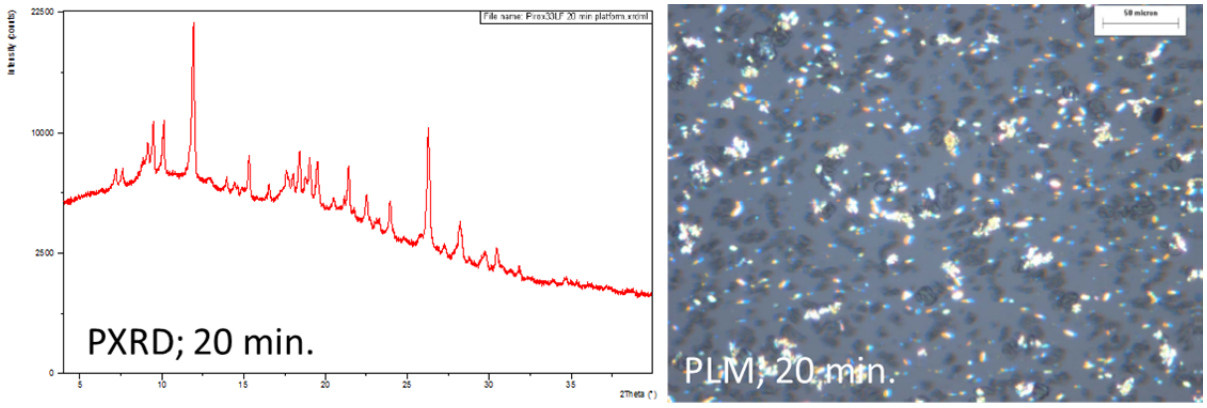

Figure 68. PXRD and PLM data for spray dried Piroxicam/HPMCAS-LF (33.3% Drug Loading) suspended in 0.5% MC + 0.25% SLS + 5 mM HCl after 20 minutes.

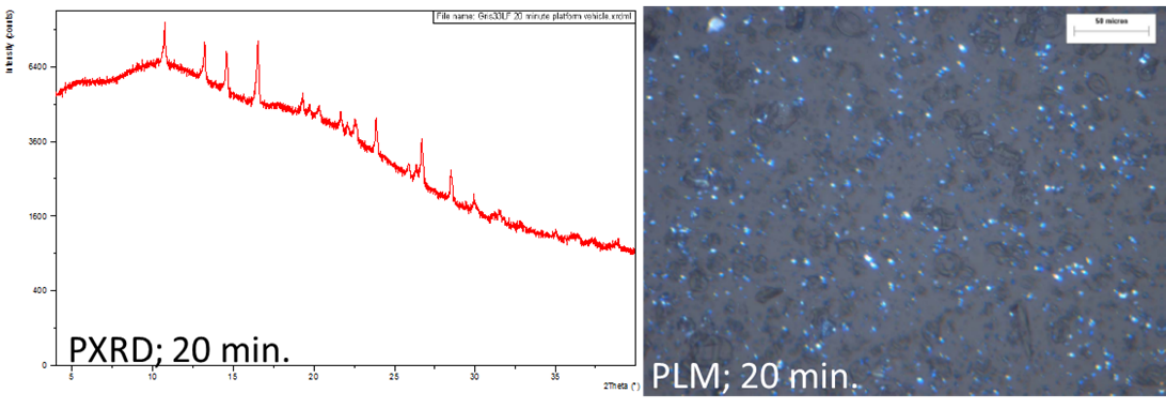

Figure 69. PXRD and PLM data for spray dried Griseofulvin/HPMCAS-LF (33.3% Drug Loading) suspended in 0.5% MC + 0.25% SLS + 5 mM HCl after 20 minutes.

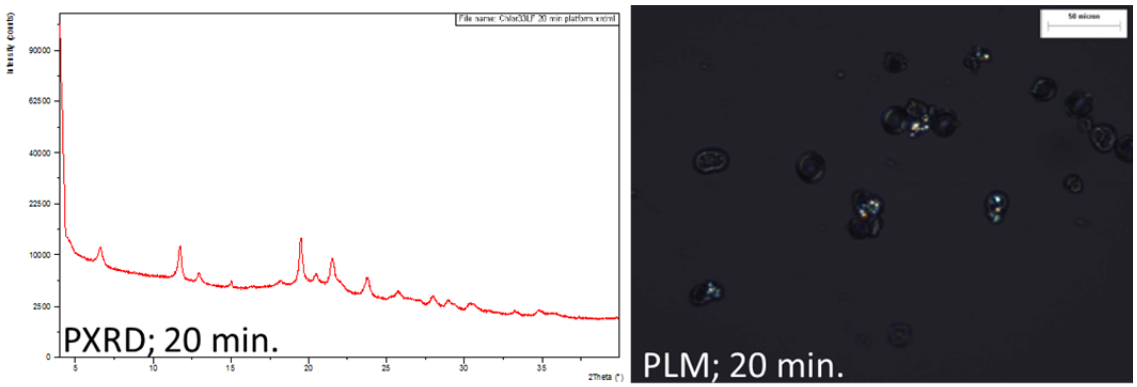

Figure 70. PXRD and PLM data for spray dried Chlorpropamide/HPMCAS-LF (33.3% Drug Loading) suspended in 0.5% MC + 0.25% SLS + 5 mM HCl after 20 minutes.

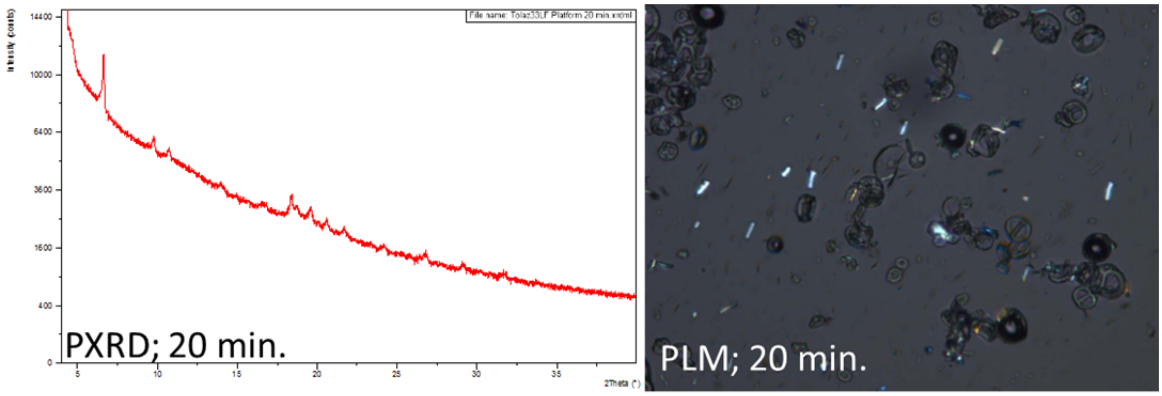

Figure 71. PXRD and PLM data for spray dried Tolazamide/HPMCAS-LF (33.3% Drug Loading) suspended in 0.5% MC + 0.25% SLS + 5 mM HCl after 20 minutes.

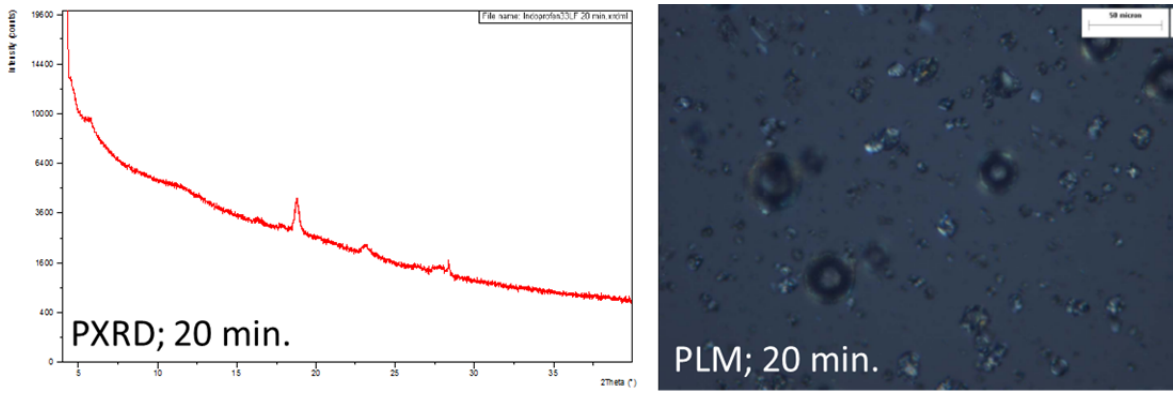

Figure 72. PXRD and PLM data for spray dried Indoprofen/HPMCAS-LF (33.3% Drug Loading) suspended in 0.5% MC + 0.25% SLS + 5 mM HCl after 20 minutes.

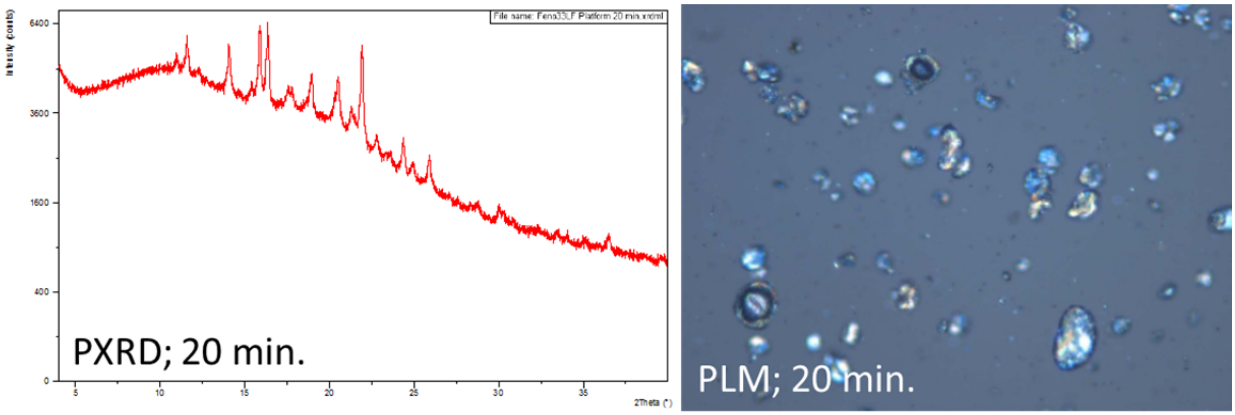

Figure 73. PXRD and PLM data for spray dried Fenofibrate/HPMCAS-LF (33.3% Drug Loading) suspended in 0.5% MC + 0.25% SLS + 5 mM HCl after 20 minutes.

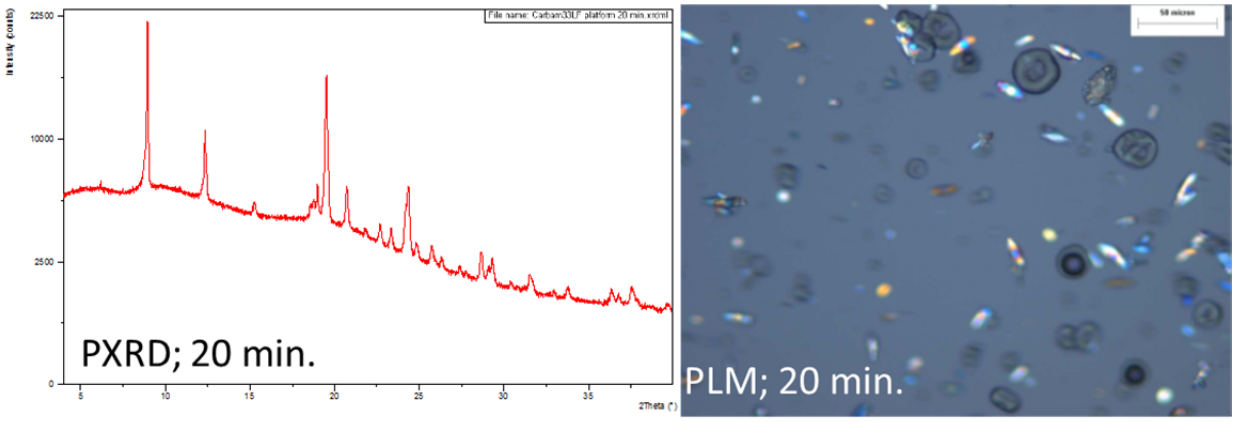

Figure 74. PXRD and PLM data for spray dried Carbamazepine/HPMCAS-LF (33.3% Drug Loading) suspended in 0.5% MC + 0.25% SLS + 5 mM HCl after 20 minutes.

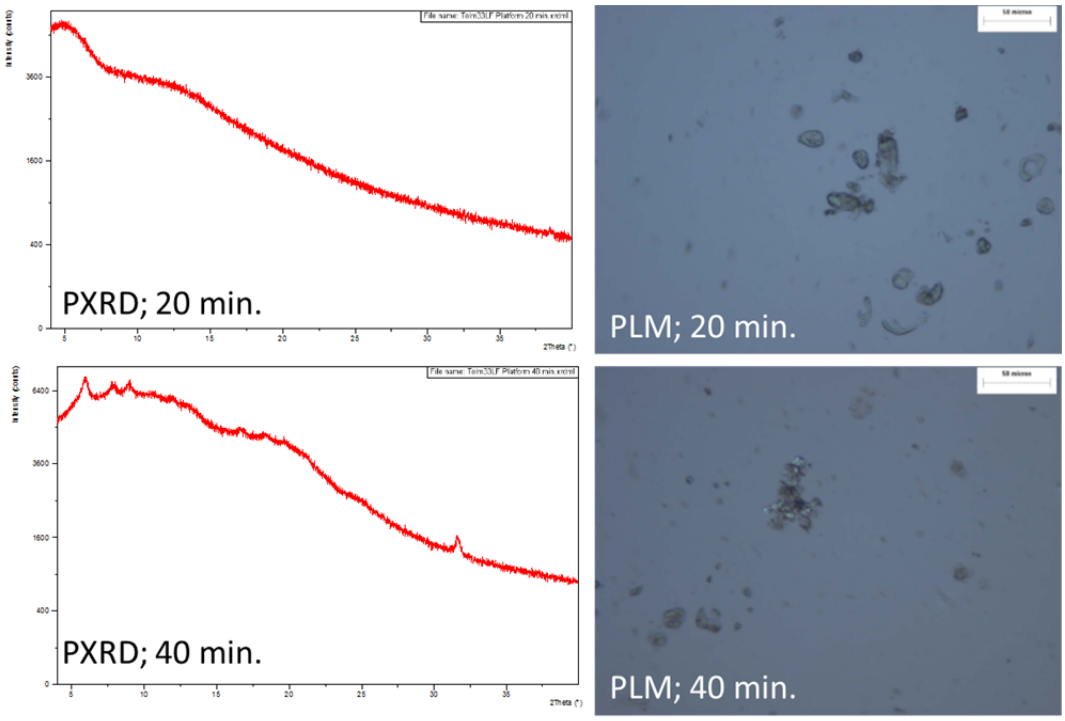

Figure 75. PXRD and PLM data for spray dried Telmisartan/HPMCAS-LF (33.3% Drug Loading) suspended in 0.5% MC + 0.25% SLS + 5 mM HCl after 20 and 40 minutes.

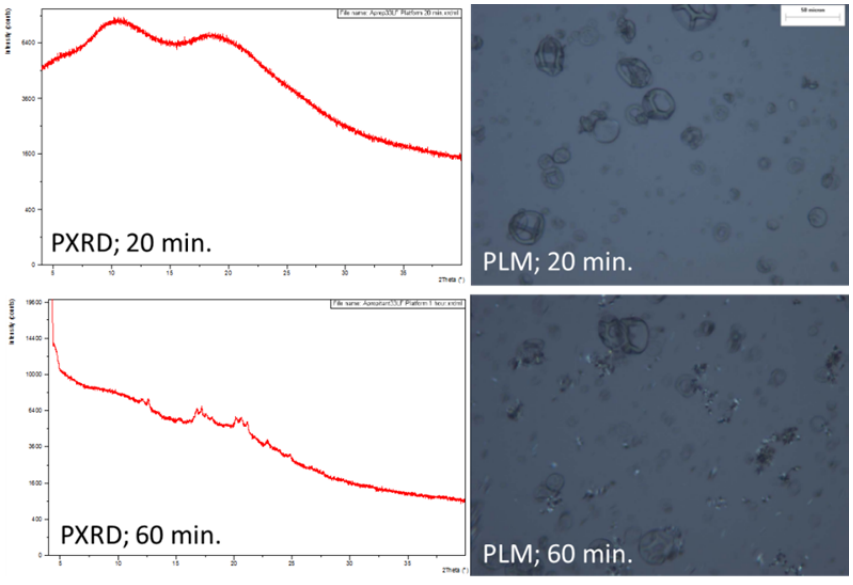

Figure 76. PXRD and PLM data for spray dried Aprepitant/HPMCAS-LF (33.3% Drug Loading) suspended in 0.5% MC + 0.25% SLS + 5 mM HCl after 20 and 60 minutes.

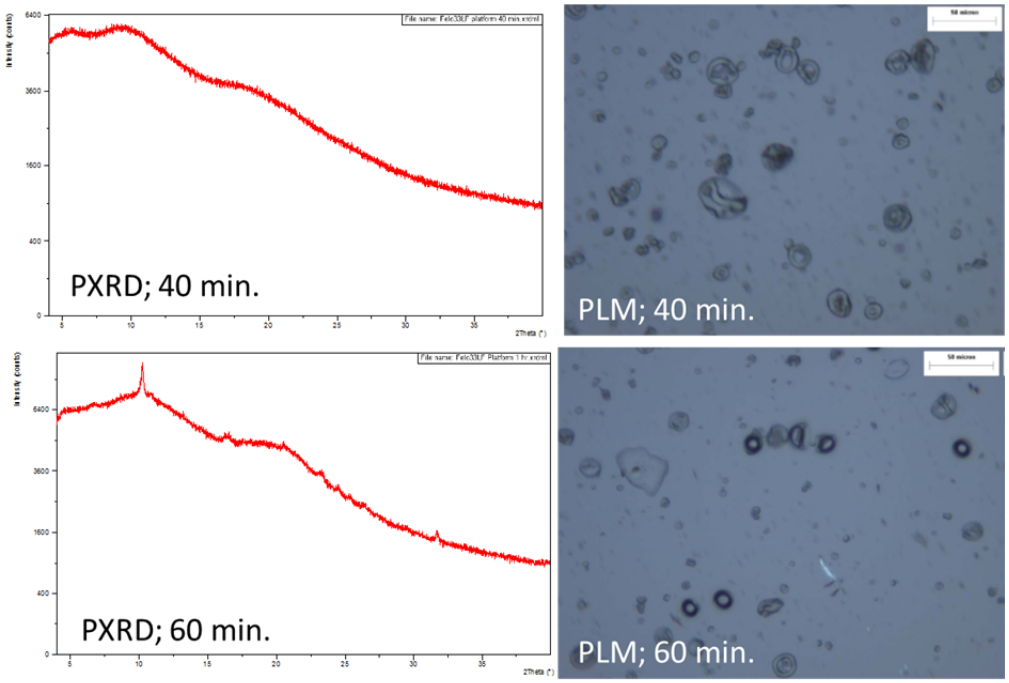

Figure 77. PXRD and PLM data for spray dried Felodipine/HPMCAS-LF (33.3% Drug Loading) suspended in 0.5% MC + 0.25% SLS + 5 mM HCl after 40 and 60 minutes.

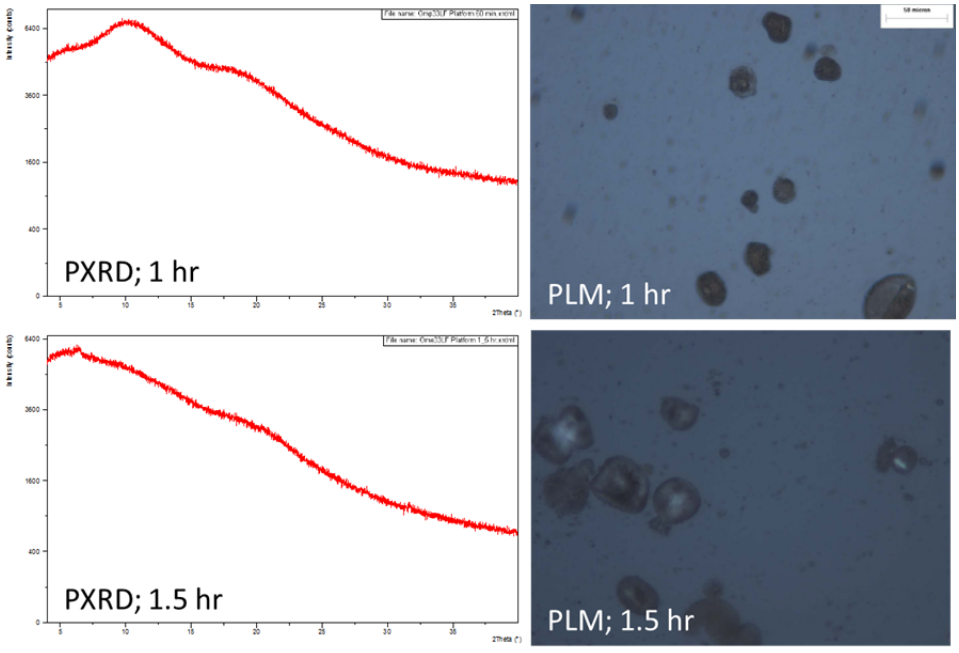

Figure 78. PXRD and PLM data for spray dried Omeprazole/HPMCAS-LF (33.3% Drug Loading) suspended in 0.5% MC + 0.25% SLS + 5 mM HCl after 1 and 1.5 hours.

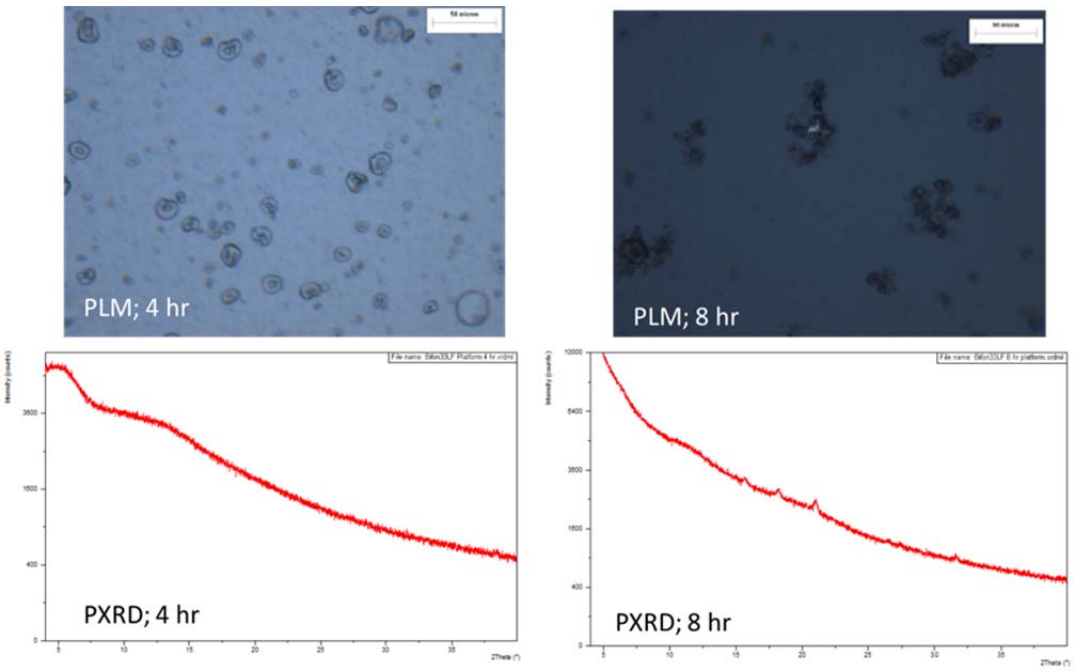

Figure 79. PXRD and PLM data for spray dried Bifonazole/HPMCAS-LF (33.3% Drug Loading) suspended in 0.5% MC + 0.25% SLS + 5 mM HCl after 4 and 8 hours.

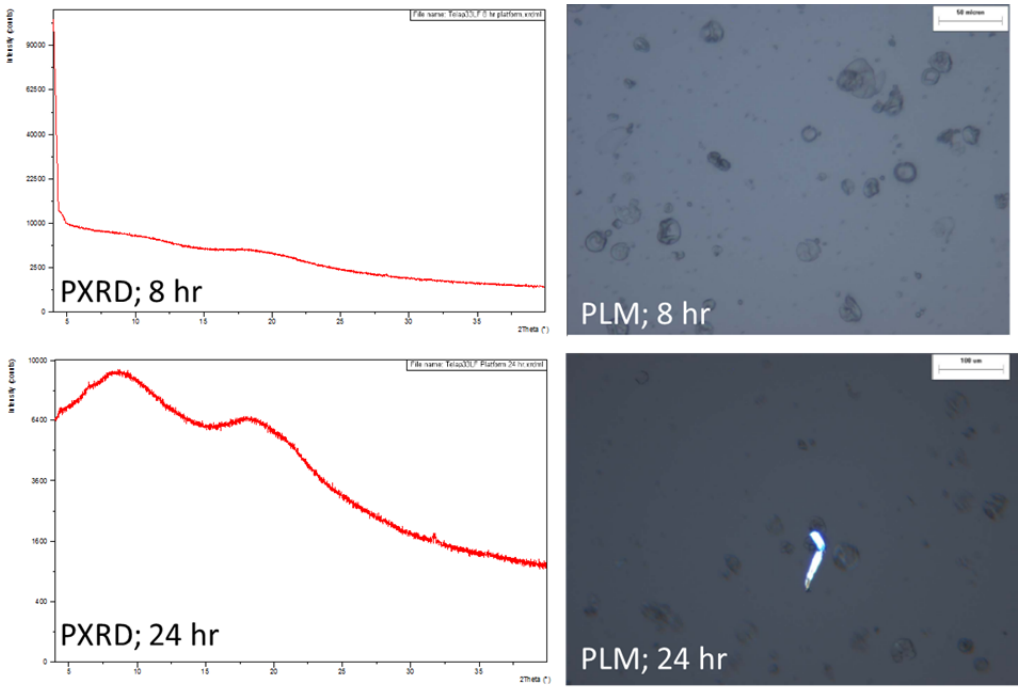

Figure 80. PXRD and PLM data for spray dried Telaprevir/HPMCAS-LF (33.3% Drug Loading) suspended in 0.5% MC + 0.25% SLS + 5 mM HCl after 8 and 24 hours.

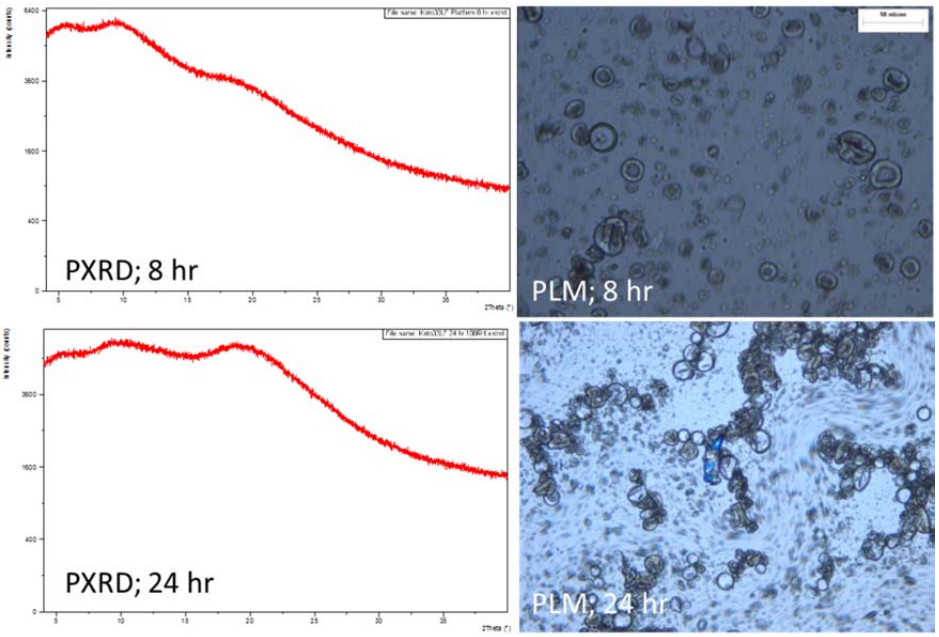

Figure 81. PXRD and PLM data for spray dried Ketoconazole/HPMCAS-LF (33.3% Drug Loading) suspended in 0.5% MC + 0.25% SLS + 5 mM HCl after 8 and 24 hours.

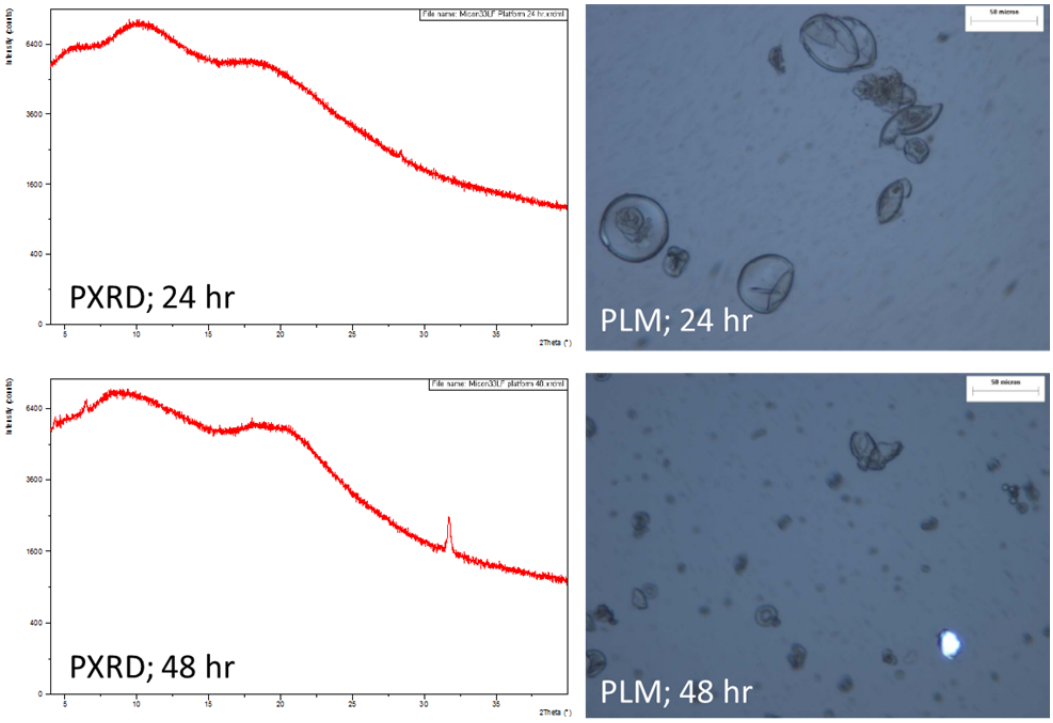

Figure 82. PXRD and PLM data for spray dried Miconazole/HPMCAS-LF (33.3% Drug Loading) suspended in 0.5% MC + 0.25% SLS + 5 mM HCl after 24 and 48 hours.

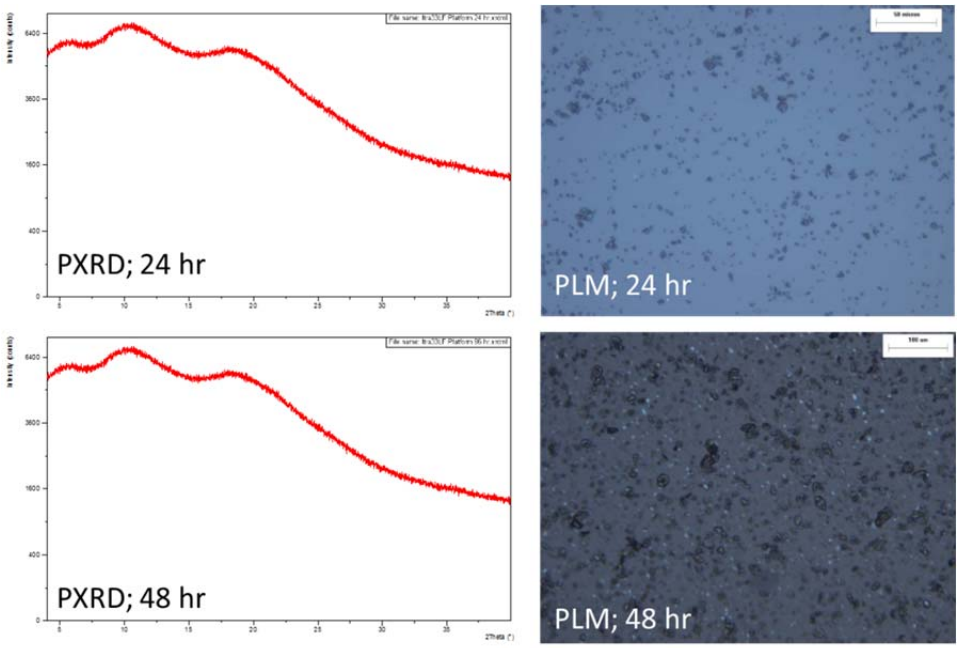

Figure 83. PXRD and PLM data for spray dried Itraconazole/HPMCAS-LF (33.3% Drug Loading) suspended in 0.5% MC + 0.25% SLS + 5 mM HCl after 24 and 48 hours.

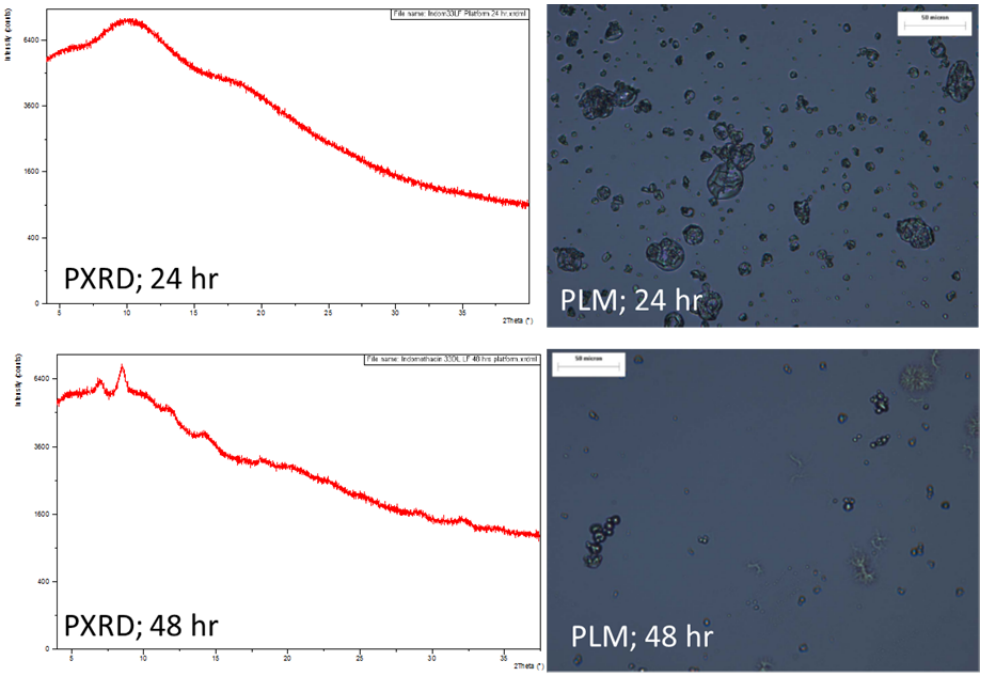

Figure 84. PXRD and PLM data for spray dried Indomethacin/HPMCAS-LF (33.3% Drug Loading) suspended in 0.5% MC + 0.25% SLS + 5 mM HCl after 24 and 48 hours.

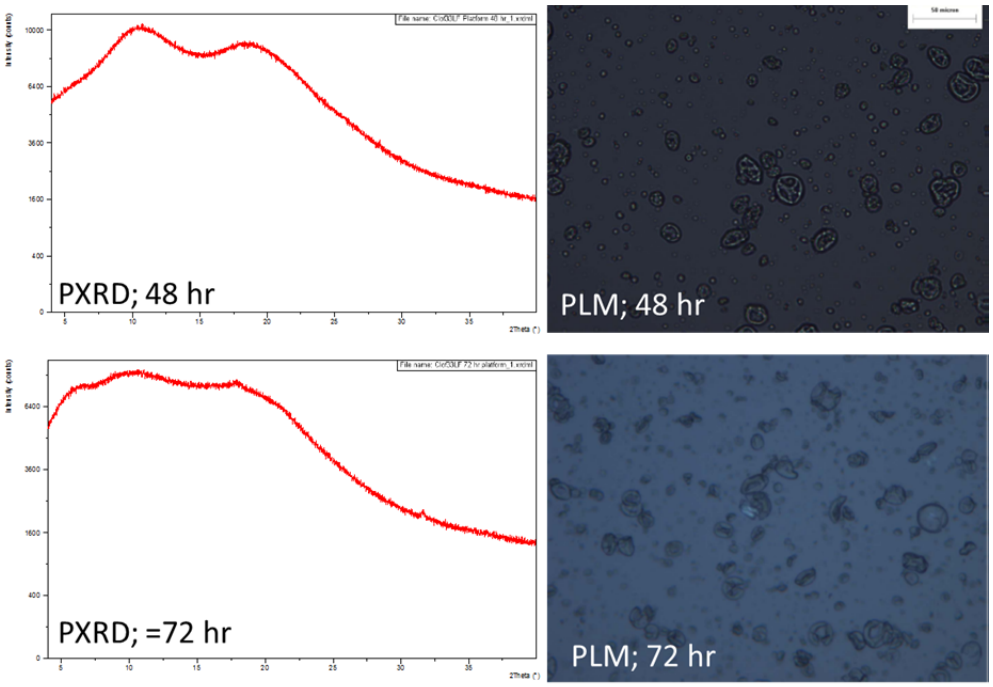

Figure 85. PXRD and PLM data for spray dried Clofoctol/HPMCAS-LF (33.3% Drug Loading) suspended in 0.5% MC + 0.25% SLS + 5 mM HCl after 48 and 72 hours.

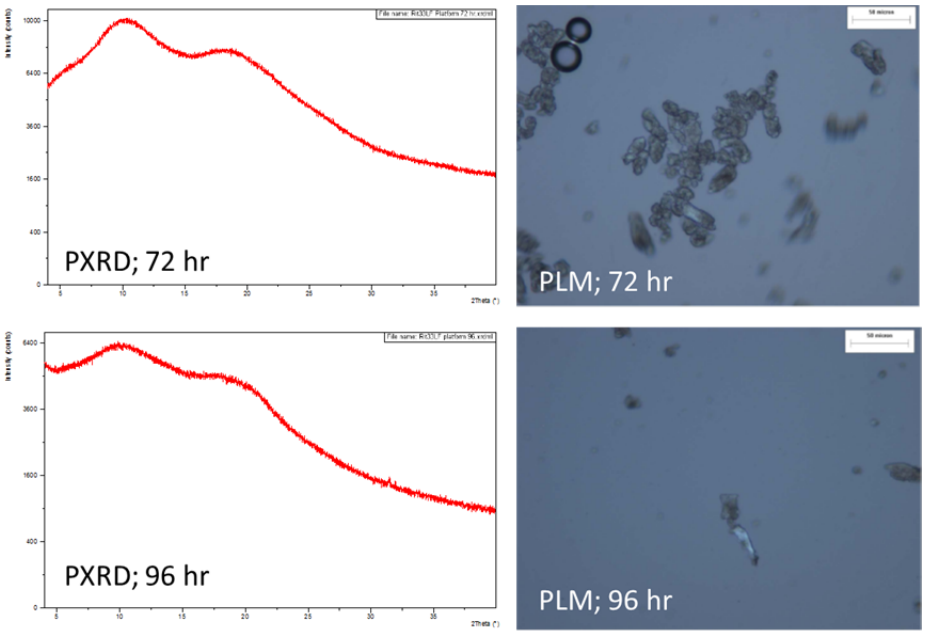

Figure 86. PXRD and PLM data for spray dried Ritonavir/HPMCAS-LF (33.3% Drug Loading) suspended in 0.5% MC + 0.25% SLS + 5 mM HCl after 72 and 96 hours.

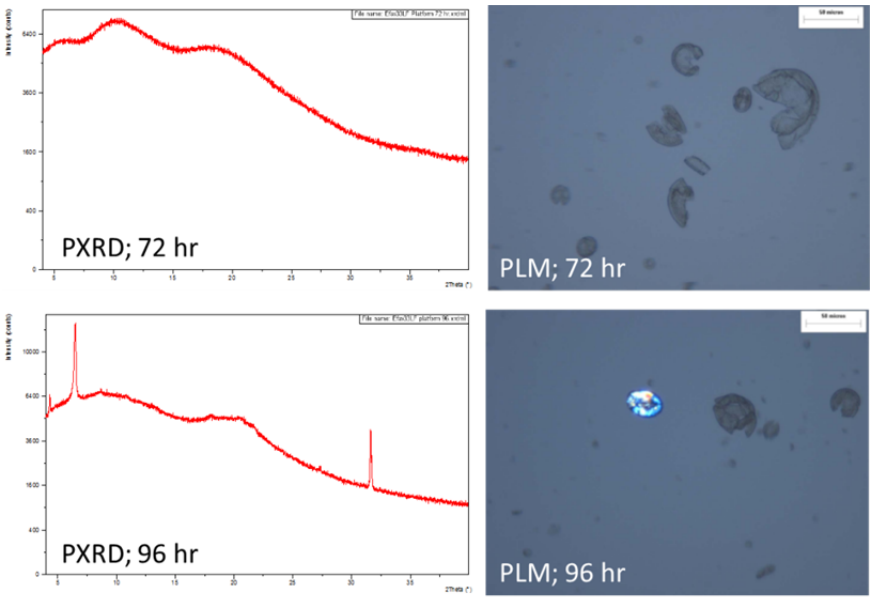

Figure 87. PXRD and PLM data for spray dried Efavirenz/HPMCAS-LF (33.3% Drug Loading) suspended in 0.5% MC + 0.25% SLS + 5 mM HCl after 72 and 96 hours.

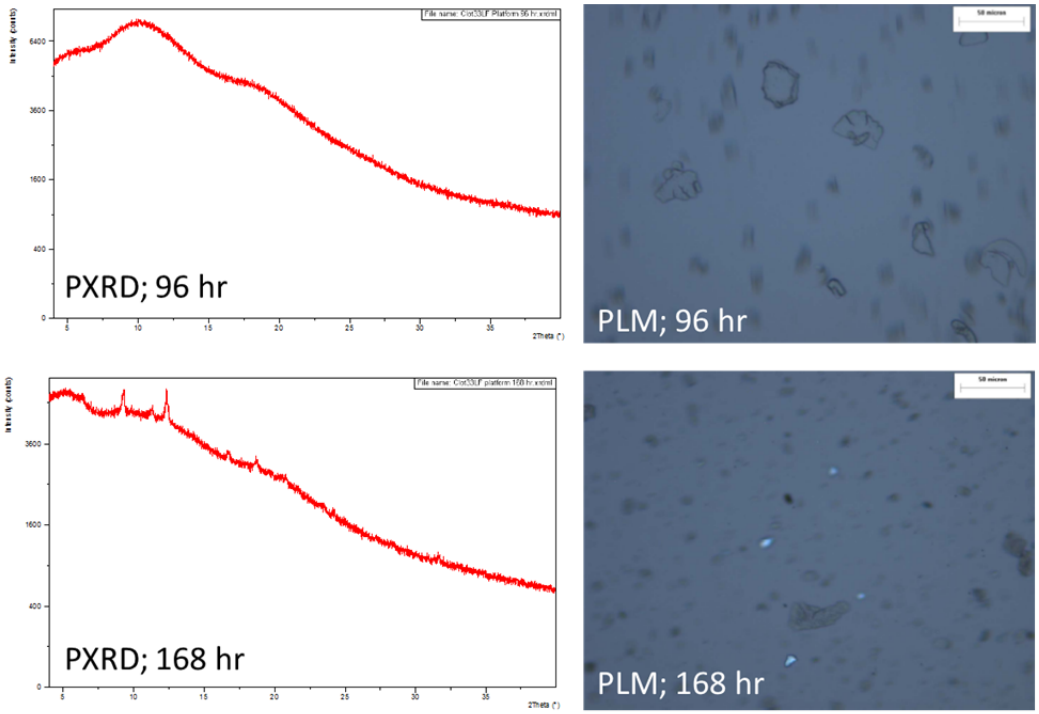

Figure 88. PXRD and PLM data for spray dried Clotrimazole/HPMCAS-LF (33.3% Drug Loading) suspended in 0.5% MC + 0.25% SLS + 5 mM HCl after 96 and 168 hours.

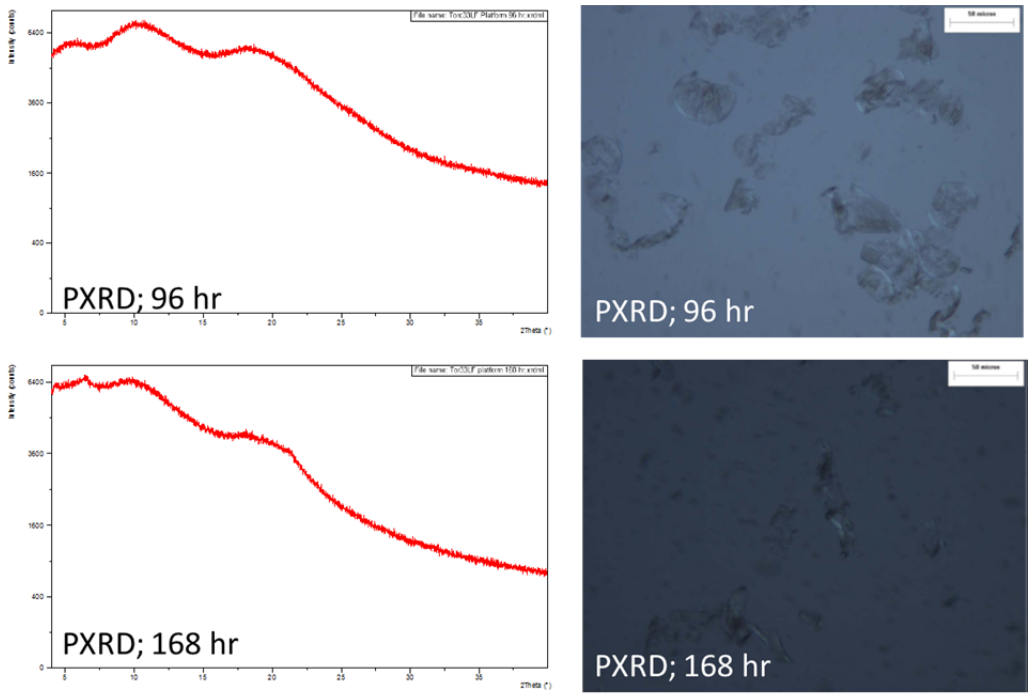

Figure 89. PXRD and PLM data for spray dried Torcetrapib/HPMCAS-LF (33.3% Drug Loading) suspended in 0.5% MC + 0.25% SLS + 5 mM HCl after 96 and 168 hours.

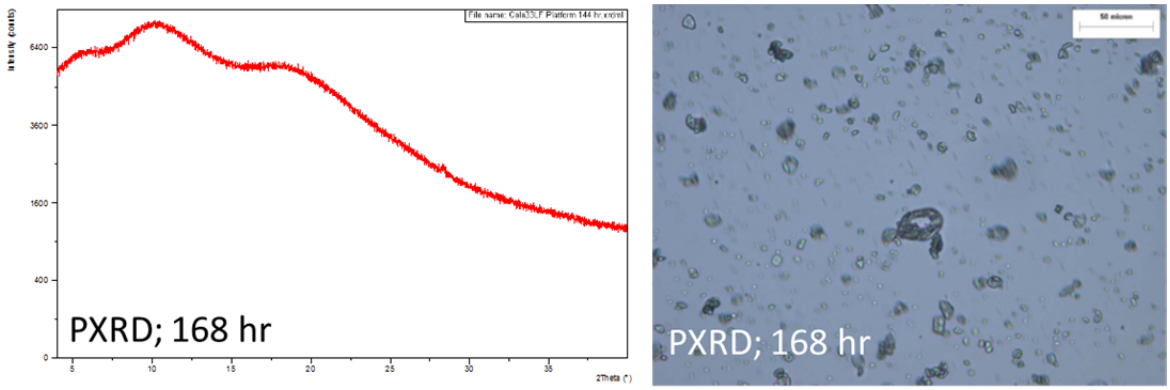

Figure 90. PXRD and PLM data for spray dried Celecoxib/HPMCAS-LF (33.3% Drug Loading) suspended in 0.5% MC + 0.25% SLS + 5 mM HCl after 168 hours.

Appendix 3: Multi-variate Descriptors Data and References

The data to support thermal and hydrophilicity analysis for each compound is provided in Appendix 3. Note that structural data is not provided, because no experiments were conducted to obtain these values.

Thermal data for thesis model compounds:

A summary of the thermal data used in this thesis appears in Table 2. The glass transition values for the dry amorphous dispersions can be found in the characterization data in Appendix 1. As mentioned in the thesis, the Gibbs Free Energy values were calculated using equation 3.

A large portion of the data appears previously in the literature by Baird[62]. This data is summarized in Table 6.

Table 6. Reference thermal data from the Baird publication[62].

Model Compound	Melting Temperature (deg C)	Enthalpy Fusion (kJ/mol)	Entropy Fusion (kJ/K*mol)	Tg, Drug (deg C)	Cyclic DSC Class
Griseofulvin	218	39.1	0.079	89	1
Indoprofen	212	36.0	0.074	50	1
Chlorpropamide	124	27.4	0.069	16	1
Tolazamide	172	43.4	0.098	18	2
Bifonazole	151	39.2	0.092	17	2
Clofoctol	88	35.1	0.097	-4	2
Celecoxib	163	37.4	0.086	58	2
Itraconazole	168	57.6	0.129	58	3
Miconazole	160	32.7	0.091	1	3
Ketoconazole	150	52.9	0.125	45	3
Clotrimazole	145	31.8	0.076	30	3
Indomethacin	161	37.6	0.086	45	3
Ritonavir	121	60.4	0.153	50	3
Felodipine	145	31.0	0.074	45	3
Carbamazepine	190	25.5	0.055	61	1
Fenofibrate	80	33.0	0.093	-19	3
Omeprazole	159	26.6	0.062	45	3

Piroxicam thermal data:

The cyclic DSC of piroxicam can be found in Figure 91. The additional data for Piroxicam was obtained from the literature[63,64].

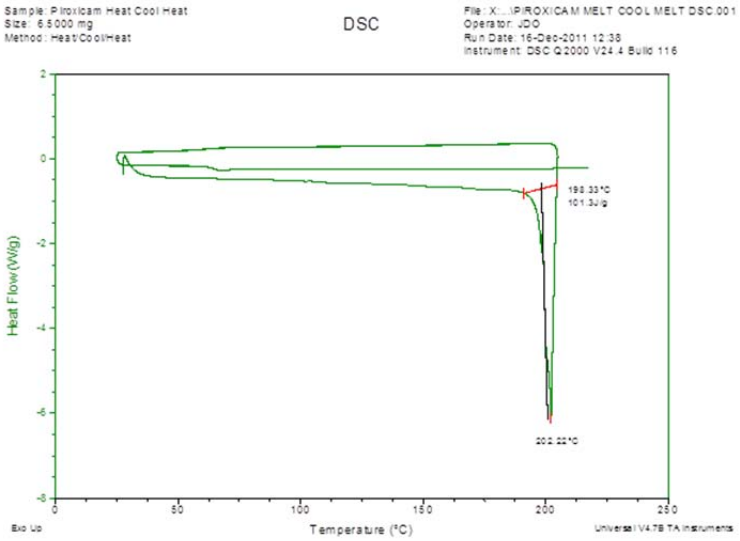

Figure 91. Cyclic DSC characterization of Piroxicam.

Telaprevir thermal data:

All thermal data for Telaprevir was generated from Figure 92, 93 and 94.

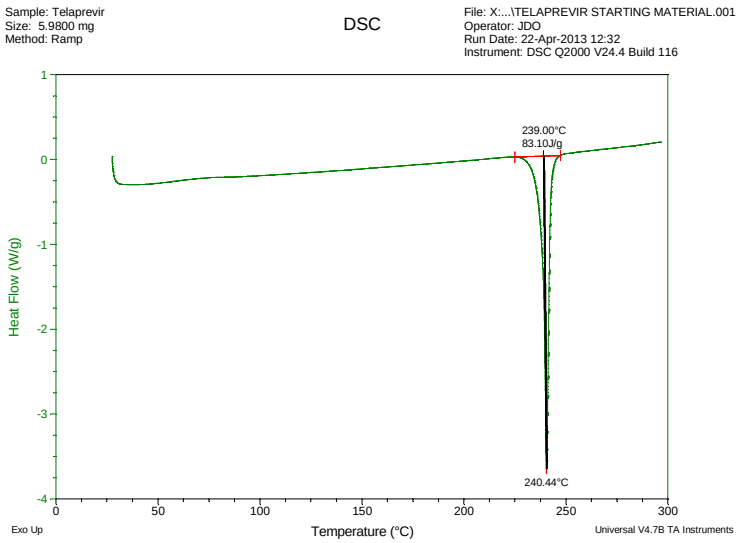

Figure 92. DSC characterization of Telaprevir.

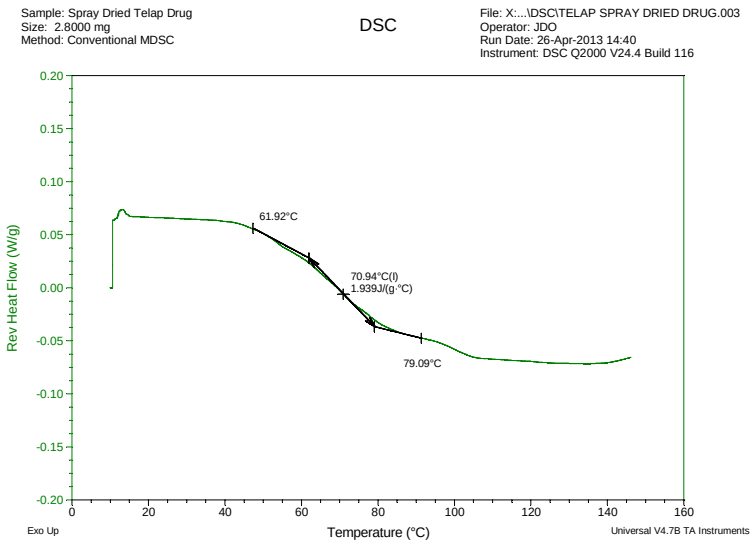

Figure 93. Modulated DSC characterization of Telaprevir.

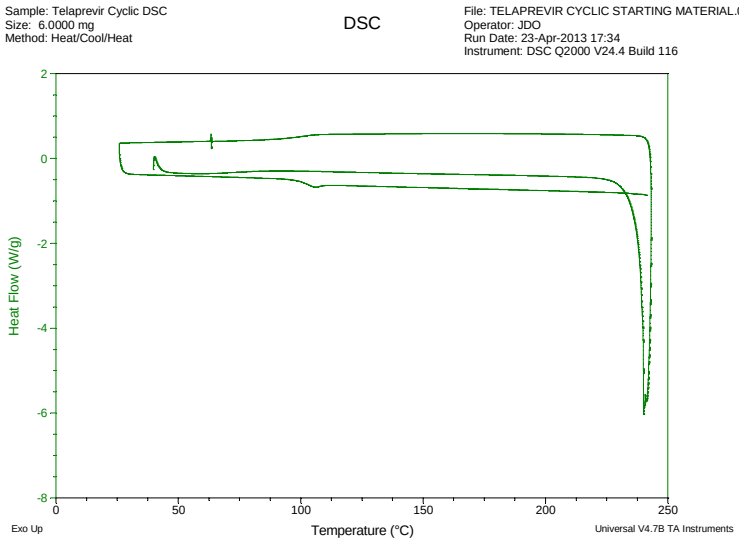

Figure 94. Cyclic DSC characterization of Telaprevir.

Efavirenz thermal data:

Efavirenz thermal data was generated by Figure 95 and 96 and by review of the literature from Ilevbare and Taylor[19].

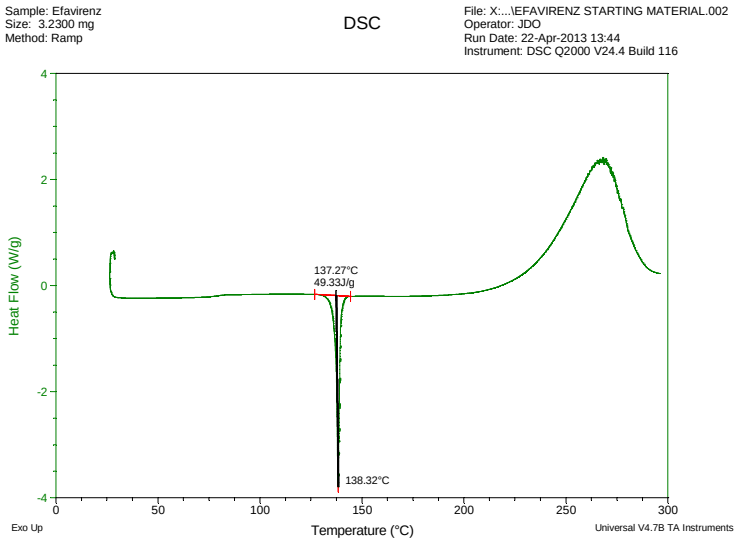

Figure 95. DSC characterization of Efavirenz.

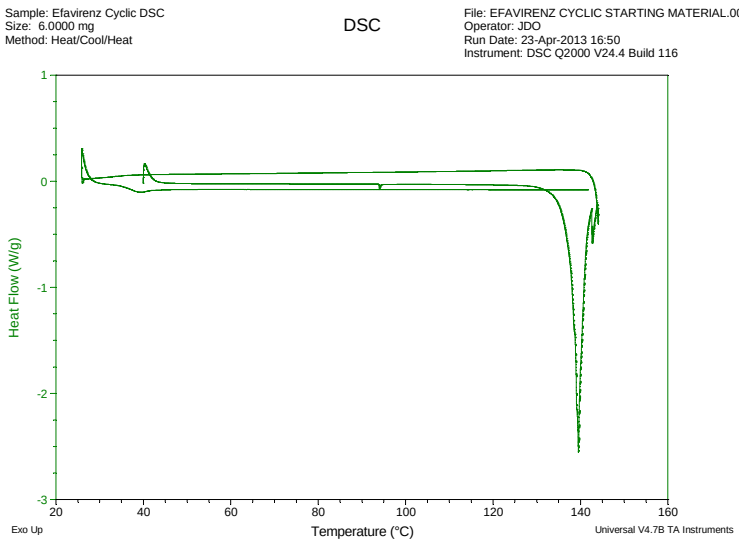

Figure 96. Cyclic DSC characterization of Efavirenz.

Aprepitant thermal characterization data:

Aprepitant thermal data was generated in Figure 97 and 98. Note that the glass transition temperature of aprepitant is taken from the cyclic DSC experiment due to the difficulty in generating amorphous aprepitant by other means.

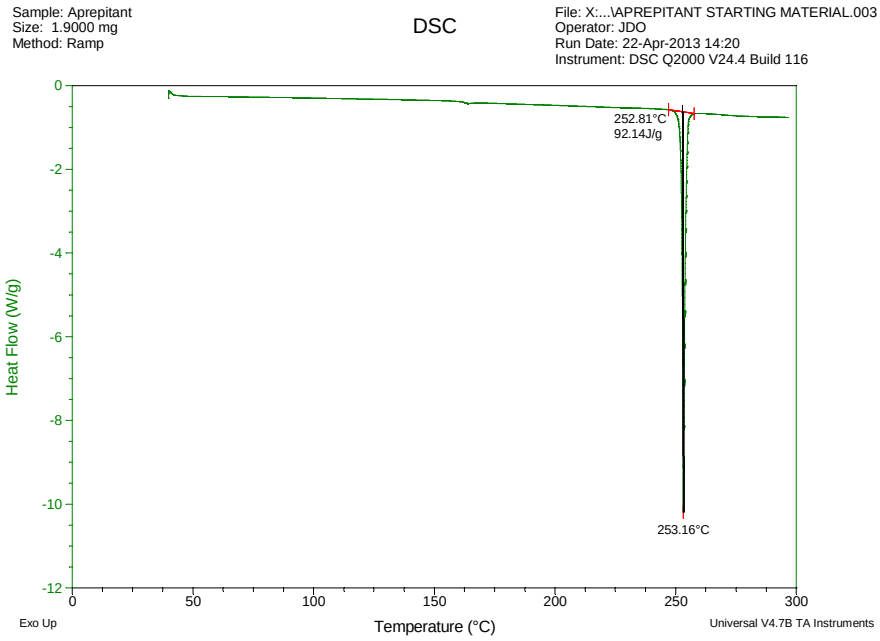

Figure 97. DSC characterization of Aprepitant.

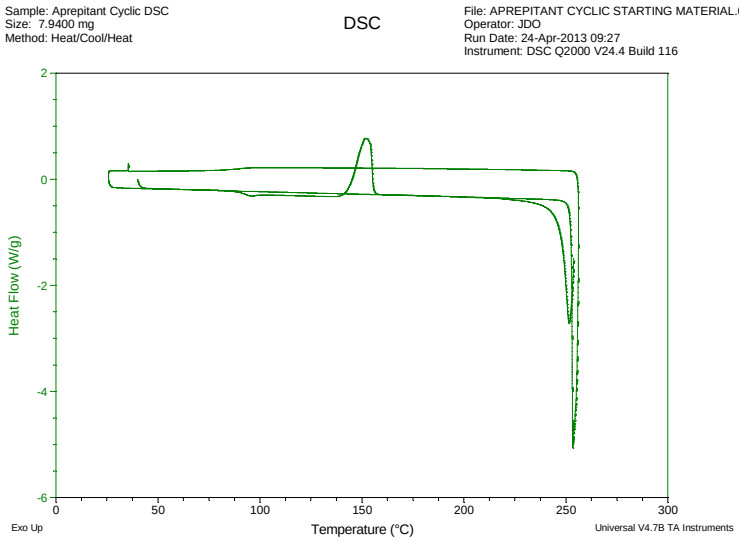

Figure 98. Cyclic DSC characterization of Aprepitant.

Torcetrapib thermal data:

Torcetrapib thermal data was generated in Figure 99, 100 and 101.

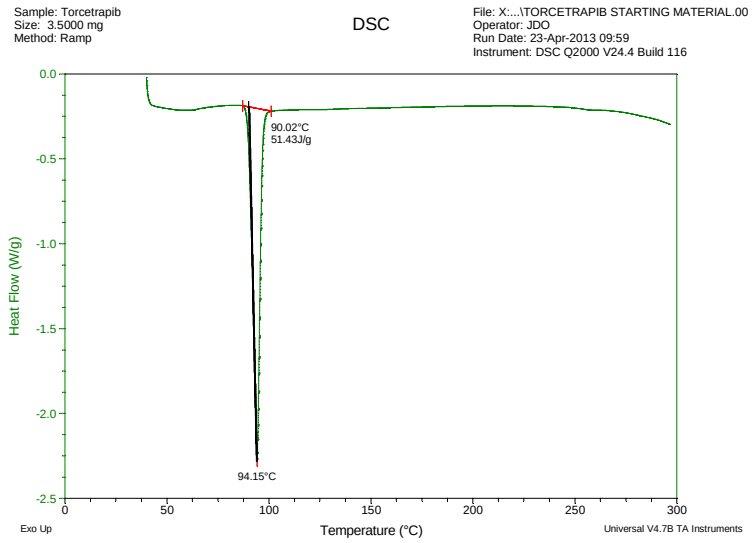

Figure 99. DSC characterization of Torcetrapib.

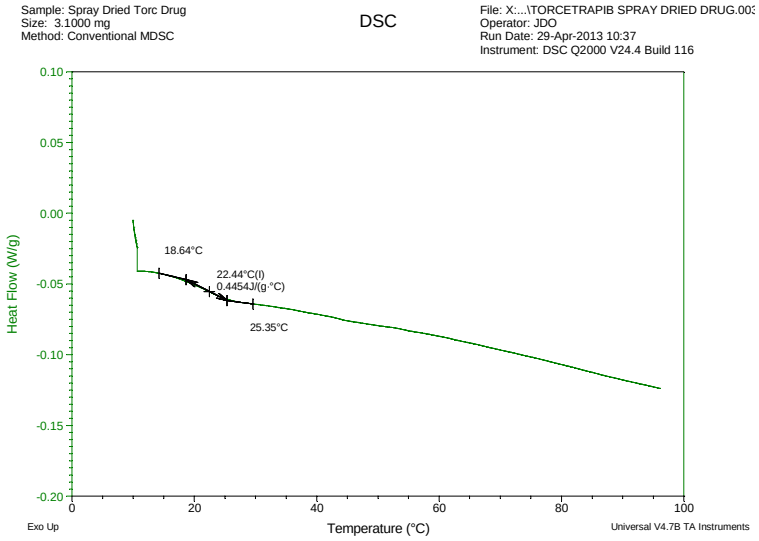

Figure 100. Modulated DSC characterization of Torcetrapib.

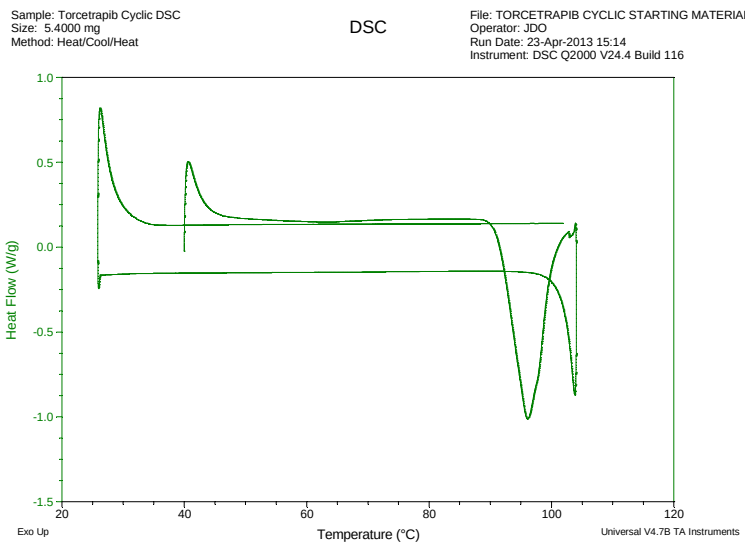

Figure 101. Cyclic DSC characterization of Torcetrapib.

Telmisartan thermal characterization data:

Telmisartan thermal data was generated by Figure 102 and 103 and by review of the literature[65].

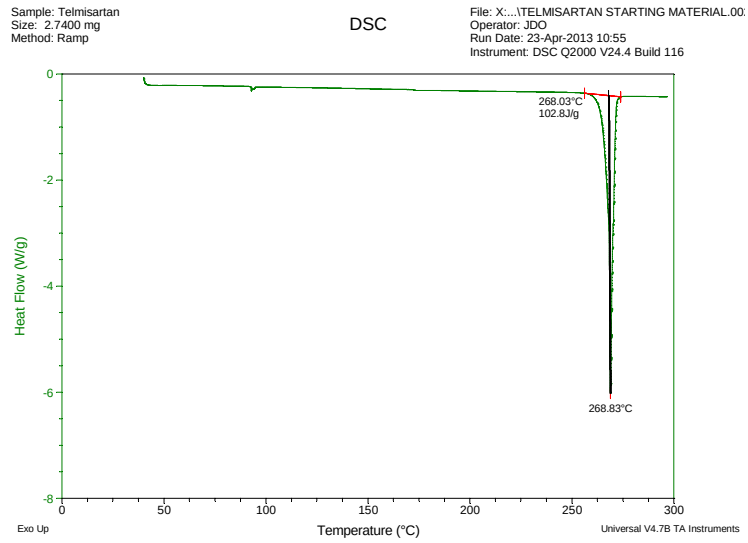

Figure 102. DSC characterization of Telmisartan.

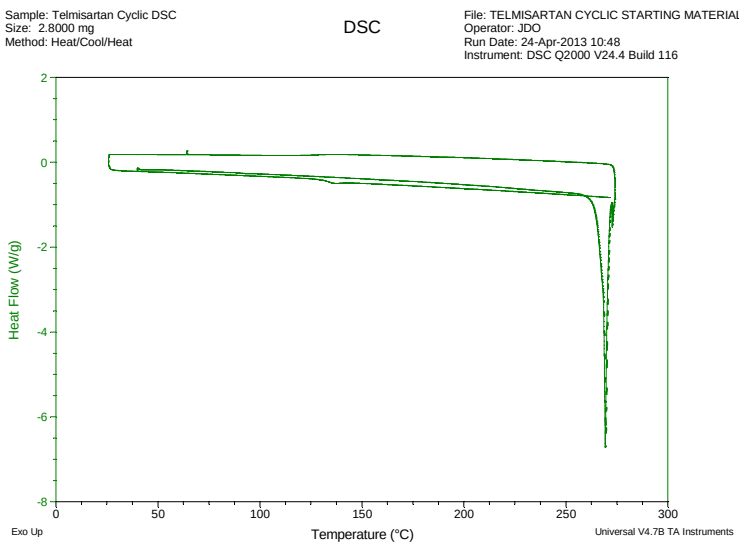

Figure 103. Cyclic DSC characterization of Telmisartan.

Nevirapine thermal characterization data:

Thermal data for Nevirapine was obtained via literature search[66] and Figure 104.

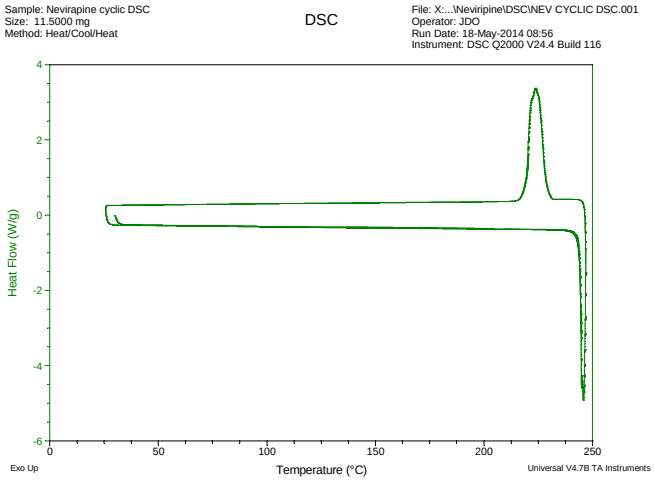

Figure 104. Cyclic DSC characterization of Nevirapine

Omeprazole thermal characterization data:

Omeprazole thermal data was generated by Figure 105, 106 and 107.

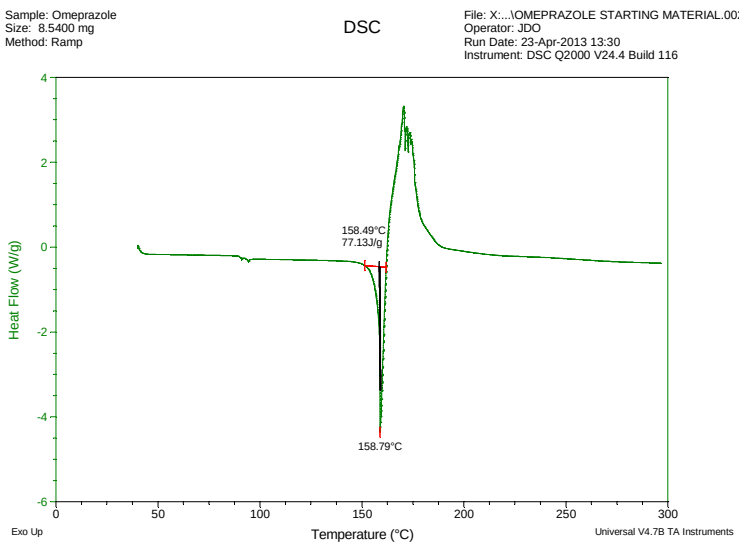

Figure 105. DSC characterization of Omeprazole.

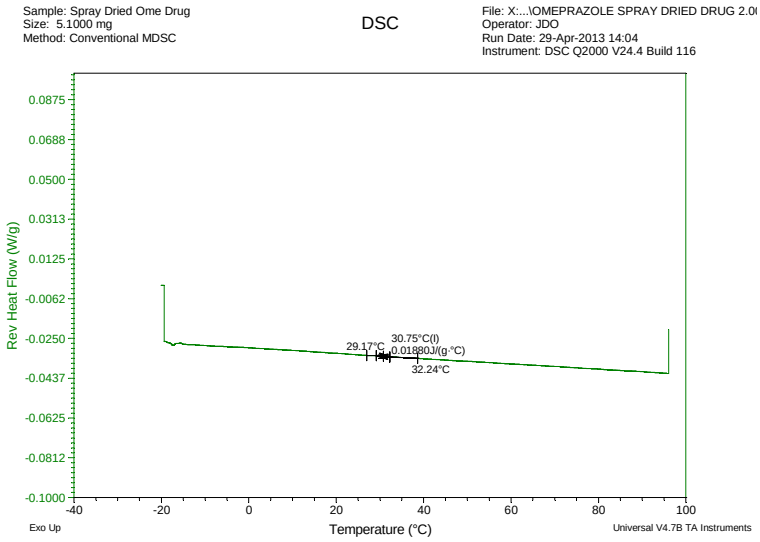

Figure 106. Modulated DSC characterization of Omeprazole.

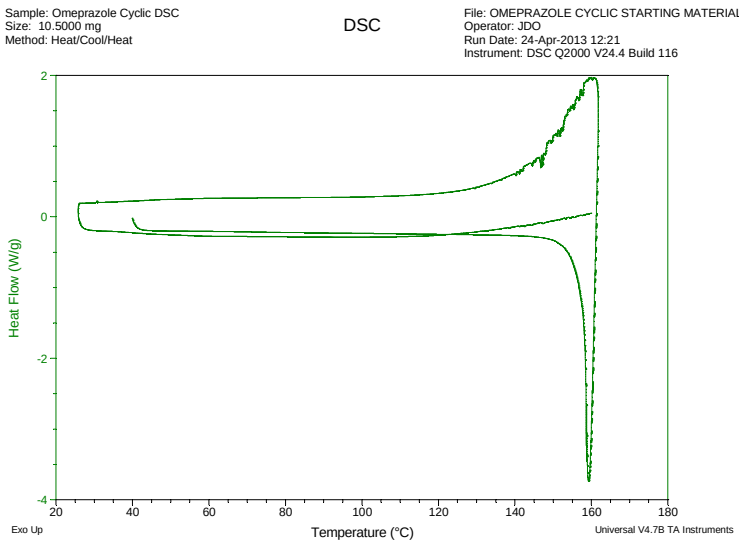

Figure 107. Cyclic DSC characterization of Omeprazole.

Hydrophilicity data for thesis model compounds:

A summary of the Hydrophilicity data used in this thesis appears in Table 3.

Log P values:

Log P values for griseofulvin, chlorpropamide, indoprofen, tolazamide, bifonazole, clofoctol, celecoxib, itraconazole, miconazole, ketoconazole, clotrimazole, indomethacin, and felodipine can be found in a publication by Baird/Taylor[62]. Log P values for ritonavir and efavirenz can be found in a publication by Ilevbare/Taylor[19]. Log P values for nevirapine, piroxicam, aprepitant, telmisartan, carbamazepine, fenofibrate and omeprazole are available at the Canadian Drug Bank Database[67]. The Log P value for torcetrapib is available at the Look Chem Online Database[68]. The Log P value for telaprevir is available in a publication by Kwong[69].

pKa values:

All pKa values listed, for ionizable molecules come from the Canadian Drug Bank Database[67], with the exception of indoprofen which is available in the literuatre[70].

Water solubility values:

All listed water solubility values were taken from the Canadian Drunk Bank[67].

General Solubility Equation Data:

All values were calculated using equation 6.

Percent w/w Gain at 90% RH:

The following data was used to calculate the wt. % gain of each amorphous dispersion at 90% RH.

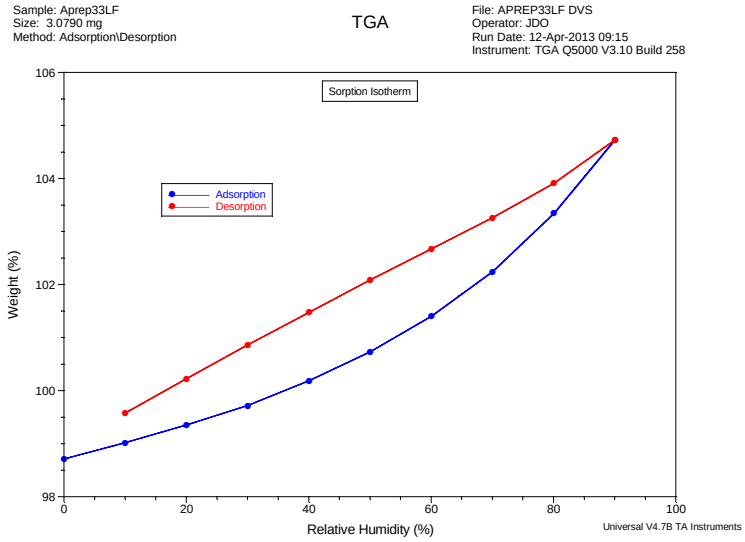

Figure 108. Moisture sorption isotherm (25 °C) for a spray dried amorphous dispersion of 33.3% Aprepitant/66.7% HPMCAS-LF.

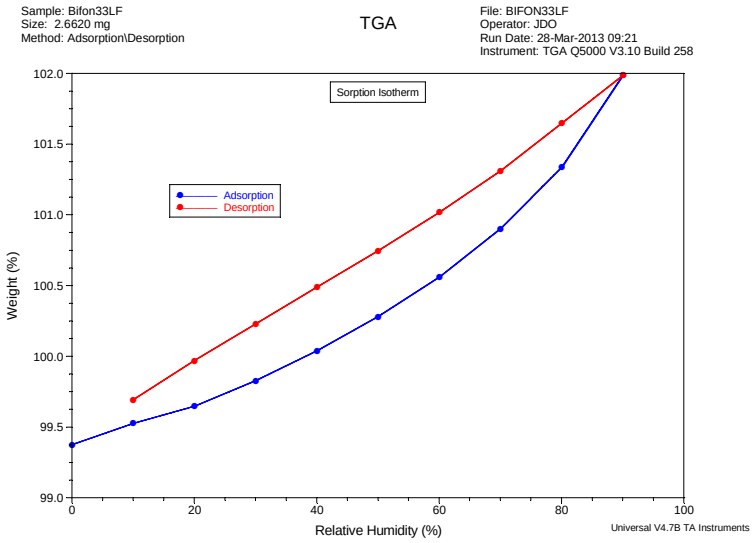

Figure 109. Moisture sorption isotherm (25 °C) for a spray dried amorphous dispersion of 33.3% Bifonazole/66.7% HPMCAS-LF.

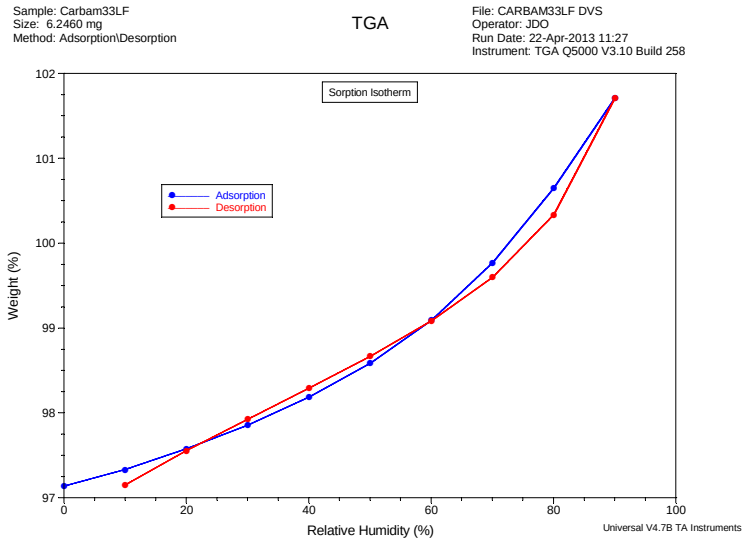

Figure 110. Moisture sorption isotherm (25 °C) for a spray dried amorphous dispersion of 33.3% Carbamazepine/66.7% HPMCAS-LF.

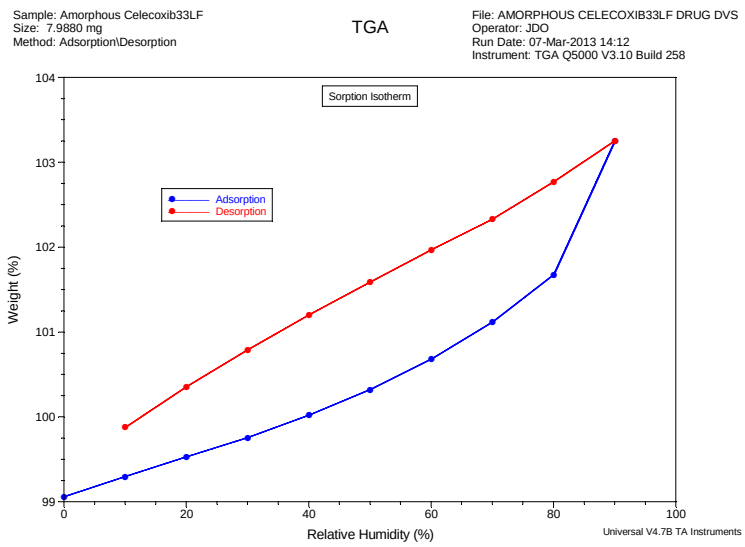

Figure 111. Moisture sorption isotherm (25 °C) for a spray dried amorphous dispersion of 33.3% Celecoxib/66.7% HPMCAS-LF.

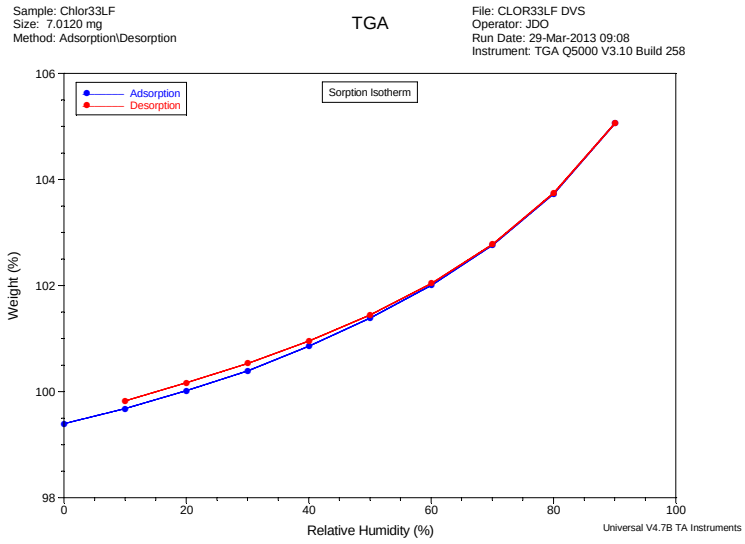

Figure 112. Moisture sorption isotherm (25 °C) for a spray dried amorphous dispersion of 33.3% Clorpropamide/66.7% HPMCAS-LF.

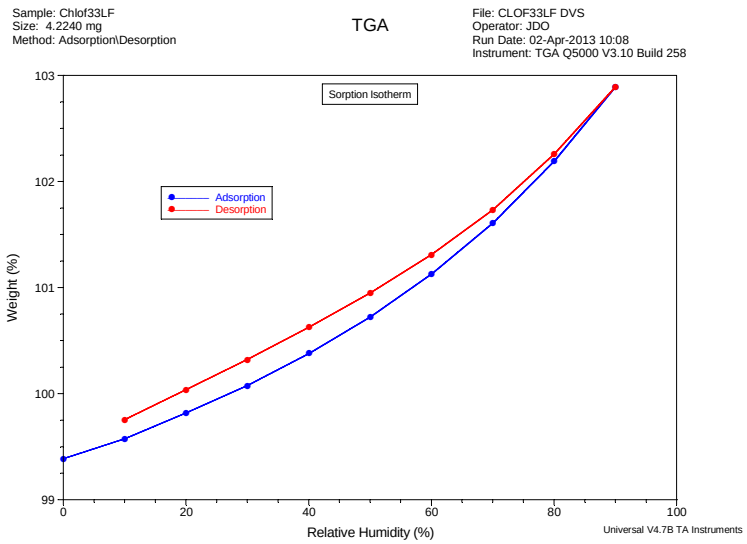

Figure 113. Moisture sorption isotherm (25 °C) for a spray dried amorphous dispersion of 33.3% Clofoctol/66.7% HPMCAS-LF.

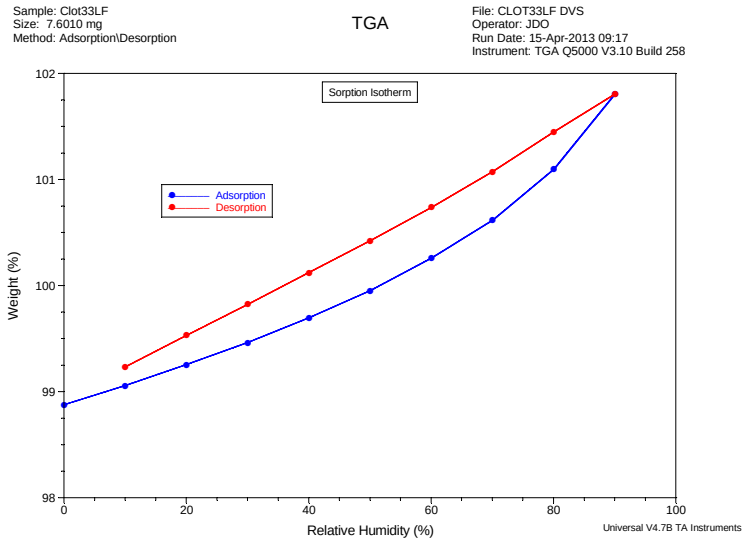

Figure 114. Moisture sorption isotherm (25 °C) for a spray dried amorphous dispersion of 33.3% Clotrimazole/66.7% HPMCAS-LF.

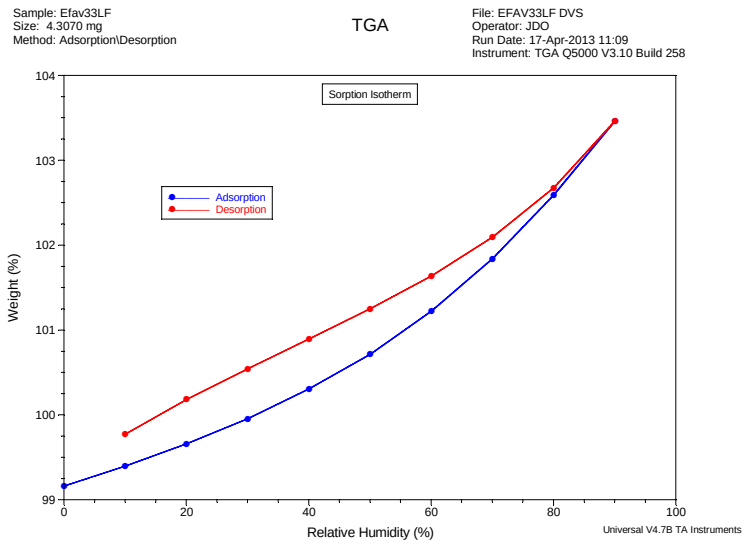

Figure 115. Moisture sorption isotherm (25 °C) for a spray dried amorphous dispersion of 33.3% Efavirenz/66.7% HPMCAS-LF.

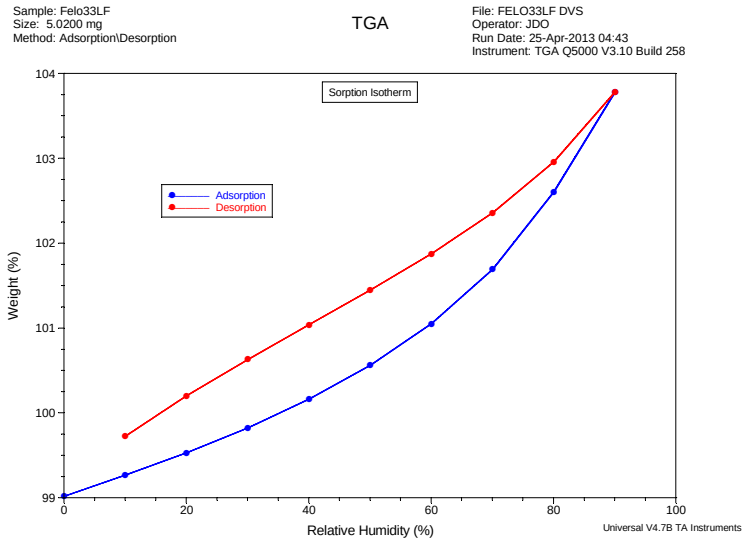

Figure 116. Moisture sorption isotherm (25 °C) for a spray dried amorphous dispersion of 33.3% Felodipine/66.7% HPMCAS-LF.

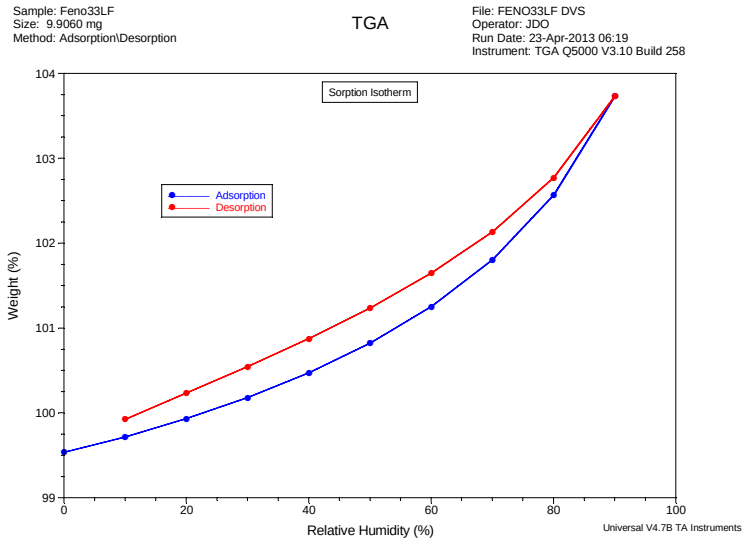

Figure 117. Moisture sorption isotherm (25 °C) for a spray dried amorphous dispersion of 33.3% Fenofibrate/66.7% HPMCAS-LF.

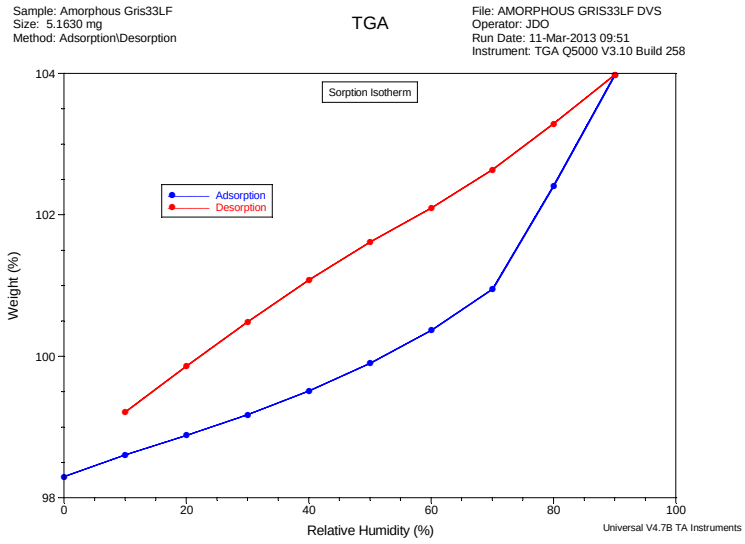

Figure 118. Moisture sorption isotherm (25 °C) for a spray dried amorphous dispersion of 33.3% Griseofulvin/66.7% HPMCAS-LF.

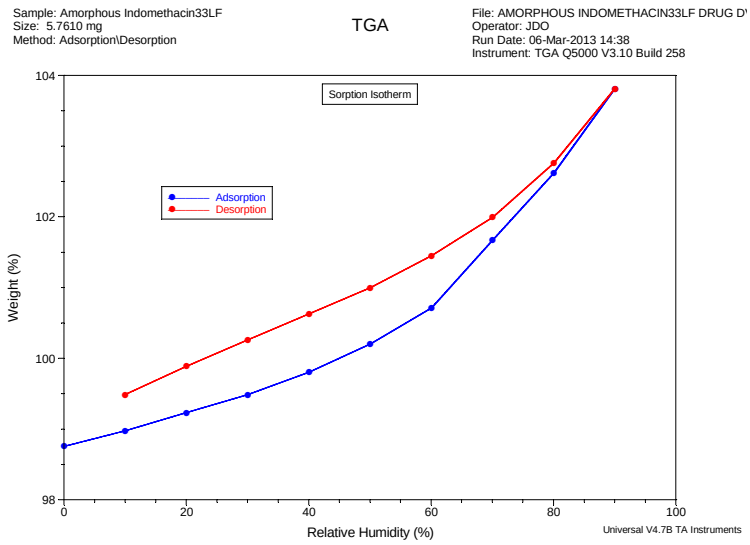

Figure 119. Moisture sorption isotherm (25 °C) for a spray dried amorphous dispersion of 33.3% Indomethacin/66.7% HPMCAS-LF.

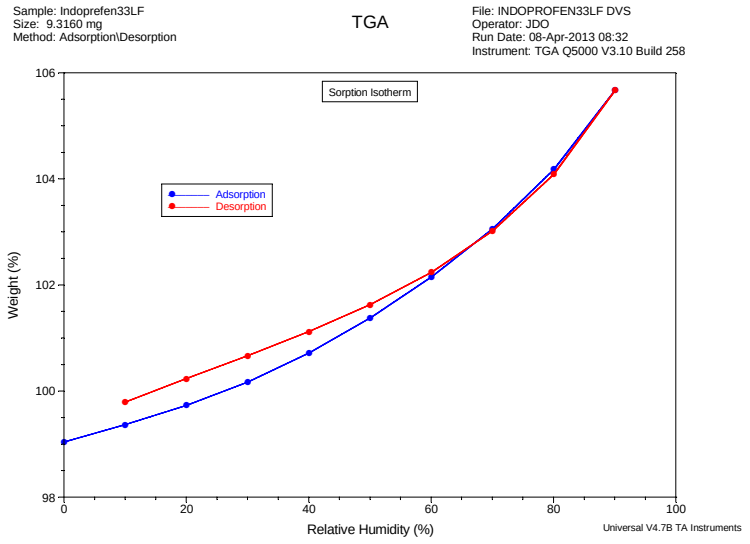

Figure 120. Moisture sorption isotherm (25 °C) for a spray dried amorphous dispersion of 33.3% Indoprofen/66.7% HPMCAS-LF.

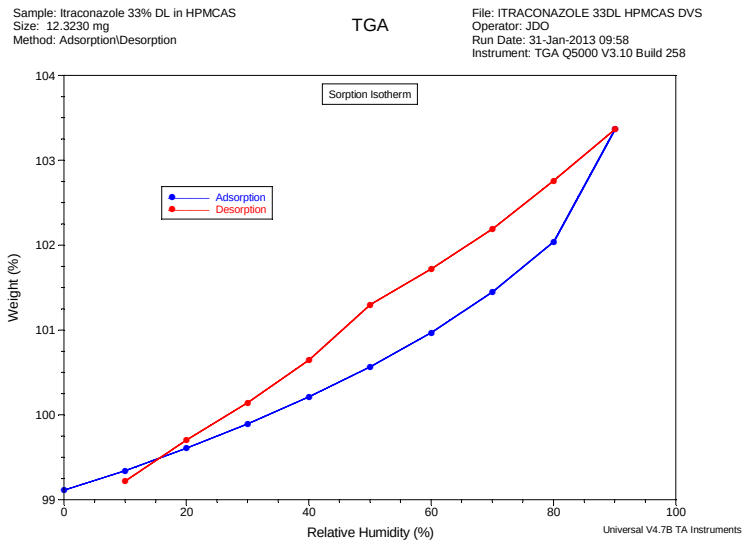

Figure 121. Moisture sorption isotherm (25 °C) for a spray dried amorphous dispersion of 33.3% Itraconazole/66.7% HPMCAS-LF.

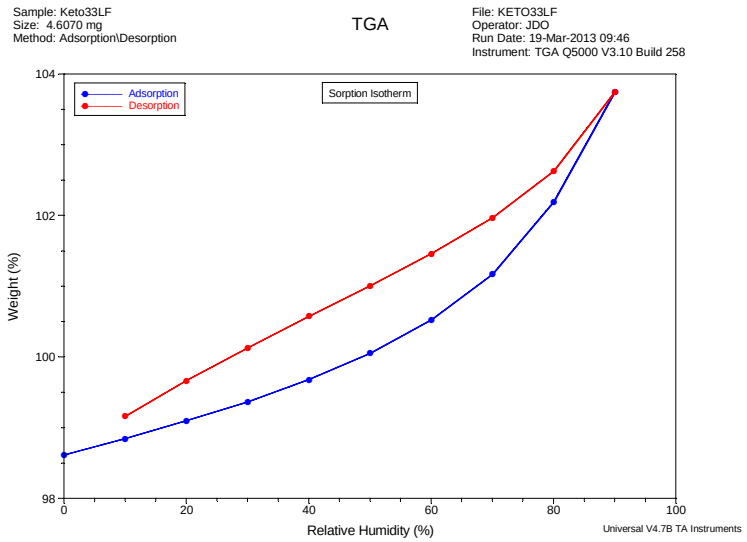

Figure 122. Moisture sorption isotherm (25 °C) for a spray dried amorphous dispersion of 33.3% Ketoconazole/66.7% HPMCAS-LF.

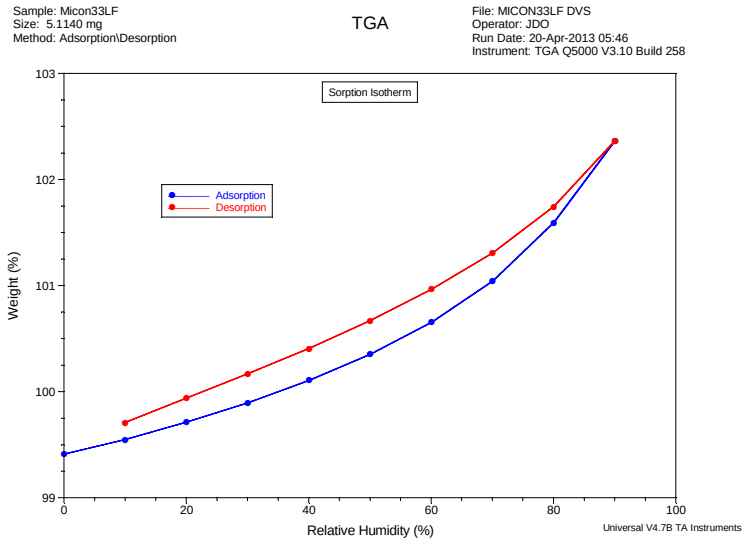

Figure 123. Moisture sorption isotherm (25 °C) for a spray dried amorphous dispersion of 33.3% Miconazole/66.7% HPMCAS-LF.

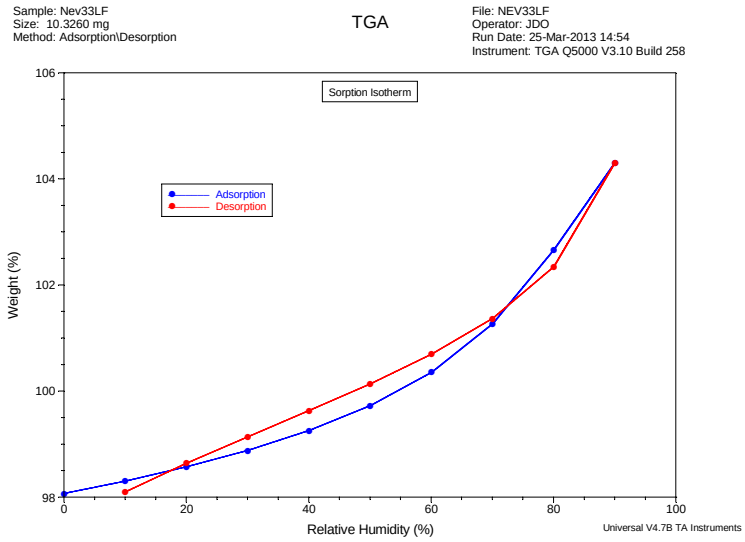

Figure 124. Moisture sorption isotherm (25 °C) for a spray dried amorphous dispersion of 33.3% Nevirapine/66.7% HPMCAS-LF.

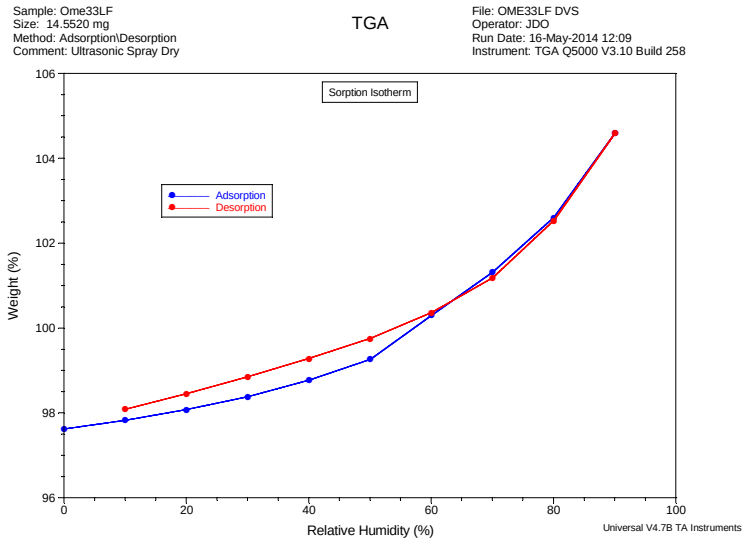

Figure 125. Moisture sorption isotherm (25 °C) for a spray dried amorphous dispersion of 33.3% Omeprazole/66.7% HPMCAS-LF.

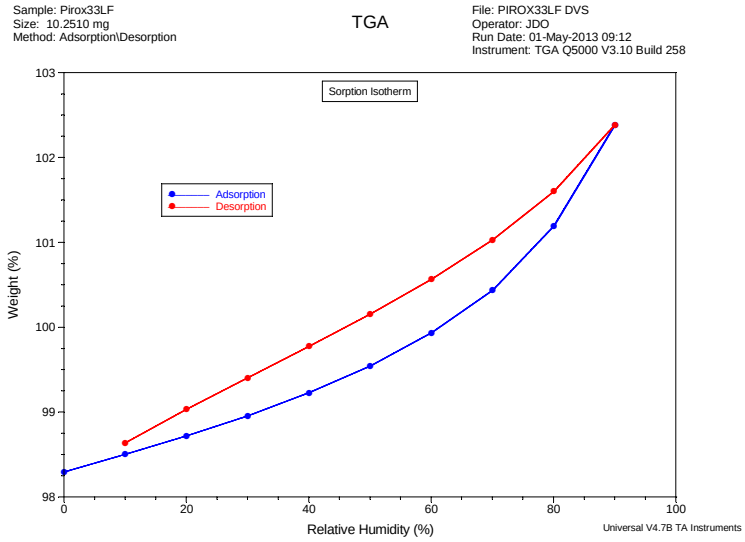

Figure 126. Moisture sorption isotherm (25 °C) for a spray dried amorphous dispersion of 33.3% Piroxicam/66.7% HPMCAS-LF.

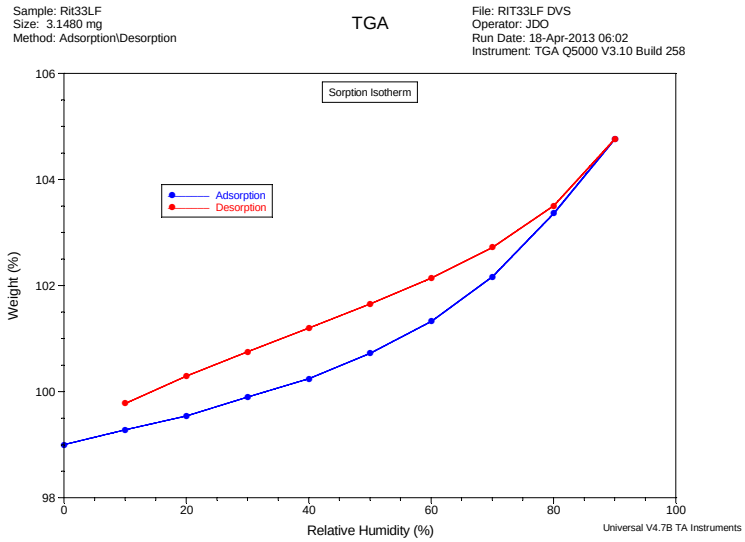

Figure 127. Moisture sorption isotherm (25 °C) for a spray dried amorphous dispersion of 33.3% Ritonavir/66.7% HPMCAS-LF.

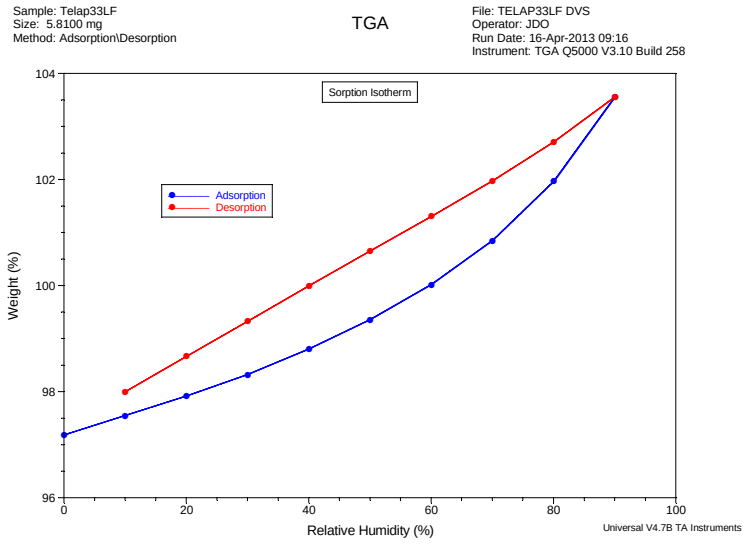

Figure 128. Moisture sorption isotherm (25 °C) for a spray dried amorphous dispersion of 33.3% Telaprevir/66.7% HPMCAS-LF.

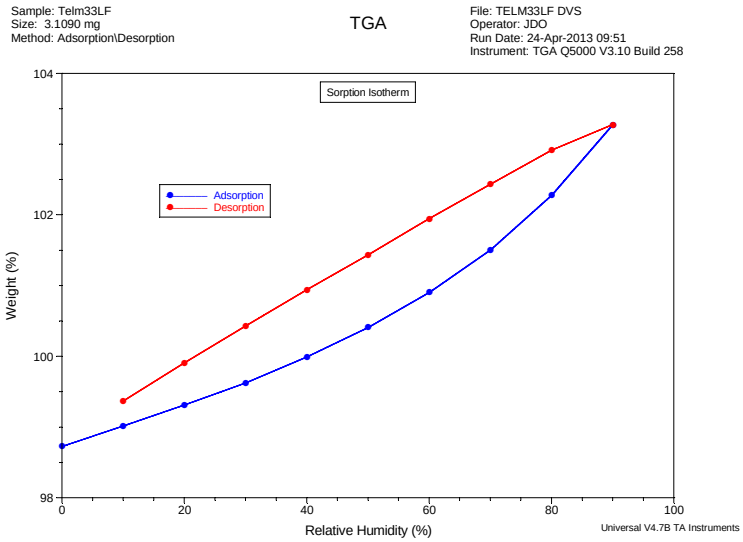

Figure 129. Moisture sorption isotherm (25 °C) for a spray dried amorphous dispersion of 33.3% Telmisarten/66.7% HPMCAS-LF.

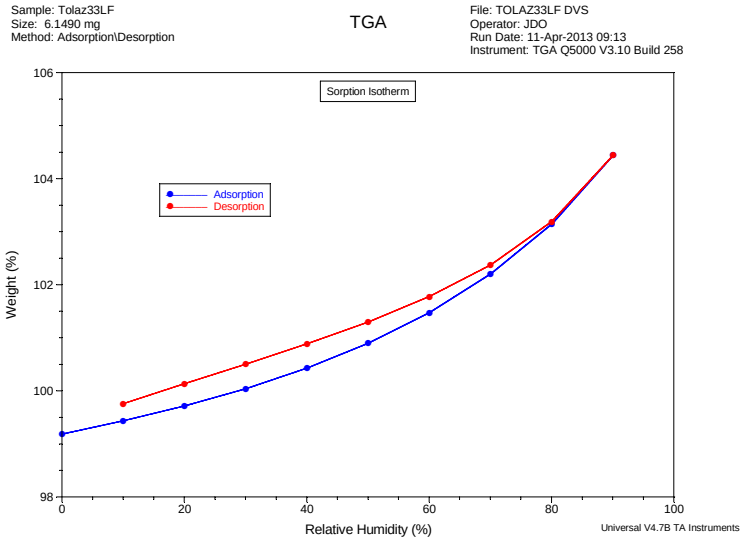

Figure 130. Moisture sorption isotherm (25 °C) for a spray dried amorphous dispersion of 33.3% Tolazamide/66.7% HPMCAS-LF.

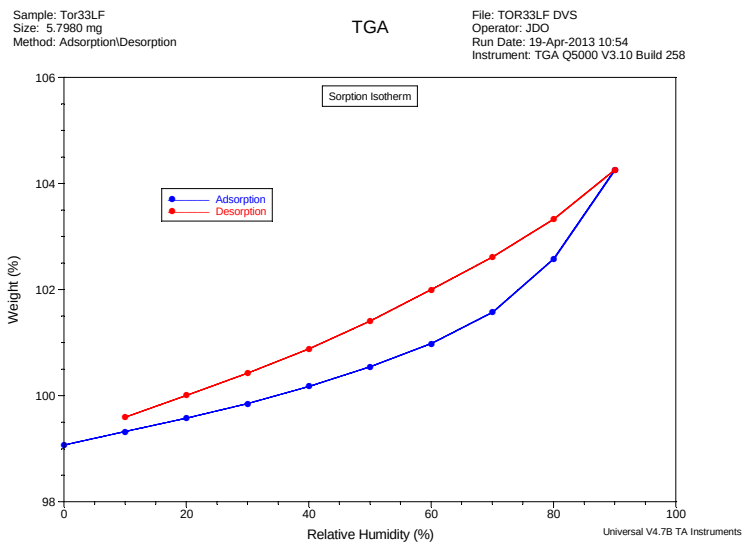

Figure 131. Moisture sorption isotherm (25 °C) for a spray dried amorphous dispersion of 33.3% Torcetrapib/66.7% HPMCAS-LF.